Fall 2013

The Effect of Composition on the Linear and Nonlinear Mechanical Properties of Particulate Filled Elastomers

Oluwaseyi Ogebule
Purdue University

Graduate School ETD Form 9
(Revised 12/07)

PURDUE UNIVERSITY
GRADUATE SCHOOL
Thesis/Dissertation Acceptance

This is to certify that the thesis/dissertation prepared

By OLUWASEYI OGEBULE

Entitled
THE EFFECT OF COMPOSITION ON THE LINEAR AND NONLINEAR PROPERTIES OF PARTICULATE FILLED ELASTOMERS

For the degree of Doctor of Philosophy

Is approved by the final examining committee:

JAMES M. CARUTHERS
Chair

WEINONG WAYNE CHEN

R. BYRON PIPES

YOU-YEON WON

To the best of my knowledge and as understood by the student in the *Research Integrity and Copyright Disclaimer (Graduate School Form 20)*, this thesis/dissertation adheres to the provisions of Purdue University's "Policy on Integrity in Research" and the use of copyrighted material.

Approved by Major Professor(s): JAMES M. CARUTHERS

Approved by: MICHAEL T. HARRIS 10/03/2013
Head of the Graduate Program Date

THE EFFECT OF COMPOSITION ON THE LINEAR AND NONLINEAR MECHANICAL PROPERTIES OF PARTICULATE FILLED ELASTOMERS

A Dissertation

Submitted to the Faculty

of

Purdue University

by

Oluwaseyi Ogebule

In Partial Fulfillment of the

Requirements for the Degree

of

Doctor of Philosophy

December 2013

Purdue University

West Lafayette, Indiana

In memory of my Dad and to my amazing Mom

Ise Oluwa li eyi

ACKNOWLEDGEMENTS

First and foremost, I give all glory, praise and honor to God Almighty. To have reached the end of this life-changing journey as a PhD student, despite the numerous ups and downs, testifies of abundant grace from. Where would I be if not for His grace, love and mercy that have carried me through this season? Truly, this doctoral degree is "the Lord's doing and it is marvelous…"(Psalm 118:23).

It has been an honor to work with some of the smartest people I have ever met. I am extremely grateful to my advisor Prof. James Caruthers for his excellent guidance. I will ever be thankful for the patience and kindness that he extended towards me. Thank you for giving me the opportunity to contribute to research and to work with and learn from an excellent scientist. I am indebted to Dr. Grigori Medvedev for his unflinching support. His patience, encouragement and advice were instrumental in successful completion of this degree. I would like to acknowledge Prof. R.Byron.Pipes, Prof. You-Yeon Won and Prof. Wayne Chen for serving as members of my PhD committee. Many thanks also go to the staff in the school of Chemical Engineering particularly Deb Bowman and Jenni Mamph for all the help with the administration side of things.

I would like to extend my gratitude to my fellow colleagues in the Caruthers research group. Many thanks to Dr. Aparajita Bhattacharya and Dr. Rasika Prabhu for help with learning how to use the instruments and other collaborative work. I appreciate the insightful research discussions and the encouragement that have so greatly contributed to the success of my research. I am grateful to Dr.JaeWoo Kim, Clancy Kadrmas and Sang Ha Son for their help with transporting of liquid nitrogen tanks. To Silei Xiong, Jeff Switzer and Anand David, your kind words and positive attitudes have made my time in the group a memorable one.

It is with immense gratitude that I acknowledge the support I received from

various organizations at Purdue. To Pastor Linda and Chi Alpha Christian Fellowship, thanks for being my family away from home. You have had an eternal impact on my life. To Mary Schweitzer and the Global Engineering Program, working with you was one of my most fulfilling experiences at Purdue. Thank you for the opportunity. To Dr. Jennifer Groh and the amazing ladies at the Women in Engineering program, especially the GMP LT 2011-2013, thanks for providing me with a platform to hone my leadership skills.

This journey would not have started without some wonderful mentors. I would like to thank the professors at Alabama A&M University who encouraged me to pursue an advanced degree. Prof. Odutola, Prof. Kim and Prof. Cooks for always seeing so much in me and encouraging me in my academic pursuits. I also appreciate the acquaintances I made at Purdue that led to my interest in research. I am grateful to Dr. Placidus Amama, Prof. Tim Fisher and Prof. Michael Harris for allowing me to participate in research as an undergraduate student.

I count it a blessing to have received the affection, care and encouragement provided by the friends I made at Purdue. I would like to acknowledge Dr. Mrs. Akande for being there for me in the most difficult time of my life. To the Yellowhouse ladies, Dr. Dahlia Campbell, Dr. Sheran Oradu and Dr.. Charity Wayua; I appreciate your genuine "sister-ship". To my sisters from Discipleship, the BlessEsther house and the DTN crew, Dr. Mopelola Akande, Dr. Sheran Oradu, Rethabile Tekane, Victor Aboh, Monique Long, JoAnna Jackson, Juan Pablo Burzaco, DeLean Tolbert, Fabiola Rojas Delgado, Zuli Melendez and Nicole Rheaume; I appreciate the prayers, encouragement and spiritual accountability. Hannah Sturtevant, Qi "Claire" Ding, Raydon Haskins and the rest of the Wiley LifeGroup, thanks for the memories and delightful times together. To my little sister, Shalyse Tindell, thanks for your genuine friendship and for ensuring I saw the sun shine occasionally. Diana Moreno, I will never forget your kind words at much needed times. To Temitope Toriola and Fally Masambuka, I appreciate your friendship and I am glad we crossed paths during our time here at Purdue. I would like to thank my African Christian Fellowship family for their prayers and support. To my Aunty and Uncle, Drs. Tayo and Lola Adedokun, I cannot find words enough to express my gratitude for all you have done for me. I will ever be grateful to God for allowing me

to meet you. To Dr. Darion Grant, thanks for your wise counsel and sincere friendship. I would also like to thank Adewale Okeleji, Dr Bismark Agbelie and family, Modurodoluwa Okeowo, Segun Ajuwon, Tolulope Omotoso, Francis Darko, Oluwatoba Omotilewa, Alain Shema and Yves Mujyambere, Ogechi Ogbonna, Nnenna Nwagbara, for their friendship, witticisms and encouragement. I will ever be grateful to Pastor Alfred and Grace Okosun. Thank you for being there for my family through the most difficult period of our lives. Your unwavering support is deeply appreciated.

Last but not least, I owe my deepest gratitude to my family, by biggest cheerleaders throughout this journey. I thank my parents John and Taiwo Ogebule for their unconditional love and untiring support. Even though my Dad did not live to see me complete this program, I know without a doubt that he would have been the proudest Dad in the world. I am indeed grateful to God even for his time here on earth and for giving me a wonderful father. I express my deepest appreciation to my Mom, a woman I very much admire. Thanks for being the most loving, selfless, and supportive mother anyone could ask for. My siblings, Abiola Ogebule, Tobi Ogebule, Taiwo Ogebule and Kehinde Ogebule, thanks for the laughter and joy you exude that has kept me going. Thank you for believing in me when I didn’t believe in myself. Ẹ se gun!

TABLE OF CONTENTS

LIST OF TABLES

LIST OF FIGURES

Figure Page

Figure Page

Figure Page

Figure Page

Figure Page

Figure Page

Appendix Figure

Appendix Figure Page

Appendix Figure Page

NOMENCLATURE

a_T – horizontal shift factors

b_T – vertical shift factors

CB – carbon black

HAM – high amplitude modulus

IIR – butyl rubber

J(t) – creep compliance

LAM – low amplitude modulus

G (t) – stress relaxation modulus

G’ – storage modulus (from shear experiment)

G’’ - loss modulus (from shear experiment)

NR – natural rubber

phr – parts per hundred rubber

PB – polybutadiene rubber

PDMS – poly(dimethylsiloxane), silicone rubber

SBR – styrene butadiene rubber

S – surface area

tan δ - loss tangent, ratio of loss modulus to storage modulus

TTS- time-temperature superposition

φ, φ_{eff} – volume fraction, effective volume fraction

ψ – interfacial area

$\phi\psi$ – loading – interfacial area

ε, γ - strain

ω - frequency

σ - stress

ABSTRACT

Ogebule, Oluwaseyi. Ph.D., Purdue University, December 2013. The Effect of Composition on the Linear and Nonlinear Mechanical Properties of Particulate Filled Elastomers. Major Professor: James M. Caruthers.

Engineering elastomers are materials capable of undergoing large deformation upon load application and recovering upon load removal. From car tires to building vibration isolator systems, elastomers are the most versatile of engineering materials. The inclusion of particulate fillers into elastomers enhances their mechanical properties (modulus, tensile strength, toughness, tear resistance, etc.) thereby extending their applicability to more demanding functions. The automotive, healthcare, construction, adhesives and consumer products are some of the many industries that produce finished goods containing elastomeric parts.

Despite the various concepts on reinforcement of filled elastomers, a complete understanding of their linear viscoelastic properties and the nonlinear mechanical properties, including stress softening (Mullins), strain dependent dynamic modulus (Payne) and others remains elusive. Furthermore, studies on filled elastomers have failed to produce a unifying perspective on the relationship between the microstructural composition and the observed macroscopic response to deformation. To further the current understanding of the underlying physics of elastomer reinforcement, a comprehensive study on the effect of composition was undertaken.

A major challenge in the application of the Time-Temperature Superposition (TTS) principle for filled elastomers rests on the difficulty of conducting experiments in their linear regime, which could be at strains even lower than 10^{-3}. In this work, the linear viscoelastic behavior of filled elastomers was studied via the successful application of TTS at extremely small strains using the double sandwich shear geometry. Well-defined

master curves were constructed for a series of carbon black filled SBR and Polybutadiene elastomers. In addition, an investigation of the effects of filler volume fraction and structure on the full linear viscoelastic response was carried out. A critical analysis of the superposed data showed correlation of linear viscoelastic properties to measurable filler parameters specifically the effective volume fraction, φ_{eff}, in which allowed for the first time collapsing on a single master curve the viscoelastic storage and loss moduli for all filled elastomers studied.

Nonlinear mechanical behavior was investigated on fumed silica filled Poly(dimethylsiloxane) rubber. For the first time, necking was observed for a lightly cross-linked poly(dimethylsiloxane) elastomer filled with 30 phr (parts per hundred rubber) or more of high surface area ($\geq$300 m^2/g) fumed silica. A series of linear and nonlinear mechanical properties of the necked material were studied including (i) linear and nonlinear dynamic shear analysis including the Payne effect, (ii) uniaxial tension experiments including the Mullins effect, (iii) tensile strength, and (iv) tear resistance via the 'trouser' test. The ultimate properties of the necked material were superior to its un-necked counterpart and both the Mullins and Payne effects were present in the necked material. The dynamic modulus exhibited anisotropy with respect to the direction of the necking deformation, where the anisotropy was not found in fumed silica filled PDMS elastomers that did not neck although the materials were pre-stretched to similar strains. Based upon these experimental observations, it was been postulated that necking occurs due to the breakage of delicate highly branched aggregates at the points of local stress concentrations. The preferential breakage of the most mechanically distressed aggregates will result in a more regular filler-matrix network, giving rise to higher ultimate properties of the necked material. This finding challenges the aggregate breakage postulate as a primary mechanism for the Mullins effect.

CHAPTER 1. INTRODUCTION

1.1 Elastomers

Engineering elastomers, synonymously rubbers, are a class of polymers. According to American Society of Testing and Materials a rubber is a "material capable of recovering from large deformations quickly and forcibly, and can be, or already is, modified to a state in which it is essentially insoluble" (ASTM D1566). The addition of particulate fillers into elastomers enhances their mechanical properties including modulus, tensile strength toughness and tear resistance. Elastomers are the most versatile of engineering materials and can be found in common everyday applications. The automotive, healthcare, construction, adhesives and consumer products are just some of the many industries that produce finished goods containing elastomeric parts. These goods include car tires, building vibrator systems, shoe soles, dental products and a wide range of applications. In their service lifetime, elastomers are subject to strains, stresses and all sorts of complex deformation histories. Relating their microscopic compositions to their macroscopic response to deformation has been an ongoing challenge for the rubber industry. An understanding of their fundamental behavior is critical to unlocking the mysteries that surround these complex materials.

Rubber reinforcement, brought about by the addition of fillers, is attributed to the filler ascribing its favorable mechanical properties on the "weak" polymer thus ameliorating the elastomers' ability to withstand deformation. From this, stems the concepts of filler-filler and filler-polymer interactions which are at the foundation of all postulates used in describing the underlying physics that corresponds to the response to deformation of filled elastomers. Despite the various concepts on reinforcement in filled elastomers, a complete understanding of key attributes such as linear

viscoelasticity, stress softening (Mullins), strain dependent dynamic modulus effect (Payne) and other mechanical properties remains elusive. In recent years, the use of computer software has become an integral part of product design to aid in reduction of manufacturing costs [1]. With computational mechanics, especially in finite element methods, simulation of stress or strain analyses on complex elastomeric networks can be performed prior to manufacturing. However, before such powerful software can be useful, a thorough understanding of the elastomer is required, meaning a complete and accurate constitutive model with the ability to predict the response of elastomeric parts to deformation is necessary. Although characterizing the mechanical properties of filled elastomers has been studied for ages, researchers are yet to develop a quantitative constitutive model that captures all the complexities of their mechanical behavior. Such models are hard to come by because a fundamental understanding of the "how" and "why" of filled elastomer mechanics is lacking. A unifying perspective on the influence of microscopic properties on the macroscopic response to deformation is needed.

Recent work by R. Prabhu [2] and A. Bhattacharya[3] utilized an extensive data set to identify the loopholes in current theories for predicting deformation in both filled and unfilled elastomers. In addition, R.Prabhu established the criteria needed to achieve time-temperature superposition (TTS) in filled elastomers [4]. Until then, the principle of TTS for filled elastomers was uncertain. As part of a concerted effort, the current work aims to expound upon recent findings by our group in order to boost the current understanding of filled elastomers. The effect of composition on the linear and nonlinear mechanical behaviour was investigated in this work.

This dissertation is organized as follows: Chapter 1 presents key concepts on filler properties and the typical response of filled elastomer. A literature review on filled elastomers and the physical mechanisms of reinforcement is provided. The linear viscoelastic behavior of filled elastomers is reported in Chapter 3 where TTS was carried out on filled elastomers. Next, a critical analysis of the effect of composition on the linear viscoelastic properties is the subject of Chapter 3 and Chapter 4. The first part is an account of the linear viscoelastic mater curves generated from TTS. Correlations between linear viscoelastic behavior and quantifiable filler parameters is the subject of the second

part. Chapter 5 is the work on nonlinear mechanical behavior that resulted in a discovery of necking, a novel phenomenon in filled elastomers.

1.2 Filled Elastomers

1.2.1 Composition of filled elastomers

A basic formulation for a filled elastomer will consist of the polymer, the filler and usually the cross-linking agent used to form a polymer network. Elastomers are amorphous polymers having a glass transition temperature, T_g, that is lower than room temperature. In the uncross-linked state, they exist as melts composed of long entangled polymer chains. With the addition of the cross-linking agent, they form polymer networks able to recover upon deformation. Besides the elastomer itself, the primary component of filled elastomers are the particulate fillers used to reinforce them. Clay, talc, carbon nanotubes, silica and carbon black are some of the many particulate fillers used to reinforce elastomers. By far, the most studied filled elastomers are composed of either carbon black or fumed silica particulates. The former because of its low cost and abundance and the latter because of its compatibility with inorganic elastomers such as silicone rubber. It is generally accepted that interactions between fillers and the polymer-filler interaction are responsible for the enhancement in mechanical properties of the elastomers. Thus, it is imperative to this work to understand the nature of the particulate, especially those used herein i.e. carbon black and fumed silica. These fillers are made up of primary particles of about 7-90nm but readily exist in aggregates composed of a fusion of primary particles (100-300nm). When describing particulate fillers, the term "structure" refers to the aggregates' properties. Fusion of aggregates produce agglomerates which can be broken down by mixing processes back to individual aggregates.

1.2.2 Types of Particulate Fillers

1.2.2.1 Carbon Black

Carbon black is manufactured from the incomplete combustion of hydrocarbon feedstock such as natural gas and aromatic oils [5]. In its industrial application, it is primarily used to reinforce elastomers especially in the tire industry but other functions also include printing inks, fibers, paper and building materials. Carbon blacks are classified into various groups based on the specific hydrocarbon feedstock and chemical processes involved. In general, there are three fabrication methods: furnace black, gas/lamp black, and thermal/acetylene black. Depending upon the feedstock material, the fabrication method or the chemical process, the property of the finished black can vary over a wide range. Figure 1.1 illustrates the surface chemistry of carbon black.

1.2.2.2 Fumed Silica

Fumed silica is distinguished from other type of silicas by its manufacturing process. The hydrolysis of silicon tetrachloride by a flame pyrolytic process produces these highly branched fumed silica particulates. The surface of fumed silica aggregates is covered by silanol groups which have a tendency to form strong hydrogen bonds and hence, they more readily form agglomerates. Hydrogen interactions allow fumed silica to entrap water (moisture) from the atmosphere. This ability to bind water renders them hydrophilic making dispersion in polar elastomeric matrices challenging. However, what might appear to be a setback is also their biggest advantage. The surface silanol groups can be chemically modified to alter its interaction with an elastomer. As such, tunable chemical modification can be done to either prevent attachment to the elastomer or can be chemically bound to the elastomer. A schematic of the fumed silica surface is provided in Figure 1.2.

1.2.2.3 Other fillers

Carbon nanotubes have in recent years become an attractive filler type due to their remarkable mechanical properties. Other fillers typically used in reinforcement studies include Silicon or Calcium aluminate, Titanium oxide, Zinc oxide and precipitated Calcium carbonate. It is worth noting that not all fillers have reinforcing abilities like fumed silica and carbon black. Some fillers like Titanium Oxide, are considered semi-reinforcing, while others like Clay are dilution fillers. Even yet, mica and talc used in polymers are mostly considered degradative fillers – that depreciate mechanical properties[5].

1.2.3 Methods of characterization of particulate fillers

1.2.3.1 Surface Area and particle size

The Brauner, Emmet, Teller (BET)[6] method is the common technique for measuring the surface area of fillers as described by ASTM D-3037/4820. This principle is based on the absorption isotherms achieved by exposing non porous fillers to Nitrogen (N_2) and determining how much N_2 is used up before a monolayer is absorbed onto the filler surface. This will be represented by key features in the adsorption isotherm. Other methods used for surface area characterization are Iodine I_2 adsorption, Cetyltrimethylammonium bromide (CTAB) or an indirect technique by measuring tint strength [5].

Another very important filler property is the average particle size as it determines the filler's ability to reinforce an elastomer. It follows that the smaller the particle size, the greater the reinforcing ability. There is no direct method of measurement for the particle size as techniques such as electron microscopy usually involve large sampling errors[5]. Therefore, the standardized approach for measuring average particle size utilizes the surface area technique. It follows that there exists an inverse relationship between the surface area per unit weight and the particle size of fillers. By measuring the surface area

of a known mass of filler, the particle size can be calculated. This is the accepted industrial convention for characterizing filler particle size as per ASTM D24.

1.2.3.2 Structure

The current industrial test standard for structure determination is the Dibutyl phthalate absorption (DBPA) number. In the case of carbon black, Dibutyl phthalate (DBP) absorption measures the relative structure by determining the amount of DBP a given mass of carbon black can absorb before reaching a specified viscous paste. Thermal blacks have the lowest DBPA numbers (32-47 ml/100g) of any carbon black, indicating very little particle aggregation or structure.

Characterizing fumed silica is not as straightforward. The fumed silica is highly branched thus is has a high structure. However the hydroxyl groups on the filler surface can be chemically modified to alter the interaction with the polymer as desired. Cabot and Evonik are some of the companies that manufacture treated fumed silica where the silanol surface have been capped with groups such as methyl in order to limit its interaction with the elastomer. Alternate chemical modifications can in fact anchor the elastomer onto the filler surface creating permanent strong chemical links.

1.2.3.3 Surface activity (Surface Energy)

The strength of the interaction between the filler and an elastomer would depend on its surface activity as dictated by its surface chemistry. Despite the lack of a standard approach for determining surface activity, certain attributes of the filler are useful in developing an understanding. The filler chemistry shows the available chemical groups that could potentially interact with the elastomer. For the case of carbon black (Figure 1.1), there are very few such chemically available groups for attachment. The case is not so in fumed silica (Figure 1.2). Thus, the ease in modification of the fumed silica surface

makes it useful for applications where specific knowledge of the polymer-filler interaction is needed.

Another parameter that indirectly characterizes the surface activity is the surface energy. The surface energy is a sum of two components: the dispersive, γ_s^d , and the polar (or specific) component, γ_s^p , expressed as.

$$\gamma_s = \gamma_s^d + \gamma_s^p \tag{1-1}$$

Table 1.1 shows the surface energy components of typical carbon black and fumed silica. Also included are the surface energies of select elastomers. As observed, carbon black has a higher dispersive component than polar component (except in the case of N550, high structure black). On the other hand, fumed silica has a higher polar component than dispersive. It follows then that carbon black would achieve reinforcement mainly by interacting with the polymer and fumed silica would favor filler-filler interactions[5,7]. In addition, it has been observed that if the surface energy of the polymer itself is much lower than the filler, the latter will tend to form agglomerates As such, there is no hindrance caused by the polymer (polymer filler interactions are minimized). Of course, other properties and filer parameters have to be taken into effect and the statements above are simply generalizations.

1.3 Mechanical Characterization of Elastomers

1.3.1 Viscoelasticity

Elastomers respond to deformation by combining the deformation response of an elastic solid and viscous liquid. Elastic solids are able to return to their original shape when deformed while viscous liquids will only stop flowing when the applied stress is removed. The combination of these characteristics renders polymers neither elastic nor viscous but both, viscoelastic. Among many others, some of the classical responses of filled elastomers include:

- Hysteresis upon stretching and un-stretching
- A time-dependent strain rate behavior

- Decrease in stress upon application of a constant strain (stress relaxation)
- Increase in strain when a constant stress is applied (creep).

1.3.1.1 Transient behavior

In response to the application of a fixed stress or strain, viscoelastic materials show creep and stress relaxation respectively. Figure 1.3 shows a typical response of a viscoelastic material to external stimuli. For a stress induced set-up, the ratio of the resulting strain, $\varepsilon(t)$ to the applied stress, σ_o to the is given by the creep compliance, J. Figure 1.3a illustrates creep and creep recovery experiments. In a strain-controlled transient experiment, the ratio of the resulting stress, $\sigma(t)$ to the applied strain, ε_o is given by the stress relaxation modulus,G. Stress relaxation is illustrated in Figure 1.3b. The expressions for the creep compliance, J(t) and stress relaxation modulus, G(t) in a shear experiment are given by:

$$J(t) = \frac{\varepsilon(t)}{\sigma_o} \tag{1-2}$$

$$G(t) = \frac{\sigma(t)}{\varepsilon_o} \tag{1-3}$$

1.3.1.2 Dynamic behavior

Dynamic tests probe the elastomers response to deformation on a frequency scale. As frequency and time are inversely proportional, tests at very low or high frequencies can enable one to obtain information at long times and very short times respectively. Hence we can obtain deformation response of a material at timescales that are experimentally inaccessible. The application of a sinusoidal strain, γ (Equation 1-4) produces a sinusoidal stress response, σ (Equation 1-5)[7]. In the equations below, the amplitude of the stress and strain is given by the σ_o and γ_o, the frequency by ω, and the time, t. As in Figure 1.4, for a viscoelastic material, stress lags behind strain by an

amount, δ. This amount, δ is representative of the difference between the dynamic response of an elastic material and that of a viscous liquid.

$$\gamma(\omega) = \gamma_o \sin(\omega t) \tag{1-4}$$

$$\sigma(\omega) = \sigma_o \sin(\omega t + \delta) \tag{1-5}$$

The stress response can be subdivided to show its elastic (in-phase with strain) and viscous component (out-phase with strain) separately as in Equation 1-6

$$\sigma = \sigma_o \sin(\omega t)\cos\delta + \sigma_o \cos(\omega t)\sin\delta \tag{1-6}$$

In terms of shear modulus, G, the in phase and out of phase components are

$$G' = (\sigma_o / \gamma_o)\cos\delta \tag{1-7}$$

$$G'' = (\sigma_o / \gamma_o)\sin\delta \tag{1-8}$$

And thus, the ratio of both gives the loss tangent expressed as

$$\frac{G''}{G'} = \tan\delta \tag{1-9}$$

1.3.1.3 Linear Viscoelasticity

Linear viscoelasticity investigates material behavior at small deformations where the materials response to stress is directly proportional. Molecular motions within polymers cause their viscoelastic response to vary over time. These relaxation processes can vary over decades; however, such timescales may not be experimentally accessible. By using Time-Temperature Superposition (TTS), the timescale of elastomer response can be extended several decades above what is experimentally accessible [8]. At very small strains, elastomers show an important temperature and frequency dependence. Above the glass transition temperature (T_g), the temperature dependence of the relaxation processes above T_g can be described by the following function via transient or dynamic experiments [9]:

$$G(t, T_1) = G(\frac{t}{a_T}, T_2) \tag{1-10}$$

By collecting data (modulus versus time/frequency) at T_2, the modulus at time, T_1 can be determined [10]. At a given strain, the modulus of a material at several temperatures above T_g can be superposed to give a master curve spanning decades on a time scale as shown in Figure 1.5. At a set reference temperature, the horizontal shift factor, a_T is used to shift the dynamic modulus data horizontally in order to compensate for the change in time brought about by changing temperature. The horizontal shift factors can be expressed using the William-Landel-Ferry (WLF) (Equation 1-11) for superposition above T_g, where C1 and C2 are WLF constants and T_{ref} is the reference temperature.

$$\log a_T = \frac{-C_1 (T - T_{ref})}{-C_1 + C_2 (T - T_{ref})} \tag{1-11}$$

Likewise, if used, the vertical shift factor, b_T, compensates for the change in modulus brought about by changing temperatures. When there is a change in the polymer-filler interaction, b_T is required for superposition otherwise, it is not always used [11]. TTS is successful if the relaxation processes show the same temperature-dependence. When this is not achievable, the material is no longer thermorheologically simple but complex[12]. This is usually the case for polymer blends[13] and multiphase systems[14].

1.3.2 Nonlinear Mechanical Behavior

1.3.2.1 Payne Effect

Named after its discoverer, A.R. Payne, this is the low frequency dynamic response of filled elastomers at small strains, <10%. It is characterized by a drop in storage modulus (G') as the strain amplitude is increased (at a constant frequency)[15-17]. The corresponding loss modulus (G'') and tan δ also show distinguished features as seen in Figure 1.6.Two linear regions exists: the low amplitude modulus (LAM) at low strains and the high amplitude modulus (HAM) at high strains. In these regions, the G' is unaffected by strain amplitudes. The difference between LAM and HAM gives the magnitude of the Payne effect (ΔG'). The point at which the drop in G' occurs coincides

with the peak at G'', known as G''max. The strain amplitude at which this occurs is the critical strain, γ_c.

It has long been accepted that fillers play a role in the Payne effect. Increase in filler loading, structure and enhanced surface activity all impact the Payne effect by increasing the magnitude of the G' response especially at the LAM end, thus increasing $\Delta G'$. The G' drop begins at strain values decreasing with increasing filler loadings[7,18-23]. Other observations include a decrease in LAM with dispersion time and temperature[24]. However, HAM is not significantly impacted by such changes[22,25,26]. The critical strain, γc has been reported by several authors and shown to be independent on frequency [18,27]. Other features of the Payne effect that have been studied in filled elastomers are

- Reversibility of Payne effect[28,29]
- Recovery - Spearheaded by Chazeau and colleagues [30], a study on the modulus recovery behavior revealed that 100% recovery is achievable within reasonable time for the Payne effect with a majority of the recover occurring within seconds [31].
- Influence of preload (static)- An effect if it is 60% or greater static pre deformation in ESBR with 50phr CB[28,29]
- Temperature[24] and frequency effects[26].

Despite the widespread view that the addition of filler particles is responsible for the Payne effect, the phenomenon is not unique to filled elastomers as several authors have reported the effect in uncrosslinked elastomers [16,31] and rubber-less systems such as carbon black in liquid paraffin[22].

Some filled elastomers showing the Payne effect (at least those of interest to this work) include carbon black filled styrene-butadiene rubber (SBR)[7,15,16,32,33]; carbon black filled polydimethylsiloxane (PDMS) [34] ; fumed silica filled SBR [35,36] and silica filled PDMS [20,24,35,37].

1.3.2.2 Payne Effect Mechanisms

Several authors including A.R. Payne himself have long argued that a breakdown of a filler network (connection of filler to filler throughout the elastomer matrix, Figure 1.7a) held my Van der Waals forces is responsible for the dramatic drop in G',storage modulus [26,33,38-41] . Pioneered by Voet *et al.*, others have used electrical conductivity studies in carbon black-SBR successfully buttress this claim[42-44]. Kraus and others pushed for the idea the breakdown and reformation of the filler network accounts for the recovery behavior in the storage modulus [40,45]. The presence of Payne in rubber-less systems supports the notion that filler-filler interaction dominates the effect and that the presence of a polymer network simply amplifies the effect and facilitates recovery[40]. In investigating the nature of the filler network, Heinrich *et al.* [40] reviewed two concepts: 1) the percolation theory and 2) the kinetic cluster-cluster aggregation (CCA).The former asserts that a filler threshold exist beyond which a filled rubber will exhibit Payne while CCA assumes a fluctuating motion of fillers within the elastomer that results in "space-filling". Both mechanisms are consistent with the idea of filler networking, and can describe the G' quite well. However, they are inadequate in their explanation of the energy dissipative process which is implied by the breakdown and reformation of the filler network [40].

Kraus was the first to suggest a phenomenological quantitative model based on agglomeration/deagglomeration of carbon black agglomerates[40,45,46]. He assumes that carbon black contacts break and reform and at a rate proportional to the number of existing contacts taking on a power law form. Although Kraus reported a good fit to actual experimental data, Ulmer [47] noted that the G''(γ_o) was deficient in its description in the very low strain amplitudes. In addition, the Kraus model cannot describe frequency and temperature effects [40]. Huber-Vilgis's take on idea of filler networking [48] asserts that the filler network is strain dependent and defined by a mean cluster size as $\xi(\gamma_o)$. They identified parameters that connected G'0 to the filler structure however, like Kraus, their model is unable of explaining temperature and frequency effects. Van de Walle *et al.* account for this inadequacy by putting forward a model comprising of a distribution of orientation and separation distance of filler aggregates as a function of strain [49].

Assuming G' and G'' are strain dependent for a two-aggregate system, a relationship between G' and G'' is facilitated through the use of a weighing function dependent on the presence and strength of contacts between aggregates ; but, as Chazeau *et al.*[30] point out, this model will not be able to predict the effect of static offsets (applying a static strain before the test) on a system.

In general, the models all contain the assumption of rearrangement of fillers in the network and are able to predict some features of the Payne effect that are independent of the specific filler types [23]. There are also several work able to predict G' for specific filler-rubber systems[5,37]. However, for these models, no explanation is rendered on the actual cause of filler network breakage and reformation.

While the filler networking view is the most common approach used to describe the Payne effect, several authors have proposed alternate perspectives attributing the Payne effect to changes in polymer-filler interactions [50]. Zhu & Sternstein's findings on the Payne effect at low filler concentration (implies no filler networking) uncrossliked system supports this notion [51] Polymer-filler interactions are evident from the formation of bound rubber, rubber physisorbed on the filler surface. Concepts on bound rubber formation were summarized by Boonstra's review article[21]. In the case of silica-silicone composite, bound rubber measurements by Aranguren and co-workers confirm that the filler surface is completely wetted by the polymer, therefore, filler aggregates can only come in contact through the polymer [19]. In addition, the fast recovery behavior of G' and G'' suggests that the origin lies in the behavior of the macromolecular structure of the matrix itself and not in the filler structure formation and destruction [30] .

Accordingly, mechanistic views focusing on this idea have been put forward by several authors[50,52]. The desorption/re-adsorption of bound rubber idea was introduced by Smit for a carbon black-SBR system [52]. This concept ascribes the drop in modulus to the adsorption and re-adsorption of polymer chains on the filler. The idea was further developed by Maier-Gortiz [50] who introduced a quantitative model involving a Langmuir-type polymer chain adsorption of filler surface. A schematic is shown in Figure 1.7b. The surface of the carbon black aggregates consist of free sites, sites occupied by stable links and those occupied by unstable links. Stable and unstable links

are weak bonds between polymer segments said to occur with strain amplitude. The nature of these links is unknown and the model fails for G'' due to its symmetry.
An alternate view on polymer-filler interactions was provided by Levresse *et al.* who investigated the amount of bound rubber, upon swelling of a an uncrosslinked system [53]. They propose a kinetic model of bound rubber formation in poly(dimethylsiloxane) (PDMS) using a second order reaction process. It follows that the reaction rate constant (of bound rubber formation), k[PDMS] °, has a weak dependence on silica loading and polymer molecular weight; however, k[PDMS] ° is very sensitive to polymer end functionality. Another perspective on polymer-filler effects suggests that the rubber occluded between filler particles behave mechanistically as part of the filler[7,54]. Bound rubber and occluded rubber are two different concepts. In the case of bound rubber, polymer chains in the vicinity of the filler are restricted from molecular motion but in occluded rubber, no reduction in polymer chain mobility is assumed. This view describes polymer-filler interactions as consisting of three parts: the filler, the a glassy shell of polymer that behaves as the filler and a polymer phase further from the glassy shell that becomes softer as the distance away from the filler is increased. The Payne effect is then assumed to be a response of the softer, more mobile phase. Table 1.2 and 1.3 summarizes mechanisms for the Payne effect, their strengths and their shortcomings.

1.3.2.3 Mullins Effect

Historically, this phenomena was first observed by Bouasse and Carriere [55]before it was extensively studied by Mullins and co-workers in the late fifties [56-59]. The Mullins effect is an elastomers' response to large deformation by a reduction in its stress for subsequent (loading-unloading) cycles beyond the first deformation cycle. Figure 1.8 is a typical example of the Mullins effect in filled elastomers. The most prominent feature is the stress softening (decrease in stress upon second loading until the previous maximum stretch). Other attributes include the presence of hysteresis upon load reversal (completion of loading-unloading cycle) permanent set (residual strain observed after

unloading), and anisotropy the material will experience if the direction of stretch of the second loading is changed as pointed out by Mullins others [56,57]. Carbon black filled SBR [56,60,61], silica filled SBR [62] and silica filled PDMS [63] are some of the many elastomers showing the Mullins effect. Like the Payne effect, the Mullins effect is not unique to filled elastomer systems. Unfilled elastomers, e.g. natural rubber and polyurethane [61,64-66] and even some biological systems [67] have been reported to show stress softening.

The influence of particulate fillers with respect to the Mullins effect are numerous. First of all, the stress-softening effect appears to be independent of filler volume fraction as implied by its presence in unfilled systems [68] and the permanent set/residual strain has been shown to increase with filler loading [69]. Filled elastomer systems show a greater strain rate dependence and hysteresis than unfilled systems [38]. There is also an anisotropy effect on the stress softening where less softening is observed if the experiment is performed in the direction perpendicular to the first stretch axis [56,63]

1.3.2.4 Mullins Effect Mechanisms

Mullins-Tobin attributed the Mullins effect to the behavior of soft and hard phases present in the composite. The soft phases are amplified upon stretching while the filler clusters (hard phases) are broken down irreversibly [58]. The fillers amplify the strain therefore, the Mullins effect is more apparent at smaller strains for a filled elastomer than it is at similar strain for an unfilled one [68]. According to Johnson-Beatty, the hard phase consists of clusters of molecular chains held together by short chain segments, entanglements or intermolecular forces [70]. As the material is stretched, chains are pulled from the clusters converting to softer regions (polymer chains). Consequently, the strain decreases in the soft region, the average chain length increases with loading, and the hard phase is oriented in stretching direction accounting for the anisotropic effect.
In line with the Mullins-Tobin concept of hard and soft phases, the strain amplification theory has been used to analyze Mullins effect data [57]. It involves the assumption that the effective strain in the rubber phase of a filled elastomer at any stress is equal to the strain

in the base elastomer without filler at the same stress, just amplified. So, the softening effect is simply a result of the change in the rubber phase (not filler phase) as supported by experiments in CB-SBR systems [64]. The strain or stretch (λ) is amplified by a factor X and rescaled to give a modified strain.

$$\tilde{\lambda} = 1 + (\lambda - 1) X \tag{1-12}$$

Several models have also utilized the X factor and related it to mechanistic damage[60,61,70-72].In the review article by Diani *et al.*, a general expression of phenomenological models is given:

$$W(F) = (1 - d) W_0\ (F) \tag{1-13}$$

where W is the strain energy density function, F is a strain tensor, and d is the damage parameter that is attributed to a physical damage concept. The "damage" idea is by far the most common perspective suggested for the mechanism behind the Mullins effect. In discussion of the "damage" evolution, Govindjee-Simo [73] approach assume that polymer chains are equally stretched and damaged. They developed a constitutive relation based on an eight chain representation of the underlying macromolecular network structure of the rubber and the non-Gaussian behavior of the individual chains in the proposed network[71,72,74]. Others have suggested that the damage parameter is only active in unloading part of the curve[75]. There has also been much discussion on what exactly is amplified in the models put forth [76].

The Mullins-Tobin [57] amplification of the uniaxial strain and the Govidjee-Simo [74] amplification of the total deformation gradient fail to predict experimental data at large strains. The Bergstrom-Boyce's approach of instead augmenting the first invariant of stretch appears to give the best estimation for chloroprene rubber under compression [76]. Recently, Mossi Idrissa *et al.* developed a new model based on the concept of hard and soft phases using Gent's strain energy (an extension of the neo-Hookean one constant constitutive relation for unfilled stress-strain behavior where the elastically stored strain energy, W is represented by a two-constant relation applicable for a wide range of strains[77]. Their new model considers filler properties such as structure and size in an attempt to predict stress softening [78] [73]. Another view on damage pioneered by Blanchard and Parkinson is the notion chain rupture [79]. On the same theory, Bueche explains that

there is an affine deformation of the filler-rubber chains and the stress softening is due to the breakage of chains [39,80].Their model accounts for the loss in stiffness due to breaking of polymer-filler bonds but is unsuccessful because it does not describe the effect in unfilled elastomers [39,79,80]. As Kraus and co-worker point out, the slow recovery after Mullins deformation does not fit the rupture assumption[38].

Generally, very few models pay attention to the anisotropic behavior of the Mullins effect. Qi and Boyce [81] proposed a phenomenological model by following the idea of soft and hard phases in rubber as proposed by Mullins and Tobin. Their model assumes that the material is isotropic and experiences no permanent set. Its damage criterion is controlled by a scalar quantity and it is able to predict data accurately for 50phr carbon-black SBR material with the underlying assumptions [61]. Other "two-phase" material models include the work by De Tommasi *et al.* [82,83] and Wineman *et al.* [84] which can model Mullins only if isotropic damage is assumed.

Miehe *et al.* [85] first proposed discontinuous and continuous damage functions based on classic damage mechanics. They later introduced a phenomenological model with an experimentally motivated *a priori* decomposition of the local stress response into three constitutive branches which act in parallel: a rubber elastic ground stress response, a rate-dependent viscoelastic overstress response and a rate-independent plastoelastic overstress response. The damage is assumed to act isotropically on all three branches and will predict Mullins assuming no anisotropy [86].

A network alteration model was proposed by Marckmann *et al.* where polymer chains are said to evolve with the maximum deformation, λ_{max}, leading to a new reference state[87-89]. The chains are eventually broken leading to dangling chains which do not contribute to stiffness, hence result in permanent set. This model assumes isothermal and isotropic systems and excludes hysteretic and non-linear viscoelastic effects. In line with this, Arruda-Boyce used a theory based on an eight-chain representation of the underlying macromolecular network structure of the rubber and the non-Gaussian behavior of the individual chains in the proposed network [90]. Both models are unable to show permanent set and anisotropy.

In support of the concept of slippage at large strains, Yamaguchi *et al.* studied the mechanical and electrical anisotropic of carbon black filled elastomers [42]. One observation is that the anisotropy effect is larger for mechanical tests than it is for electrical (measuring resistivity). They report that this difference is due to anisotropic slippage occurring at the filler–rubber surfaces and electrical behavior is more governed by breakdown of filler network. The changes to the mechanical behavior from the first cycle to subsequent strain cycles are much less dramatic than the changes in the electrical resistivity. Also, this indicates that the carbon black network breakdown has little effect on the mechanical behavior but a much greater effect on the resistivity.
Bhattacharya *et al.* put forth a jamming/unjamming mechanism based on motion of fillers within the matrix [3]. They proposed a phenomenological model describing the total stress as a sum of hyperelastic and viscoelastic contributions, where only the hyperelastic term is modified by jamming. The results look promising but will require further study. A summary on the mechanisms, pros and cons of the Mullins effect is provided in Table 1.4 and Table 1.5.

1.3.3 Summary of Nonlinear effects

Tables 1.2 and 1.5 provide a summary of mechanisms for the Payne and Mullins effects along with their advantages and shortcomings. They are two categories of models used to describe the non-linear behavior of filled elastomers – phenomenological and micro-mechanical. While phenomenological models have been shown to work in many cases, they utilize several parameters and there is difficulty relating them to physical quantities. Micro-mechanical models on the other hand relate macroscopic mechanical behavior to the physical chemical structure. Ideally, a model should contain as few parameters as possible that can be related to physical quantities if one is to manufacture rubber parts with tunable properties. It should be able to reproduce arbitrarily complex deformation behavior, and not only dependent on one deformation state as is the case in several models. In actuality, most models have to compromise certain attributes because they are unable to fit both criteria. Also several models are generally inferred from a

specific set of experimental data and thus, they work well for the particular materials being studied but cannot be easily extended to other types of rubbers or loading conditions.

All mechanisms and models are inadequate in their ability to fully describe the Payne and Mullins effect. In the case of the Payne phenomenon, these theories are "elastically driven", mainly focusing on the G' storage modulus and less on the loss properties, G'' [30,40]. They also do not address the influence of the filler structure on both G' and G'' simultaneously. As for the Mullins effect, most models focus on describing stress softening ignoring the permanent set (residual strain) and anisotropy observed in the effect [61]. Other approaches are purely mathematically derived, based on fitting experimental data to equations.

We also find that the Payne and Mullins effect are usually dealt with as two separate mechanical entities. Whilst the amount of deformation is different for both, the material is intrinsically the same .The nature of the underlying microstructure must be consistent for explaining both phenomena. i.e. if Mullins is caused by jamming of aggregates, one must account for its non-existence or presence in the Payne effect and provide an explanation for the why it may not be the governing mechanism in Payne. A better unifying perspective on how the microscopic heterogeneity is related to macroscopic deformation is needed.

1.4 Research Goals

Since the development of important reinforcement concepts by Payne, Mullins and Medalia, a significant breakthrough in the understanding of filled elastomers has long been overdue. Several theories for rubber reinforcement have been put forward; however, no consensus had been established on the underlying physics behind the response of filled elastomers to deformation. The lack of a unifying perspective is a major challenge in rubber research that needs to be addressed. There has also been a tendency to come up with complicated proposals without exhausting the simple options. An assessment of what is difficult to understand and what is really understood is needed. In our group, a lot

of effort has been dedicated to distinguishing between the two. This is the third contribution of a concerted effort to understand the physics of polymer reinforcement. Certain questions that needed be posed, some of which were addressed by the first and second contribution concern the following:

1. An understanding of the base unfilled elastomer must be attained before the effect of adding fillers can be understood. Through studies by R. Prabhu on linear viscoelasticity, small amplitude behavior was investigated for both unfilled elastomers and their filled counterparts[2]. Time-temperature superposition showed that only good experiments at low strain amplitudes are needed to obtain high-quality results. This is an important advancement and building block for this work. The lingering questions are (i) what is the effect of composition on TTS of filled elastomers and (ii) how are the concepts like the effective volume fraction and other filler parameters affected in the linear viscoelastic region?
2. Work by A. Bhattacharya with respect to the Mullins effect showed that the phenomenon can be explained by viscoelasticity considering damage[60]. It was shown that the hysteresis of all Mullins cycles are viscoelastic but that of the virgin material after the first deformation cannot be explained. The question remains, what explains Mullins once viscoelasticity is taken care of. In the course of addressing these questions, we studied the effect of fillers where viscoelasticity was eliminated by selecting systems way high above T_g where viscoelasticity was not an issue. The explanation for the Mullins effect is complicated and identifying the "damage" type is an important issue. The unanswered question here has to do with the role of filler properties on the nonlinear mechanical behavior.

The objective of this work is to identify the important parameters needed to further the current understanding on both the linear and nonlinear mechanical behavior of filled elastomers. The focus of this work is two-fold: (i) To determine the effect of composition on the linear viscoelastic properties. Once this is established, a critical analysis of linear viscoelastic behavior is needed with emphasis on correlating key features to measurable filler parameters. (ii) To study the nonlinear behavior as a function of filler properties.

The question of whether the mechanical response provides any additional insights into the mechanistic picture of the Payne and Mullins is the subject of this part.

Pursuant to these goals, a study on three different sets of filled elastomers was undertaken. Linear viscoelastic characterization of carbon black filled styrene butadiene rubber (SBR) and polybutadiene (PB) was carried out via the successful application of the time-temperature superposition principle as presented in Chapter 2. The extension of the dynamic master curves through the use of transient creep and creep recovery experiments provide an insight on the long term behavior. Chapter 3 and Chapter 4 deals with the critical analysis of the effect of composition on carbon black filled SBR. In Chapter 4, key features from Chapter 3 were studied for their correlations with measurable filler parameters. The effective filler volume fraction concept and other filler parameters were also investigated. Chapter 5 is an account on the effect of composition as it pertains to fumed silica filled silicone rubber. The unexpected discovery of necking, led to additional investigation of the necked material.

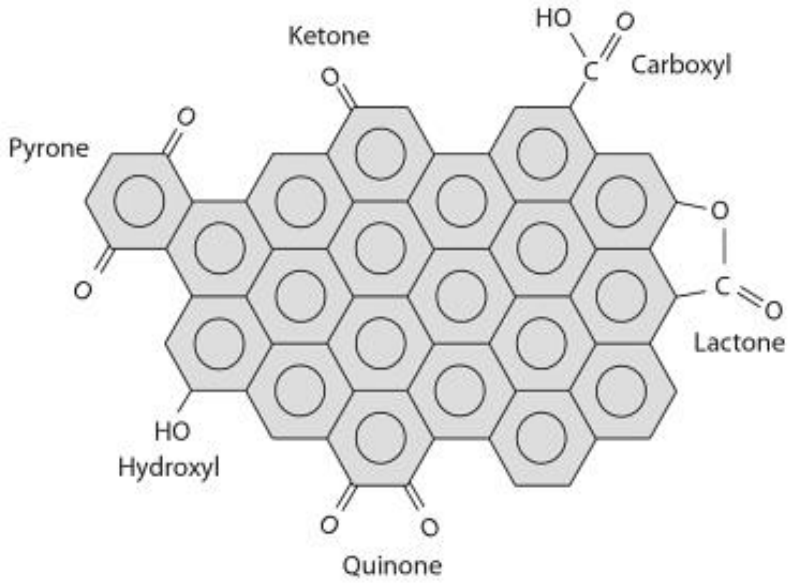

Figure 1.1: Surface chemistry of carbon black[5]

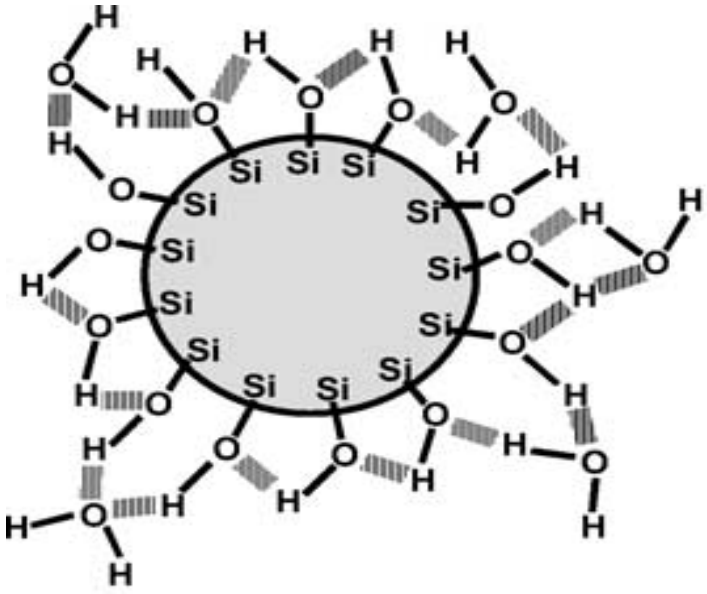

Figure 1.2: Surface chemistry of fumed silica

Table 1.1: Surface Energies of some filler and elastomers

Material	$\gamma_{specific}$ (mJ/m^2)	$\gamma_{dispersive}$ (mJ/m^2)	γ (mJ/m^2)
Elastomers			
SBR[91]	17.10	16.07	33.17
NR[91]	0.12	34.99	35.11
PDMS[92]	0.9	19.5	20.4
Carbon Black*			
N550	134.4;173.4	75.0;75.0	209.9; 248.4
N762	77.7;74.0	126.4;132.8	204.1;206.8
N990	56.6;58.8	71.8;78.7	128.4; 137.5
Fumed Silica*			
A130	48.1;45.4	27.3;30.7	75.4; 76.1
A200	57.4;55.1	40.9;44.3	98.3; 99.4
A300	51.0	55.0	106

*Surface energy values taken from Leblanc[5] unless otherwise specified

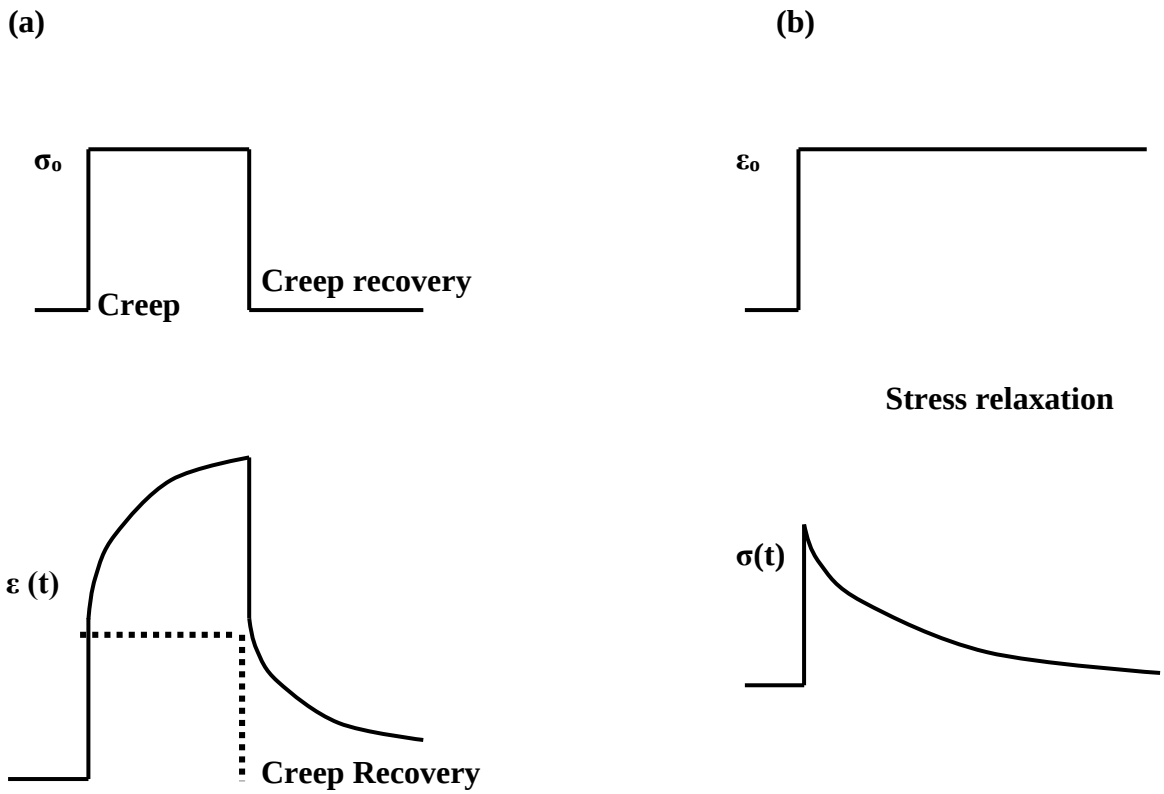

Figure 1.3: Schematic showing (a) creep with creep recovery and (b) stress relaxation behavior for a viscoelastic material.

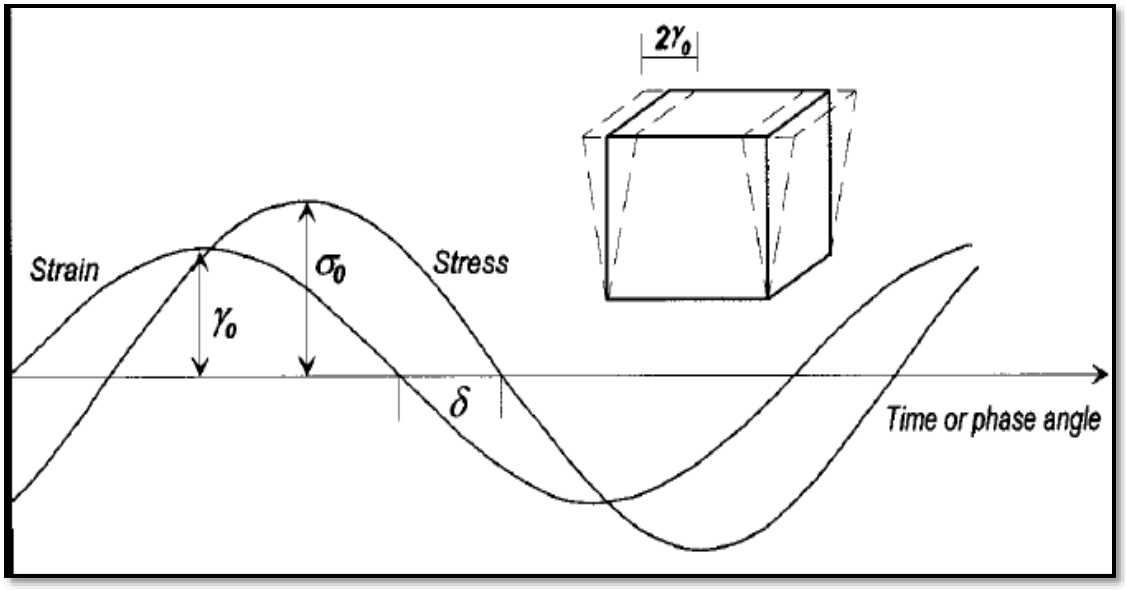

Figure 1.4: Dynamic mechanical response of a viscoelastic material. The applied strain amplitude, γ_o, the resulting stress, σ_o, and the phase angle delay, δ, are shown. Figure from Wang [7]

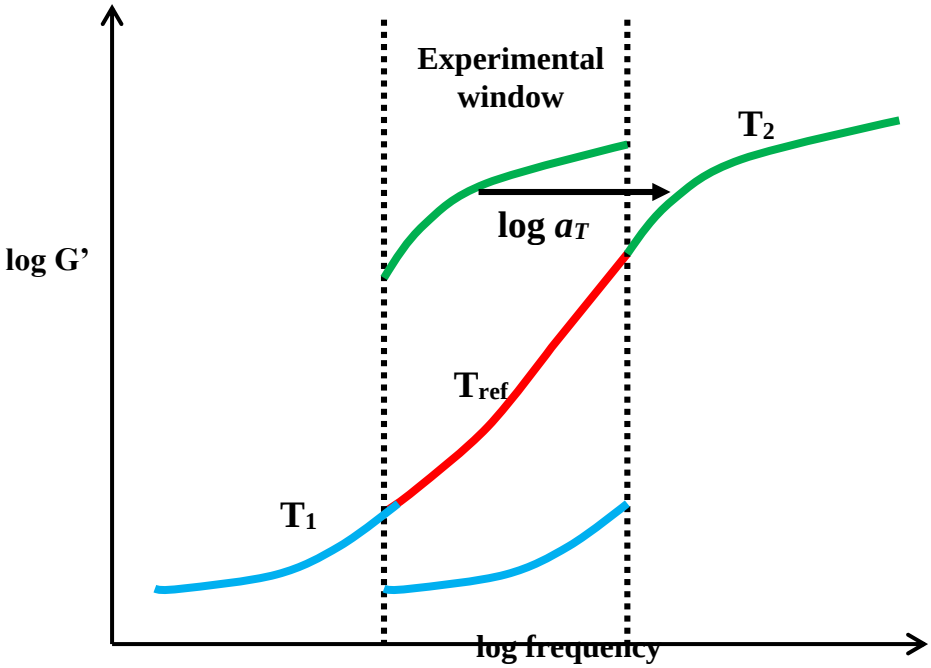

Figure 1.5: Schematic showing time-temperature superposition.

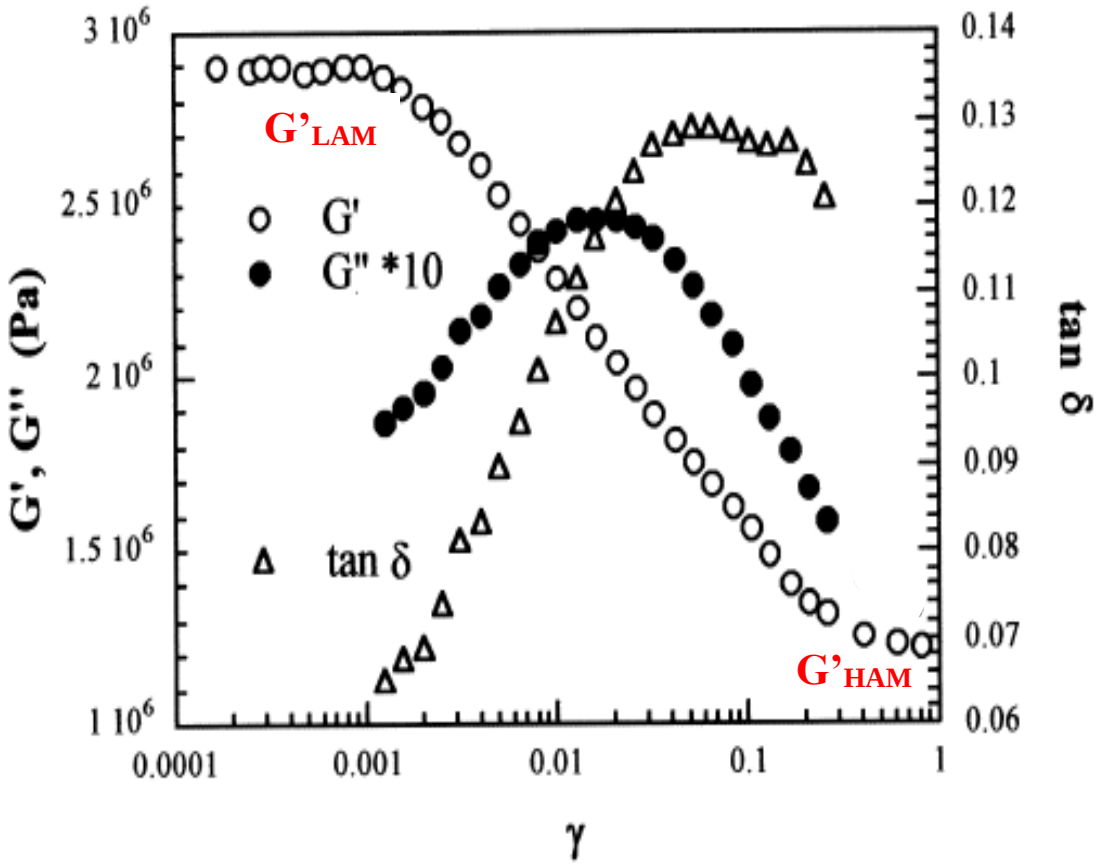

Figure 1.6: The Payne effect showing the storage modulus, G', loss modulus, G'' and loss tangent, tan δ. The low amplitude modulus, G'_{LAM} and the high amplitude modulus, G'_{HAM} are also shown. Figure adapted from Clement *et al.* [24]

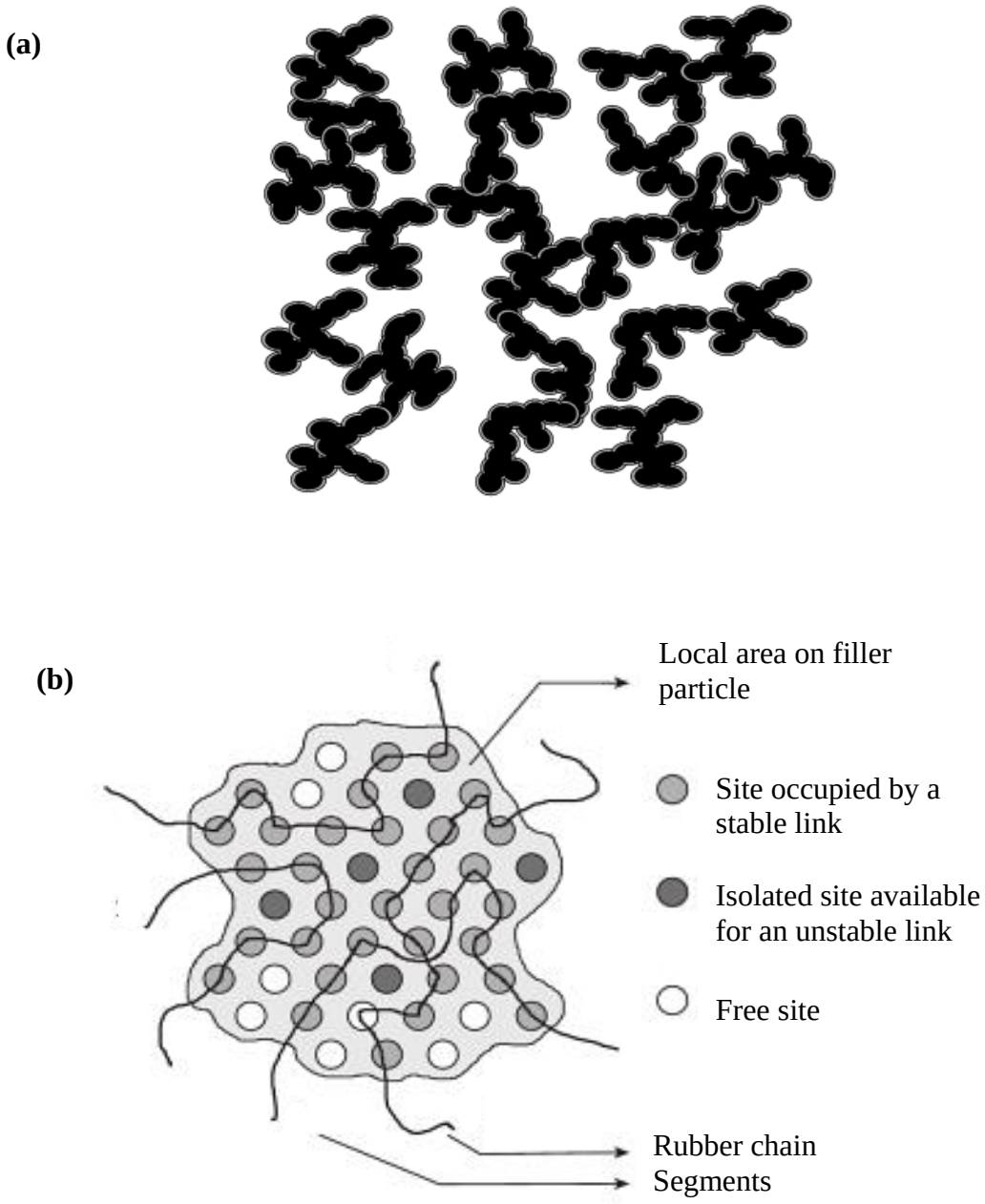

Figure 1.7**:** Illustration of filler-filler and filler-polymer interactions. (a) Filler networking by Heinrich *et al.*[93]. (b) Maier-Goritz[50] filler-polymer adsorption adapted from Leblanc[5].

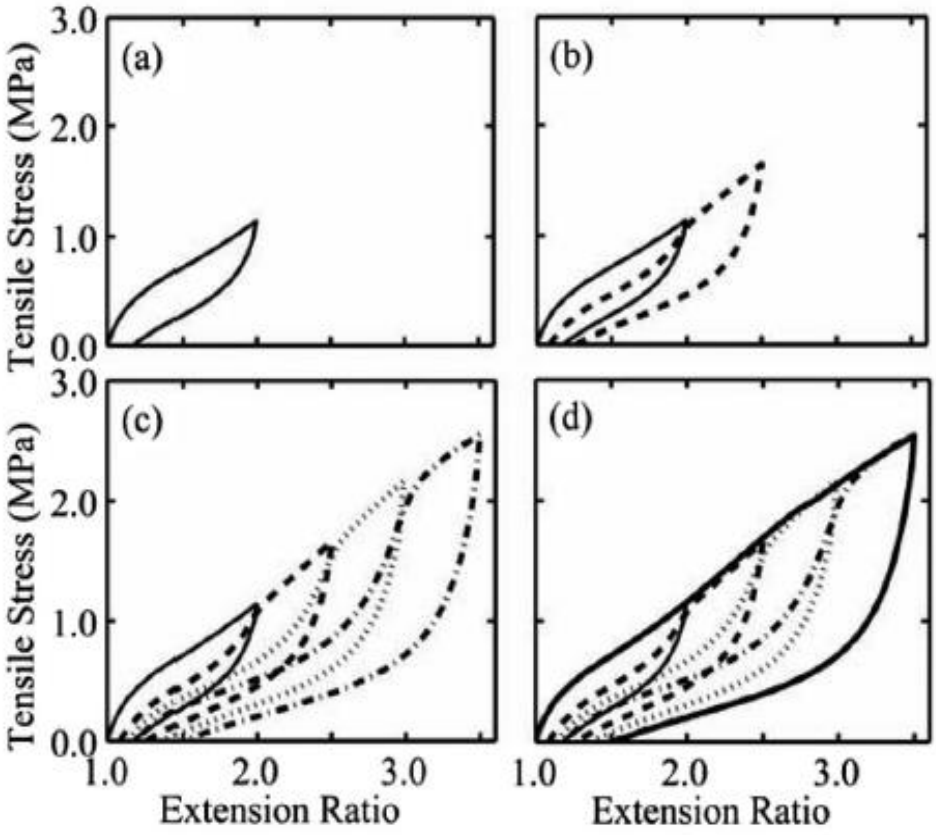

Figure 1.8: Mullins experiment for a filled elastomer. (a), (b), (c) corresponds to the first, second, and third & fourth cycles, respectively. The thick solid black line in (d) corresponds to a single loading. Figure adapted from Bhattacharya *et al.*[60]

Table 1.2: Payne effect mechanisms

Payne Effect			
Ref #	Physical Mechanism	Pros	Cons
15,38,45,49,94	Breakage and reformation of filler-filler network; agglomeration/deagglomeration	-Explains why filled uncrosslinked elastomers and low molecular weight melts exhibit Payne since it is a filler only effect -Reformation explains complete recovery of Payne	-Fillers must be connected throughout the composite (this is called percolation). However, Payne has been observed for systems below the percolation point [95]
7,19,50,53	Breakage of weak polymer-filler bond during deformation	-Transient interactions between polymer and filler -Explains the drop in G'	-Does not predict reversibility of Payne since bond breakage is permanent.. - Graphitized CB (less filler-rubber interaction) shows even more Payne effect[33]

Table 1.3: Constitutive models for the Payne effect

Constitutive Models for the Payne Effect			
Ref #	Physical Mechanism	Pros	Cons
45,47,49	-Filler network models -Filler-polymer network models	-Predicts G' accurately	-Usually fails in description of G'' at small strain[5] -temperature effect is not always accounted for -Whole set of model parameters have to be reconsidered if frequency is changed
96-98	3D models by Lion *et al.*	-Predicts G' accurately -Has a time dependent damage term that could possibly explain recovery	-Purely phenomenological

Table 1.4: Mechanisms for the Mullins effect

Mullins Effect			
KEY: Stress softening (S); Anisotropy (A); Permanent set (P); Recovery (R); Stress relaxation (SR)			
Ref #	Physical Mechanism	Pros	Cons
38,39,87,89	Chain Scission; bond rupture; network alteration theory	-Explains S, A and P	-ESR studies for chain scission showed carbon radicals for both filled and even unfilled SBR-results are inconclusive [62]. -cannot explain R since bond rupture is permanent
79,80,99-102	Chain adsorption-desorption; Chain slippage	-Explains S, R and P	-A will be hard to explain
42	Breakage of aggregates; Breakage of agglomerates	-Explains S,A, and P	-Does not explain R since aggregates breaking is irreversible
63	Removal of entanglements by chain slippage	-Explains S, R and A	Will not be able to explain R
103	Influence of a glassy layer	-Explains S and R	-Should be much more temperature sensitive than has been shown -does not account for A
3,104	Jamming of filler aggregates	-Explains S, P, A and R	-New idea, further study needed

Table 1.5: Constitutive models for the Mullins effect

Constitutive Models for the Mullins Effect			
Ref #	Physical Mechanism	Pros*	Cons *
61	1. Damage-based models		
105	a. Hyperelastic	-Will return to original curve after λmax for the second loading	-No consideration of SR -Cannot account for A and P
71,72,74,75,78,86	b. Hyperelastic with Viscoelasticity	-Will predict S, P,	-Poor prediction of SR[60] -Usually ignores A
106	c. Plasticity-based models	-Explains P	-Will not predict SR - Cannot account for A
3,104	2. "Jamming Models	-Predicts SR	-Needs to be tested with other systems

*Refer to Table 1.4 for key

CHAPTER 2. THE APPLICATION OF TIME-TEMPERATURE SUPERPOSITION FOR CARBON BLACK FILLED ELASTOMERS

This Chapter is Derived from a Recently Submitted Manuscript with Authors R. Prabhu, O. Ogebule, R. Klitkou, G.A. Medvedev and J.M. Caruthers. The Dynamic Data was Collected by R. Prabhu. I Worked on the Transient Creep and Creep Recovery Experiments.

2.1 Introduction

The linear viscoelastic response of filled elastomers is only observed for very small deformations as compared to the unfilled material, where filled elastomers can exhibit nonlinear viscoelastic response to dynamic loading at strains lower than 10^{-3} [26,27,107]. This nonlinear dynamic phenomenon in filled elastomers is known as the Payne effect,[15] where the dynamic storage modulus decreases with increasing strain amplitude while the loss modulus goes through a maximum. There have been numerous studies of the Payne effect in filled elastomers and several physical mechanisms have been proposed to explain the significant decrease in modulus with increasing strain amplitude, including (i) filler-filler interactions[22,45] where there is breakage of filler clusters with deformation and (ii) filler-polymer interactions[50,95] where it is assumed that the polymer chains detach from filler surface. The primary focus of previous research has been on the nonlinear Payne effect. The focus of this communication is a viscoelastic characterization of filled elastomers at small strains, where the response is linear.

For materials deformed in the linear regime, it may be possible to determine the viscoelastic master curve via time-temperature superposition (TTS). A summary of studies of viscoelastic properties of carbon black filled elastomer systems where the TTS

procedure was employed is given in Table 2.1; however, in some cases non-standard vertical shifting was needed in addition to the horizontal shifting as described by $\log a_T$ in order to effect TTS. The standard $\rho_0 T_0/\rho T$ vertical shifts from rubber elasticity theory[9,108] has been employed in some of these studies[109,110], whereas other authors employed non-standard vertical shifts, including no vertical shift[111-113].A key issue is that linearity of the stress-strain response was only clearly established in a few of these studies,[109,110] where in other studies one cannot ascertain if the applied strains are small enough to ensure linearity. In other studies traditional TTS failed[114-116] or unusual shifting procedures were employed[117,118]. For example, Ferry and coworkers[117,118] studied the dynamic linear viscoelastic behavior of carbon black filled polybutadiene, where the tanδ data could not be superposed by horizontal shifting. In that study the modulus of the carbon black filled rubbers decreased with temperature, which was attributed to dissociation of the junctions between filler aggregates; thus, the superposition of storage and loss moduli isotherms in the rubbery region was achieved using just a vertical shift without any shifting along the log(frequency) axis. These vertical shifts were significantly different from the ones obtained for unfilled SBR, where the temperature dependence was Arrhenian.

There have also been dynamic studies of filled elastomers carried out at larger strain amplitudes such that the material response is in the non-linear regime, where TTS was still employed.[114,116,119-121]. For example, Klüppel and Fritzsche[119,120] reported superposition of frequency dependent isotherms for several carbon black and silica filled SBR and EPDM elastomers; however, different vertical shift factors were required to superpose the storage and loss moduli. This is problematic because the storage and loss moduli come from the Fourier transform of the time dependent shear modulus and thus must have the same vertical shift. Adicoff and Lepie[114] and Stacer, *et al.*[116] have also used different vertical shift factors to superpose storage and loss moduli, which they indicated was evidence of thermorheologically complex behavior.

Although TTS of nonlinear viscoelastic data may provide insights into the reinforcement mechanism for filled elastomers, there is inherent uncertainty in any extension of a nonlinear viscoelastic response along the log time/frequency axis. The purpose of this work is to investigate the linear viscoelastic response of filled elastomers

at sufficiently small strains with a focus on (i) the applicability of TTS for filled systems and (ii) understanding how particulate fillers modify the linear viscoelastic relaxation processes. Pursuant to this objective, the dynamic linear viscoelastic behavior has been studied for a series of SBR elastomers filled with two different types of carbon black and one polybutadiene elastomer filled with carbon black.

2.2 Experimental

The principal material used in this study was a styrene-butadiene elastomer, which was chosen because it (i) does not crystallize, (ii) is chemically stable for the temperature range of interest, (iii) is a single phase and (iv) has a T_g between -45°C to -60°C[122] so that both the transition and rubbery region are experimentally accessible. An SBR random copolymer containing 23.5% styrene by weight was provided by the Goodyear Rubber Company (SBR, Plioflex 1502). The SBR elastomer did not contain extending oil so that the effect of the filler on the linear viscoelastic behavior could be studied without additional complications from the oil. Carbon blacks N990 and N550 and an Acetylene black were provided by Cabot Corporation, where the surface area and structure are given in Table 2.2. The SBR gum stock was first masticated in a Brabender internal mixer (C.W. Brabender Inc.) at 30rpm for 5 minutes. Then 40phr (i.e. parts per hundred parts of rubber) of carbon black and 0.1phr of a Dicumyl Peroxide (Sigma-Aldrich) cross-linking agent were added to the mixer and masticated with the SBR for 10 minutes. The filled rubber mixture was finally subjected to 20 passes through a two-roll mill (C.W. Brabender Inc.) to ensure complete dispersion of the carbon black into the rubber matrix. The mixture was cured in a 100mm x 100mm square mold using a hot press (Carver Inc.) at 170°C under 20,000lbs for 30 minutes. The rubber sheets were bagged and stored at 4°C prior to testing. Filled rubber specimens for dynamic experiments were cut into the required dimensions from the cured sheet using a parallel cutting assembly with a microtome blade.

In addition to the SBR elastomer, the behavior of a filled polybutadiene elastomer was studied. Polybutadiene (Diene™ Polybutadiene) was provided by Bridgestone

Americas. The polybutadiene gum stock was mixed with 36phr of N990 and N550 carbon black directly in the two-roll mill (20 passes), where no crosslinking agent was added to polybutadiene. The filled polybutadiene was then subjected to 20 additional passes through the two-roll mill to ensure complete dispersion of the carbon black. The material was then molded into a sheet with the hot press using the same conditions as for the filled SBR material described above.

The G' and G'' dynamic shear storage and loss moduli were measured using a Dynastat mechanical spectrometer[123] with double shear sandwich grips. The specimen dimensions were 25mm by 17mm with a thickness of 3.3mm, where the shear deformation was applied along the 25mm length of the sample. The dynamic moduli were measured as function of frequency between 0.1 to 100Hz at various temperatures from -30° to 70°C. To facilitate the mechanical measurements at sub-ambient temperatures, the Dynastat apparatus was encased inside a plexiglass chamber where -50°C dew point air was circulated to reduce moisture condensation. Because of the sensitivity of the Dynastat, strains as small as 3×10^{-4} could be reliably used enabling linear viscoelastic measurements for filled systems that display nonlinearity at small strains.

Creep and creep recovery experiments were conducted on an AR-G2 rheometer (TA Instrument) for unfilled SBR and SBR filled with N550 and N990 carbon black. Tests were performed using both torsion bars and cylindrical samples between parallel plates. Cylindrical cured elastomer specimens with a length 19mm and diameter 25mm were glued onto disposable aluminum plates using a quick curing epoxy (Loctite®). The aluminum plates with a cylindrical rubber specimen were mounted in the AR-G2 and a small normal force was applied to eliminate slippage between the specimen assembly and the test fixture. After loading into the AR-G2, the specimens were allowed to anneal for 12 hours at 30ºC before testing in order to eliminate any effects due to the sample loading procedure. Isothermal creep experiments were performed for filled materials in 10ºC increments from -10ºC to 60ºC and for the unfilled SBR from 20ºC to 60ºC. All samples were allowed to equilibrate for 30 minutes at each temperature prior to the creep experiments, which lasted an additional 30 minutes. Care was taken to ensure that the

applied torque produced strains within the linear viscoelastic regime. Using the same experimental setup, creep recovery tests were performed at 30ºC, where the materials were first allowed to creep for 1hr followed by recovery for 12 hours for the unfilled SBR and 24 hours for the filled SBR.

2.3 Results

Dynamic Behavior of SBR Filled Elastomers

The G' and G'' as a function of applied dynamic strain amplitude ε_o, where the dynamic strain is $\varepsilon(t) = \varepsilon_o \sin\omega t$, are shown in Fig. 2.1 for lightly crosslinked SBR filled with 40phr of N990, N550 and AcB at a frequency of 10Hz and 30°C. The storage modulus for each filled material was normalized using the lowest strain amplitude modulus, $G'(\varepsilon \rightarrow 0)$, which was 1.01MPa for N990, 2.37MPa for N550 and 1.97MPa for the AcB. From the flat portion of the storage modulus, the linear viscoelastic limit is a strain amplitude of 0.5% for N990 filled SBR, 0.2% for N550 filled SBR and less than 0.03% for the AcB filled SBR. In agreement with a previous study,[124] the onset of the Payne effect occurs at lower dynamic strains for higher surface area and higher structure carbon blacks for a constant given filler content. AcB, which is the filler with the highest structure and surface area, exhibits nonlinear strain softening even at strain amplitude of 0.03%, which was the lowest strain where forces could be reliably measured in the Dynastat.

An important question is whether the identified linear response range applies to all temperatures and all frequencies that will be used in construction of the master curve via TTS. Some authors have reported that the onset of Payne effect is insensitive to both temperature and frequency for carbon black-natural rubber and carbon black-emulsion SBR systems.[27,28] Alternatively, other researchers have reported that for carbon black filled natural rubber and fumed silica filled poly(dimethylsiloxane) the onset of Payne occurs at slightly higher strain amplitudes as temperature is increased[15,24] In order to determine the effect of temperature on the linear limit of the dynamic response, the modulus was measured as a function of applied strain amplitude at -30°C, which was the

lowest test temperature for dynamic experiments in this study. The amplitude dependence of G' for SBR filled with 40phr N990 and polybutadine filled with 36phr of N550 at both 30°C and -30°C were determined, where the onset of nonlinearity occurs at marginally lower strain amplitudes at -30ºC (data shown in Appendix A). Frequency sweeps over 0.1 to 100Hz at the lowest test temperature were also performed at two strain amplitudes within the linear range to ensure that the filled material response was linear at all frequencies. Based upon these amplitude studies, the response will be linear at the frequencies and temperature of interest for strain amplitudes of 10^{-3} and 5×10^{-4} for N990 and N550 filled SBR respectively, and the strain amplitudes were 10^{-3} for N990 and 6×10^{-4} for N550 filled polybutadiene. The frequency isotherms to be reported in the following time-temperature superposition studies will be for strain amplitudes less than or equal to these values. The linear region for the SBR filled with 40phr of AcB could not be achieved with the current instrumentation and, thus, this material will not be included in this study.

The shear storage moduli, G', and loss moduli, G'', isotherms were measured at frequencies from 0.1 to 100Hz for temperatures from -30 to 70ºC. The G', G'' and $\tan\delta = G''/G'$ isotherms are shown in Fig. 2.2 for SBR filled with 40phr of N990. Similar isotherms for SBR filled with 40phr of N550 are shown in Appendix A. The traditional application of TTS superposition for isotherms in the rubber and transition region first requires vertically shifting the isotherms by log b_T, where $b_T = \rho_0 T_0/\rho T$. [110,125] This shifting procedure assumes that the strength of both the equilibrium rubber response and the viscoelastic transition is governed by rubber elasticity. This assumption has a long, successful history for unfilled polymers, where the entropic spring is the key physical phenomenon both in the response of the equilibrium rubber and in the Rouse model for describing the transition zone. However, for highly filled systems there is no assurance that the traditional method of applying $\rho_0 T_0/\rho T$ vertical shifts to the isotherms is appropriate. Using an analysis method described elsewhere,[126] there is a TTS procedure that can be used without presupposing the form of the vertical shifts. In this method $\tan\delta$ isotherms are shifted horizontally along the log frequency axis, and if superposition is achieved it implies that $d_T = b_T$, where d_T is the change in strength of the equilibrium

modulus and b_T is the change in strength of the viscoelastic component of the modulus. Subsequently, $\log G'(\omega)$ and $\log G''(\omega)$ isotherms are first shifted along the $\log\omega$ axis and then the same vertical shift is applied to the $\log G'(\omega)$ and $\log G''(\omega)$ isotherms in order to achieve superposition. If superposition is achieved, the material is thermorheologically simple and the $\log b_T$ (or equivalently $\log d_T$) is determined from the vertical shifts. The data may show the traditional $\rho_0 T_0/\rho T$ vertical shift or the data may exhibit a different vertical shift, which was the case for uncrosslinked and lightly crosslinked SBR.[117,118,126].

Using the procedure described above, the $\tan\delta$ isotherms were shifted along the log frequency axis. As shown in Fig. 2.3, the $\tan\delta$ master curve for SBR filled with 40phr of N990 has excellent superposition using the horizontal shifts $\log a_T$ given in Fig. 2.4. The temperature dependence of $\log a_T$ is well described by the WLF equation with parameters given in Table 2.3. Using the $\log a_T$ shifts in Fig. 2.4, the shear storage and loss isotherms were shifted along the log frequency axis as shown in Fig. 2.5a, where there is obvious lack of superposition. Then the same empirical vertical shift was applied to both the G' and G'' data, which effected excellent superposition as seen in Fig. 2.5b. The b_T vertical shift needed for superposition of the SBR filled with 40phr of N990 is shown in Fig. 2.6 along with the curve for the traditional $b_T = \rho_0 T_0/\rho T$ vertical shift. The b_T vertical shift has an unexpected increase from approximately -10°C to 30°C, where b_T exhibits the traditional $\rho_0 T_0/\rho T$ behavior for temperatures less than -10°C and greater than 30°C. Although b_T does not have the traditional $\rho_0 T_0/\rho T$ form, the material is still thermorheologically simple and can be analyzed completely using TTS. Similar b_T behavior was observed for the unfilled SBR[126], where several postulates concerning the origin were made. The key finding of this analysis is that when the amplitude of the dynamic strain is such that the material is linear (i.e. at strains less than the one at which the decrease in G' seen in the Payne effect) a particulate filled elastomer is thermorheologically simple in the entanglement and transition region and can be effectively analyzed using time-temperature superposition.

G', G'' and $\tan\delta$ isotherms were also measured for SBR filled with 40phr of N550 carbon black, where the isothermal data are reported in Appendix A. Just as in case of the N990 filled material described above, $\tan\delta$ isotherms could be superposed by just

horizontal shifts along the log frequency axis, where excellent superposition is observed as shown in Fig. 2.7 using the $\log a_T$ shift factor shown in Fig. 2.8. Similarly to the N990 filled SBR, if the G' and G'' isotherms for the N550 filled SBR are horizontally shifted along the log frequency axis using $\log a_T$ determined from the $\tan\delta$ master curve, there is lack of superposition like that observed in Fig. 2.5a. However, if the horizontally shifted $\log G'$ and $\log G''$ isotherms are then shifted vertically, then excellent superposition is achieved for both the G' and G'', resulting in the master curves shown in Fig. 2.9a and Fig. 2.9b. The empirically determined b_T shift factor for the N550 filled material is shown in Fig. 2.10, where it has the same non-standard temperature dependence as observed for the unfilled SBR and the N990 filled SBR. G', G'' and $\tan\delta$ isotherms in the linear region have been previously reported for unfilled SBR[126] and the resulting master curves are also reported in Figs. 2.7 and 2.9.

Examining the data in Fig. 2.9a and Fig. 2.9b, upon the addition of significant amounts of carbon black the shapes of the G' and G'' master curves are remarkably similar to these of the unfilled material. At fa_T = 1Hz the G' and G'' master curves for N550 filled SBR are approximately 3.5 times greater than unfilled SBR master curves and the N990 filled SBR master curves are approximately 1.5 times greater than unfilled SBR master curves. The fact that the G' and G'' moduli of the N550 filled material is greater than these of the N990 filled material (at the same volume fraction of carbon black) is consistent with the fact that N550 has a higher structure than N990 as given in Table 2.2. Although the shapes of the G' and G'' master curves are similar for the filled and unfilled materials, there are some difference as clearly shown in the $\tan\delta$ master curves in Fig. 2.7. The addition of carbon black has a minimal effect on $\tan\delta$ in the transition region, where the reported difference at the highest frequencies for the N550 filled material is most probably an artifact due to the stiffness of this material at low temperatures. Specifically, the sandwich shear geometry was optimized to obtain a strong force signal at the lower levels of stress exhibited when testing the unfilled material at high temperatures and low frequencies. Since the N550 filled material is stiffer for the low temperatures and high frequencies than any other system reported in this study, there may be experimental difficulties for this particular low temperature isotherm. At low

frequencies, there is a significant difference in the tanδ master curves, where the filled materials exhibit a significantly longer relaxation response. The long time tail in the relaxation process clearly increases with the addition of carbon black, where the relaxation response of the higher structure N550 carbon black appears somewhat longer than the lower structure N990 carbon black.

Creep Behavior of SBR Elastomers

The difference in the low frequency region of the relaxation spectrum between filled and unfilled elastomers illustrated in the tanδ plot in Fig. 2.7 warrants further investigation. It is experimentally impractical to access still lower frequencies using dynamic mechanical measurements; hence, creep and creep-recovery experiments were performed on the same materials reported in Fig. 2.7 using the ARG2 rheometer. Creep compliance isotherms are shown in Fig. 2.11 for SBR filled with 40phr of N990. The creep compliance master curve was constructed by using the same loga_T horizontal shift factors as the ones used in the TTS of the dynamic data shown in Fig. 2.8. With respect to the vertical shift factor b_T, the quality of superposition of the creep compliance isotherms was not significantly affected by either (i) applying the b_T values from Fig. 2.10 or (ii) just assuming b_T =1. This insensitivity to b_T is because unlike the dynamic storage and loss moduli isotherms the creep compliance isotherms lack distinguishing features. The creep compliance master curves are shown in Fig. 2.12. Similar isothermal creep data were experimentally determined for the unfilled SBR material and SBR filled with 40phr of N550, where the data is reported in Appendix A. The linear viscoelastic compliance master curves for the unfilled SBR and the SBR filled with 40phr of N550 are shown in Fig. 2.12 and were constructed using the loga_T shown in Fig. 2.8 and the b_T values from Fig. 2.10.

Long term creep of a material that is near the rubbery plateau can have experimental artifacts in the AR-G2 rheometer. Specifically, when the rate of creep is very small (as in the terminal relaxation region of a crosslinked rubber) any small instrument drift in the rheometer will be an issue. An alternative way to probe the long

term behavior in the linear viscoelastic region is to perform a creep-recovery experiment, where during the recovery period the power that causes the torque is turned off and the angular displacement is in the instrument's 'sweet spot.' For the creep recovery experiments, the specimen was (i) subjected to torsional creep for 1 hour, where the maximum strain at the outer end of the specimen was never greater than 0.13%. and (ii) the torque was turned off and the specimen allowed to recover for 12 hours or more. The creep-recovery response $\gamma(t)$ is shown in Fig. 2.13 for the two filled and one unfilled SBR elastomers. For a linear viscoelastic material $\gamma(t)$ is related to the creep compliance $J(t)$ by

$$\frac{\gamma(t)}{\sigma} = J(t) - J(t - t_1) \qquad for \qquad t \geq t_1 \tag{2-1}$$

and is a function of the time since the removal of the load, i.e. $t - t_1$.

The challenge is now to combine (i) the linear viscoelastic G' and G'' master curve data with (ii) the creep data and (iii) the creep-recovery data so that the time/frequency range of the overall viscoelastic response is extended. The method for combining of the dynamic and creep data is as follows:

1. The compliance is assumed to have a Prony series form of

$$J(t) = \sum_{i=1}^{n} J_i \left(1 - \exp\left(-\frac{t}{\tau_i}\right)\right) \tag{2-2}$$

   where τ_i relaxation times are evenly distributed on the log scale and modal values J_i define the relaxation response.

2. The $\gamma(t)$ creep-recovery data can also be parameterized in terms of the $\{J_i\}$ spectrum by combining Eqns. 2-1 and 2-2.
3. The dynamic compliances expressed in terms of $\{J_i\}$ spectrum are given by

$$J'(\omega) = \sum_{i=1}^{n} J_i \frac{1}{1+(\omega\tau_i)^2} \qquad J''(\omega) = \sum_{i=1}^{n} J_i \frac{\omega\tau_i}{1+(\omega\tau_i)^2} \tag{2-3}$$

The dynamic moduli master curve data shown in Fig. 2.9 are converted using the standard formulae[9]

$$J'_{dyn}(\omega) = \frac{G'(\omega)}{\left[G'(\omega)\right]^2 + \left[G''(\omega)\right]^2} \qquad J''_{dyn}(\omega) = \frac{G''(\omega)}{\left[G'(\omega)\right]^2 + \left[G''(\omega)\right]^2} \qquad (2\text{-}4)$$

where subscript 'dyn' indicates that these dynamic compliances are determined from the converted Dynastat data.

4. The $\{J_i\}$ spectrum is determined by simultaneously fitting the three different types of linear viscoelastic data; specifically, (i) *J(t)* master curve data shown in Fig. 2.12 is fit to Eqn. 2-2, (ii) the $\gamma(t)/\sigma$ creep recover data shown in Fig. 2.13 is fit to Eqn. 1 using the$\{ J_i \}$ spectrum defined in Eqn. 2-2 and (iii) the G' and G'' master curve data shown in Fig. 9 are converted to $J'_{dyn}(\omega)$ and $J''_{dyn}(\omega)$ via Eqn. 2-4 and then fit to Eqn. 2-3. The objective function for optimization is the standard sum of squares of the differences between the predicted response and the experimental data, where the each of the (i) (ii) and (iii) contributions are normalized by the number of data points in that data set in order that each data set's contribution is approximately equal. As the resulting objective function is quadratic in terms of the unknown J_i's, the 'quadprog' function in MATLAB was used to determine the $\{J_i\}$ spectrum.
5. Once the $\{J_i\}$ spectrum has been determined, then the material response can be extended over the full time/frequency range using information from the full complement of experimental data.

The caveat in the above program is that there is a slight mismatch between the data obtained using the Dynastat apparatus and the ARG2 apparatus. It was found that the compliance data from ARG2 torsion creep measurement needed to be multiplied by a factor of 1.2 in case of the filled materials and the factor of 1.4 in case of the unfilled material to obtain the compliance/modulus values consistent with the ones measured by the Dynastat in the double sandwich shear configuration. At this point we have no explanation for the mismatch.

The results of the above procedure using the optimized $\{J_i\}$ set are shown as model predictions in Figs. 2.12 through 2.14, where there is excellent agreement between the predictions using the $\{J_i\}$ spectra and the data. The only slight inconsistency is the short time compliance behavior of the unfilled SBR, where the compliance predicted using $\{J_i\}$ spectrum is slightly less than the experimental compliance at short times. The most important conclusion from combining the transient creep with the dynamic modulus is that there is a rapid decrease in the intensity of the long time relaxation processes for the unfilled material as shown in $\tan\delta$ vs. log(frequency) response shown in Fig. 2.14. This significant difference between the unfilled and filled systems can been seen in the creep and creep-recovery data in Figs. 2.12 and 2.13. Specifically, in Fig. 2.12 at longer times the creep compliance for the unfilled material clearly levels off, indicating that the equilibrium compliance has been reached; and in a similar manner, in Fig. 2.13 the recovery from creep in case of the unfilled material is clearly completed within the experimentally accessible time window of 12 hours, whereas for the filled materials relaxation is still continuing for times in excess of 24 hours.

TTS of filled Polybutadiene data

Because of the non-standard b_T vertical shift with the unfilled and carbon black filled SBR elastomers, dynamic measurements were performed with a lightly crosslinked polybutadiene gum stock filled with 36phr of N550 and N990 carbon black and cured with 0.1phr of DCP. Unlike unfilled SBR, unfilled polybutadiene was previously found to exhibit the standard $\rho_0 T_0/\rho T$ vertical shifts[126]. G', G'', and $\tan\delta$ isotherms were obtained for the two N990 and N550 filled PB and are given in Appendix A. The data were analyzed in a similar manner to that used for the filled SBR material. The $\tan\delta$ isotherms were shifted along the log frequency axis and excellent superposition was achieved as shown in Fig. 2.15 using the $\log a_T$ horizontal shifts shown in Fig. 2.16. The temperature dependence of $\log a_T$ is essentially the same for the unfilled and two filled polybutadiene elastomers. Using this $\log a_T$ shift, the G' and G'' isotherms were horizontally shifted, where there was lack of superposition just like for the carbon black filled SBR

elastomers; however, when the vertical shift shown in Fig. 2.17 was applied to both the G' and G'', excellent superposition was obtained as shown in Fig. 2.18. Examining the data in Fig. 15, the temperature dependence of the vertical shift for the unfilled polybutadiene is the traditional $\rho_0 T_0/\rho T$ vertical shift consistent with rubber elasticity. For the filled polybutadiene elastomer b_T is a monotonic function of temperature, unlike the b_T temperature dependence observed for the SBR polymers, but the slope of $b_T(T)$ is significantly less than $\rho_0 T_0/\rho T$ from rubber elasticity. In a similar manner to the filled SBR materials, the $b_T(T)$ curve for the lower structure N990 carbon black has a larger difference from the $\rho_0 T_0/\rho T$ response of the unfilled material than the N550 carbon black with the higher structure.

Both the G' and G'' master curves have nearly the same shape as the master curves for the unfilled polybutadiene. Using the master curve response at $fa_T = 10^2$ Hz, the 36phr N990 G' and G'' master curves are approximately 1.8 times greater than the unfilled material and the 36phr N550 master curves are 2.9 times greater than the unfilled polymer. Small differences between the carbon black filled polybutadiene and the unfilled elastomer is more clearly exposed in the $\tan\delta$ master curves shown in Fig. 14. The unfilled and N550 filled $\tan\delta$ master curves are essentially identical and the N990 $\tan\delta$ master curve overlap with the other two master curves, except at small frequencies, where the N990 filled material has a stronger low frequency response. The ordering of the $\tan\delta$ response for N550 and N990 at low frequencies is reversed for the polybutadiene materials as compared to the SBR filled elastomers, where the N990 has a more significant long time response for the polybutadiene materials.

2.4 Discussion

This work clearly shows that time temperature superposition is valid for several carbon black filled elastomers provided the applied strain is less than the linear viscoelastic limit. As shown in Figs. 3, 5b, 7, 9, 13 and 18 the superposition of isotherms is excellent, when the appropriate horizontal and vertical shifts are used. Because the

linear viscoelastic data reported in this work is of sufficient precision and the frequency range is large the validity of TTS could be critically assessed. The $\log a_T(T)$ shift function for the carbon black filled elastomers was the same (within experimental error) as the $\log a_T(T)$ shift function of the unfilled SBR and polybutadiene elastomers. Thus filler addition does not affect the temperature dependence of the relaxation times, consistent with the behavior observed by Ferry and Fitzgerald for carbon black filled butyl rubber.[110] The similarity in the WLF behavior for unfilled and filled elastomers indicates that the relaxation behavior in the temperature region above T_g is unaffected by the addition of filler, which is consistent with the literature.[25,127] The data did not extend to sufficiently low temperature to make any conclusions concerning the effect of particulate fillers on the viscoelastic response in the glassy state.

The $\tan\delta$ isotherms did not require any vertical shift for superposition, which implies that $b_T=d_T$ and is consistent with the traditional method of TTS that has been successful for unfilled, single phase elastomers. The vertical shift factor required to effect superposition of the G' and G'' data shows qualitatively different behavior for polybutadience vs. SBR. The traditional $\rho_0 T_0/\rho T$ vertical shift works for the unfilled polybutadiene,[126] where the addition of carbon black decreased the temperature dependence b_T with a larger decrease for the higher structure N550 black (see Fig. 10). The significant decrease in the temperature dependence of b_T is consistent with previous research, where a temperature independent vertical shift i.e. $b_T = 1$, was sufficient to achieve TTS for both SBR and natural rubber filled with carbon black,[111-113] The observed b_T temperature dependence results from two competing trends: (i) the entropic spring of rubber elasticity causing the modulus (or equivalently the b_T vertical shift factor) to increase with temperature and (ii) thermally activated filler-filler and/or filler-matrix interactions that cause the modulus to decrease with increasing temperature. The decrease in modulus with temperature for filled materials is well known[15,22,24,25,120,124,128]. There are several mechanistic proposals for why the modulus decreases with increasing temperature. First, the modulus decrease with temperature has been attributed to reversible dissociation of filler junctions.[15,22,117,118] where it was also found that at much higher temperatures (~100^{o}C) the traditional rubber elasticity behavior was recovered, i.e.

modulus increased with increasing temperature. Second, it has been proposed that the modulus softening with temperature is the consequence of glass-like polymer bridges that connect filler aggregates, where the glass-like bridges undergo a glass-to-rubber transition as the temperature is increased.[120] Finally, Onogi. *et al*.[121] have attributed the increase in b_T with temperature to variation of volume fraction of carbon black filler arising from the difference in the thermal expansion coefficients for filler and polymer. The structure of the filler appears to be an important parameter, where the higher structure fillers cause the modulus to decrease more with temperature, which is consistent with the filler-filler dissociation mechanism.[22] Specifically, carbon black with higher structure and/or more surface area would have more contacts between adjacent filler particles, resulting in more particle-particle interactions. Since these particle-particle interactions will dissociate with increasing temperature, the higher structure black with more particulate interaction will have a greater reduction in the modulus with temperature as compared with a lower structure black. The modulus reduction with temperature due to particulate-particulate breakup is combined with the increase in modulus with temperature due to rubber elasticity; thus, the temperature dependence of b_T should be less for the higher structure black in agreement with the data shown in Fig. 17. Even though $b_T(T)$ data for the filled polybutadience is consistent with the filler junction postulate, the temperature dependent modulus data for the carbon black filled elastomers reported in this study does not clearly discriminate between the above mechanisms.

The filled SBR systems exhibit a qualitatively different vertical shift, where there is an unusual increase in the vertical shift factor in the temperature range from -10 to 30°C as shown in Fig. 10. We have previously reported that a non-standard increase in the vertical shift factor near 20°C is required to effect superposition of G' and G'' isotherms for both uncrosslinked and lightly crosslinked unfilled SBR, where the traditional $\rho_0 T_0/\rho T$ vertical shift predicted by rubber elasticity was required for the more highly crosslinked SBR.[126] As reported in this communication the SBR filled with carbon black requires vertical shifts that have a similar increase near 20°C, where the magnitude of the b_T increase was larger for the filled elastomers. Two possible mechanisms proposed for the unanticipated increase in the vertical shift SBR with increasing

temperature are phenyl ring stacking or the melting of micro-crystallites, where phenyl stacking and/or micro-crystallization is reduced for the highly crosslinked SBR.[126] From this perspective, the presence of filler appears to promote whatever is the underlying mechanism, since as shown in Fig. 10 the unusual increase in b_T at 20°C increases upon addition of the carbon black filler and the larger structure N550 black has a larger increase in b_T.

An important observation is the presence of a significant low frequency relaxation processes for the filled systems as compared to the dynamic response of the unfilled polymer. This long time response is consistent with a simple picture, where the time scale of the relaxation is related to the size of the molecular/mesoscopic unit that is undergoing relaxation. First consider the unfilled polymer, where the low frequency behavior in an unfilled network is controlled by the longest Rouse modes[129]. Thus, the unfilled polymer will not exhibit relaxation times longer than that determined by the distance between crosslinks, which is clearly seen in the dependence of the loss peak on the crosslink density for the unfilled SBR[126] where the peak shifts to higher frequencies for higher crosslink densities. In contrast, in the presence of filler the longest relaxation processes are not the Rouse modes of the polymer network, but rather the cooperative movements that involve a number of chains attached to a given filler particle. The characteristic length of the particulate-polymer structure will be much larger than the distance between crosslinks, and consequently the time scale of the relaxation will be significantly longer.

The dynamic moduli G' and G'' master curves for both the carbon black filled SBR and the filled polybutadiene exhibit a similar shape as the unfilled master curves (see Figs. 9 and 17). The similarity in shape is nearly exact in the transition and entanglement region, but there are differences in the long time (i.e. low frequency) response as shown in the tan δ master curves (see Figs. 7 and 14) This similarity in shape of the logG' and logG'' vs. logfa_T implies that to a first approximation the filled material's behavior is a multiplicative constant of the unfilled material, where that multiplicative constant is 1.8 for the N990 filled polybutadiene system and 2.9 for the N550 filled polybutadiene system. The reinforcing effect of fillers has been explained

using the Guth-Smallwood relation[130] with corrections for filler structure via occluded rubber.[25] This type of hydrodynamic corrections for the presence of fillers have been successfully used in the high strain amplitude region of the Payne effect.[17] However, to the best of our knowledge, this type of hydrodynamic model for describing the effect of particulate fillers on the modulus of elastomers has not heretofore been reported for the low strain amplitude region that is the focus of this communication. A more complete study of use of this type of hydrodynamic analysis to describe the composition dependence of the small amplitude dynamic behavior of filled elastomers will be the subject of a future publication. It should be noted that a simple hydrodynamics will not be sufficient to fully describe the effect of particular fillers on the G' and G'' master curves, because it cannot account for a new low frequency mechanism that is clearly manifested in the $\tan\delta$ master curves.

In this chapter, we have established that if the strain amplitude is sufficiently small, well defined master curves can be constructed using TTS for highly filled elastomers. Consequently, this work enables an investigation the effects of filler volume fraction, structure and surface area as well as the matrix rubber and its crosslink density on the full linear viscoelastic response. The similarity in shapes of the G' and G'' master curves in the transition and entanglement regions and the change in shape of the $\tan\delta$ master curve in the flow region suggest that it may be possible to develop a more fundamental picture of compositional variations on the linear viscoelastic processes that control the deformation behavior of filled elastomers. This will be the subject of future investigation.

Table 2.1: Studies of time-temperature superposition in carbon black filled elastomers

Material	Ref #	Vertical shift	Linearity in the stress-strain?
SBR + CB +oil	109	Standard b_T	Yes-Linear
NR + CB	111	b_T =1(filled); standard(unfilled)	Not established
SBR + CB (U/C) (w and w/o oil)	112	b_T = 1	Not established
Butyl rubber + CB Polyisobutylene + CB	110	Standard b_T TTS was not observed	Linear
SBR + CB + oil	113	b_T = 1(filled); standard(unfilled)	Linear
Polybutadiene + CB	114	b_T = 1	Not established
Polybutadiene + Ammonium Perchlorate	115	b_T = 1	Not established
Nitrile-Butyl Rubber + Asbestos + Silica	116	b_T = 1	Not established
SBR + CB + oil	117	b_T = non-standard	Not established
Polybutadiene + CB + oil	118	b_T = non-standard	Not established

Table 2.2: Composition of filled elastomers

Rubber	Filler type	Filler structure DBPA number (ml/100g)*	Surface area (m^2/100g)*	Filler Amount (phr)	DCP amount (phr)
SBR	N990	40	7-12	40	0.1
	N550	121	38-46	40	0.1
	Acetylene black (AcB)	310	70	40	0.1
Polybutadiene	N990	40	7-12	36	0
	N550	121	38-46	36	0

*Data supplied by the manufacturer

Table 2.3: WLF constants for filled SBR and filled polybutadiene at a reference temperature of 20°C

Material	C_1	C_2
SBR (unfilled) + 0.1phr DCP[126]	5.5	131.3
SBR + 40phrN990 + 0.1phr DCP	5.6	132.1
SBR + 40phr N550 + 0.1phr DCP	6.7	149.7
Polybutadiene[126]	4.6	186.0
Polybutadiene + 36phr N990	4.4	183.4
Polybutadiene + 36phr N550	4.7	185.5

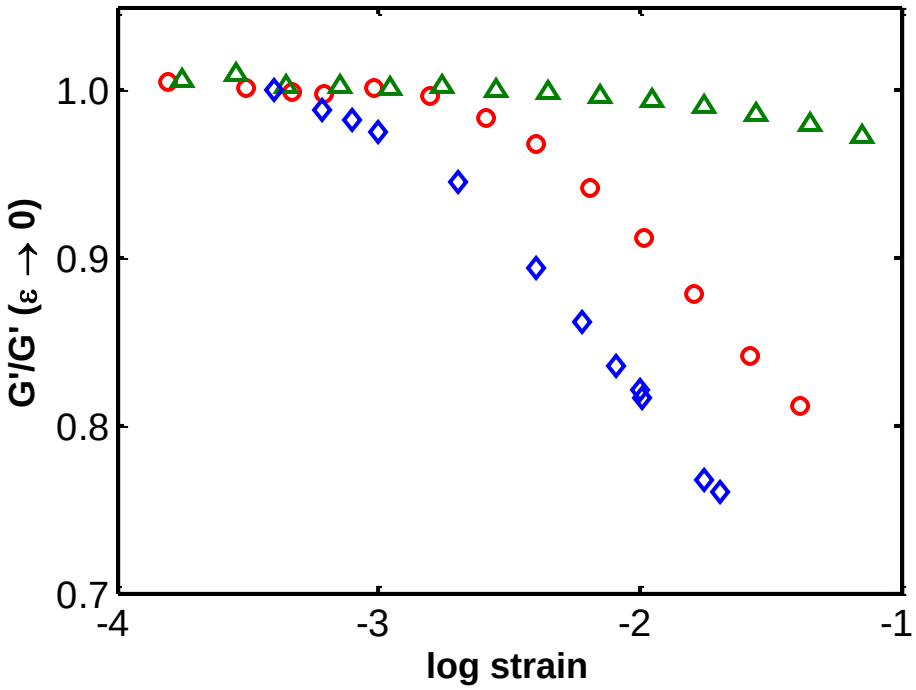

Figure 2.1: Payne experiment at 30°C: Variation of shear storage modulus as a function of strain amplitude at a frequency of 10 Hz for lightly cross-linked SBR containing 40phr carbon black: N990 (Δ); N550 (○); Acetylene Black (◊).

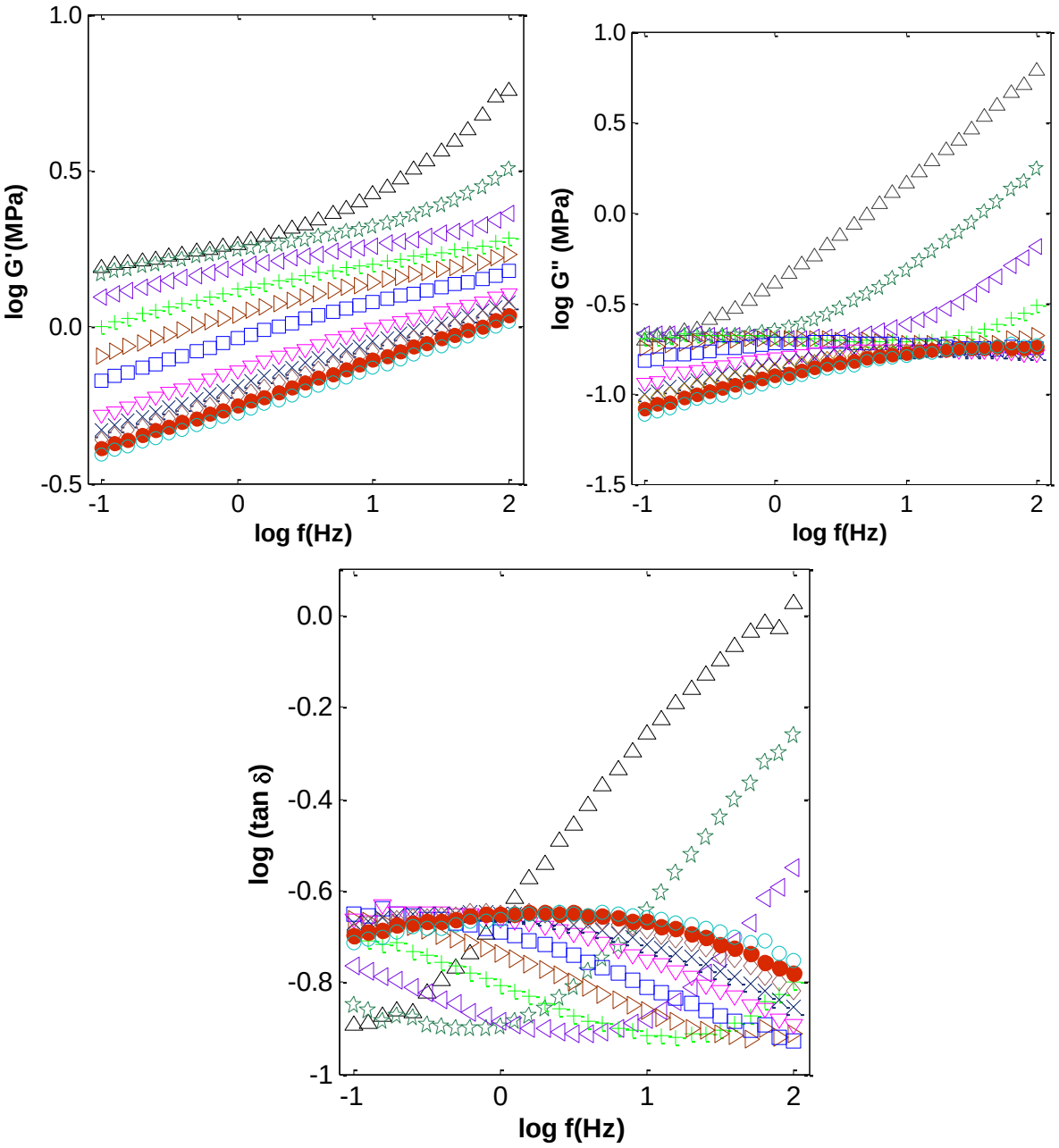

Figure 2.2: G', G'' and tanδ isotherms for SBR with 40phr of N990 cured with 0.1phr of DCP. Temperatures (in ^{o}C) are as follows: Δ -30, ☆ -20, ◁ -10, + 0, ▷ 10, □ 20, ▽ 30, × 40, ◇ 50, • 60, ○ 70.

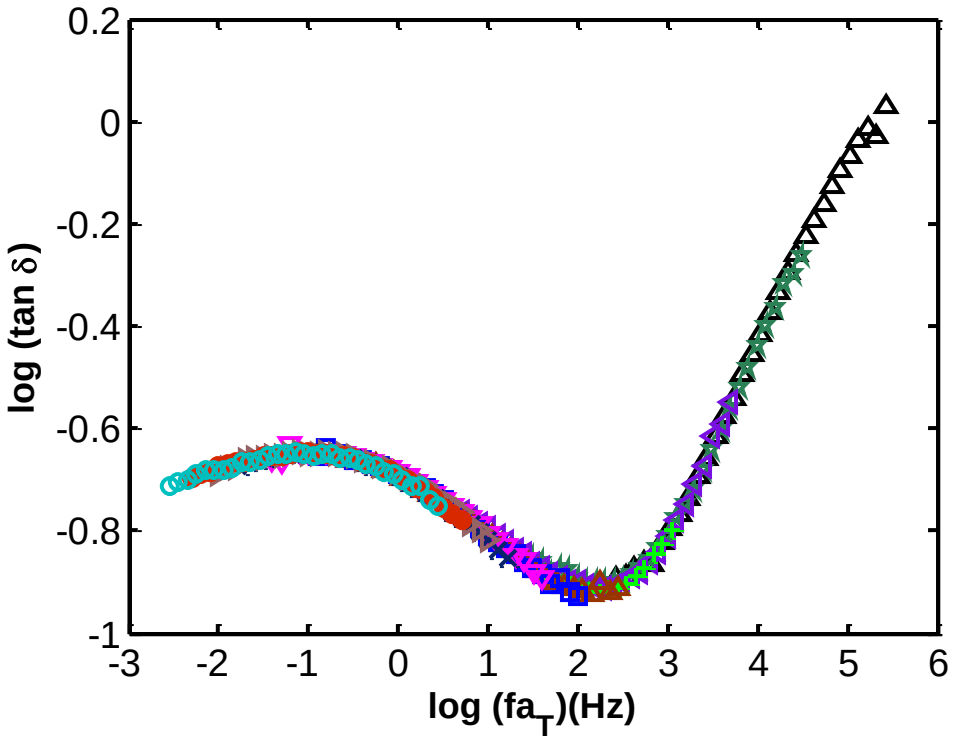

Figure 2.3: Tanδ master curve for SBR with 40phr of N990 cured with 0.1phr of DCP. Symbols are same as in Fig. 2.2.

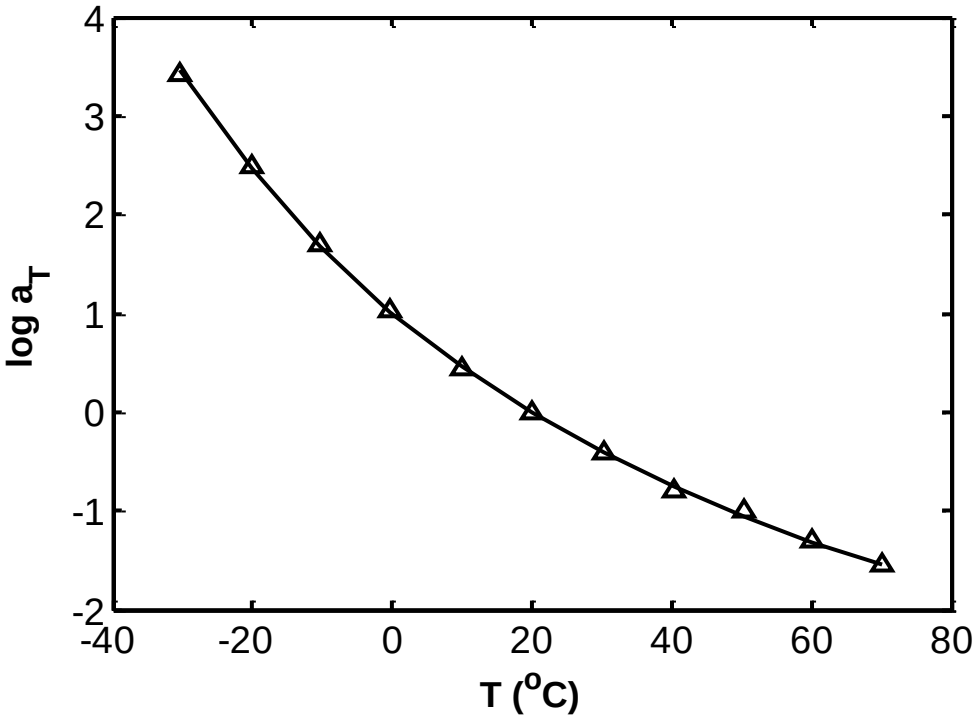

Figure 2.4: Temperature dependence of loga_T for SBR with 40phr of N990 cured with 0.1phr of DCP. Line is the WLF fit with C1 and C2 constants given in Table 2-3.

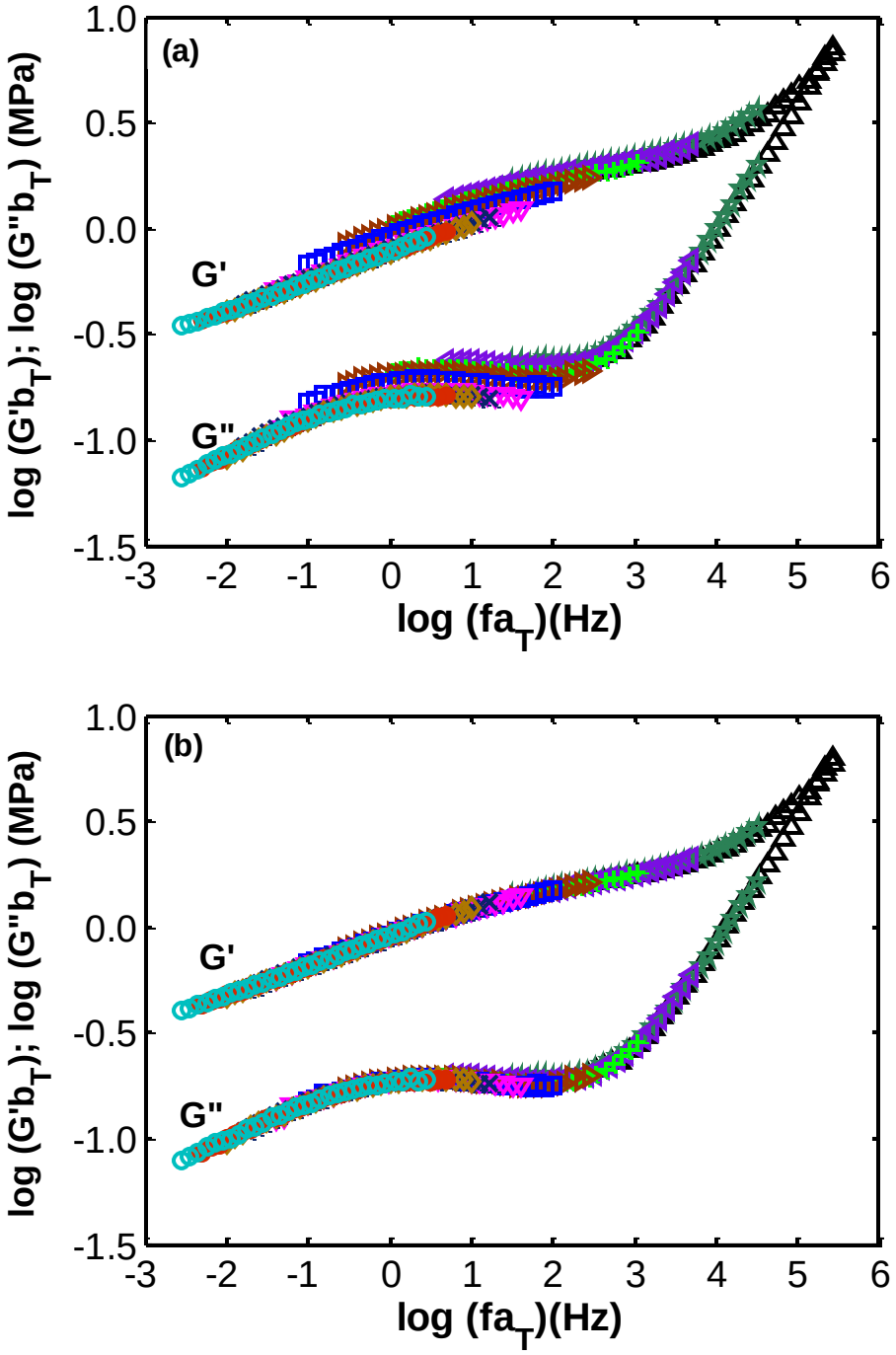

Figure 2.5: G' and G" master curves for SBR with 40phr of N990 cured with 0.1phr of DCP using (a) the standard vertical shifts and (b) the non-standard vertical shifts shown in Fig. 2.6. Symbols are same as in Fig. 2.2.

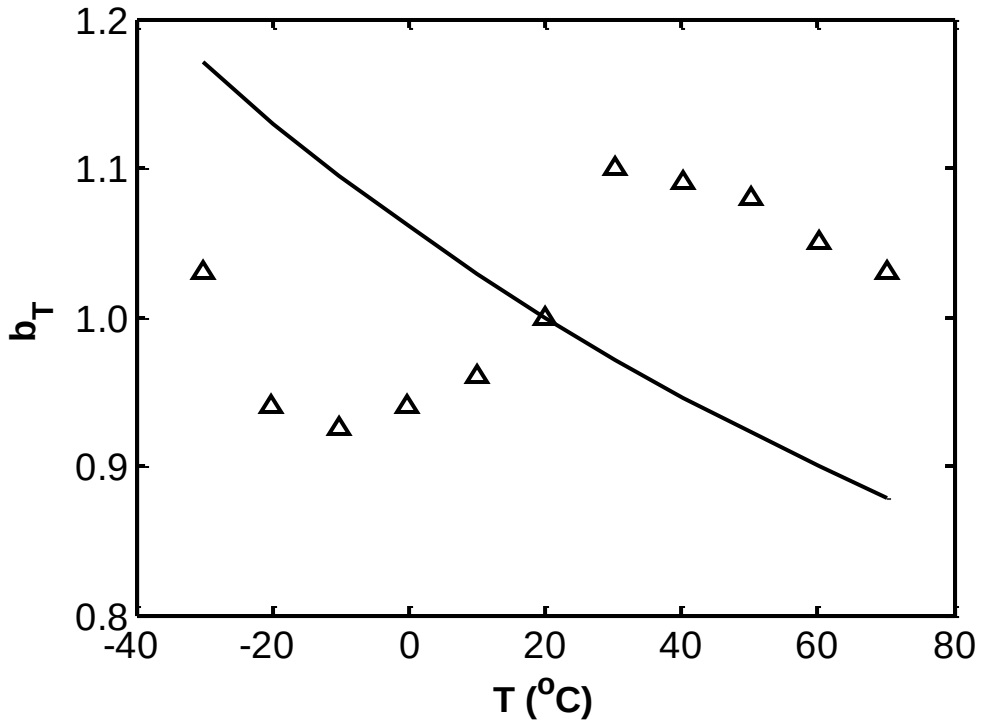

Figure 2.6: Temperature dependence of b_T for SBR with 40phr of carbon black cured with 0.1phr DCP. The line is the standard $\rho_0 T_0/\rho T$ vertical shift from rubber elasticity.

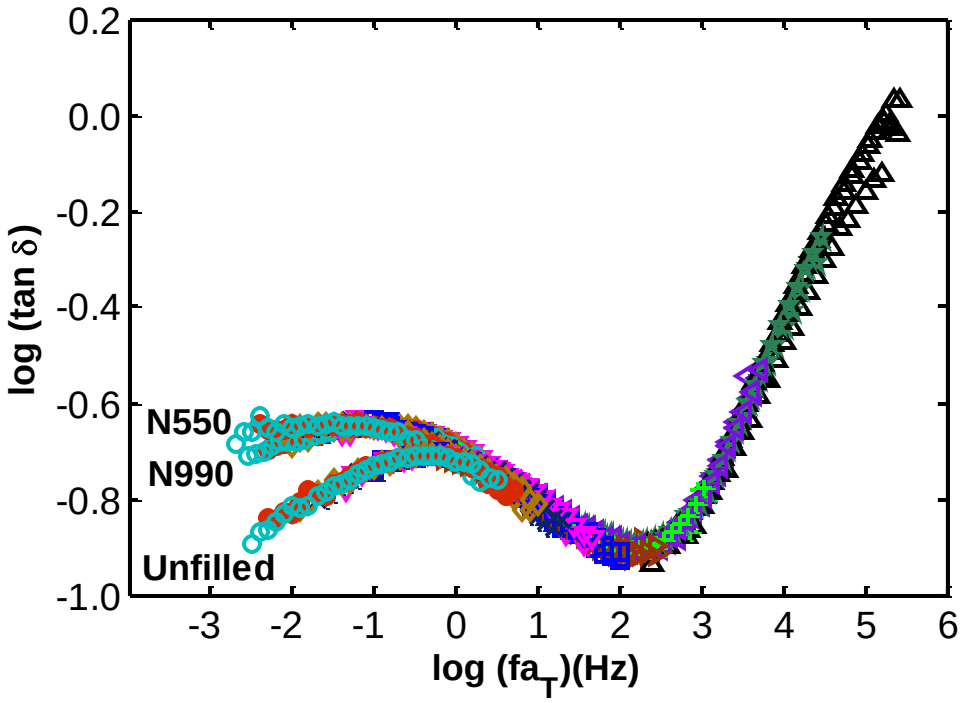

Figure 2.7: Tanδ master curves for unfilled SBR[126] and SBR filled with 40phr of N550 and N990 carbon black. Symbols are same as in Fig. 2.2.

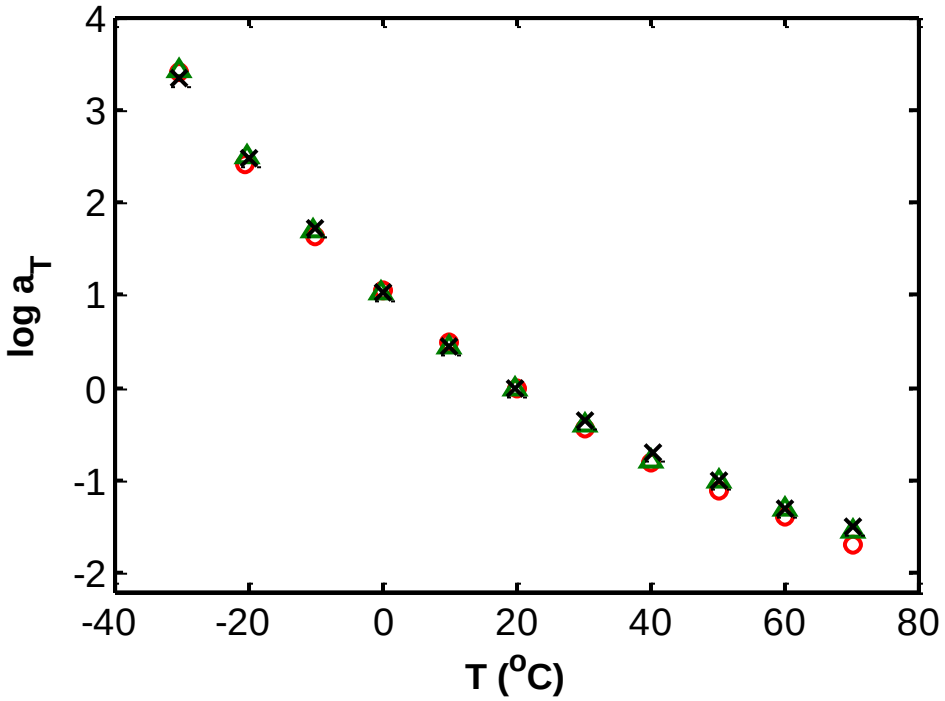

Figure 2.8: Temperature dependence of loga_T for unfilled SBR[126] (×) and SBR filled with 40phr of N550 (○) and N990 (△) carbon black.

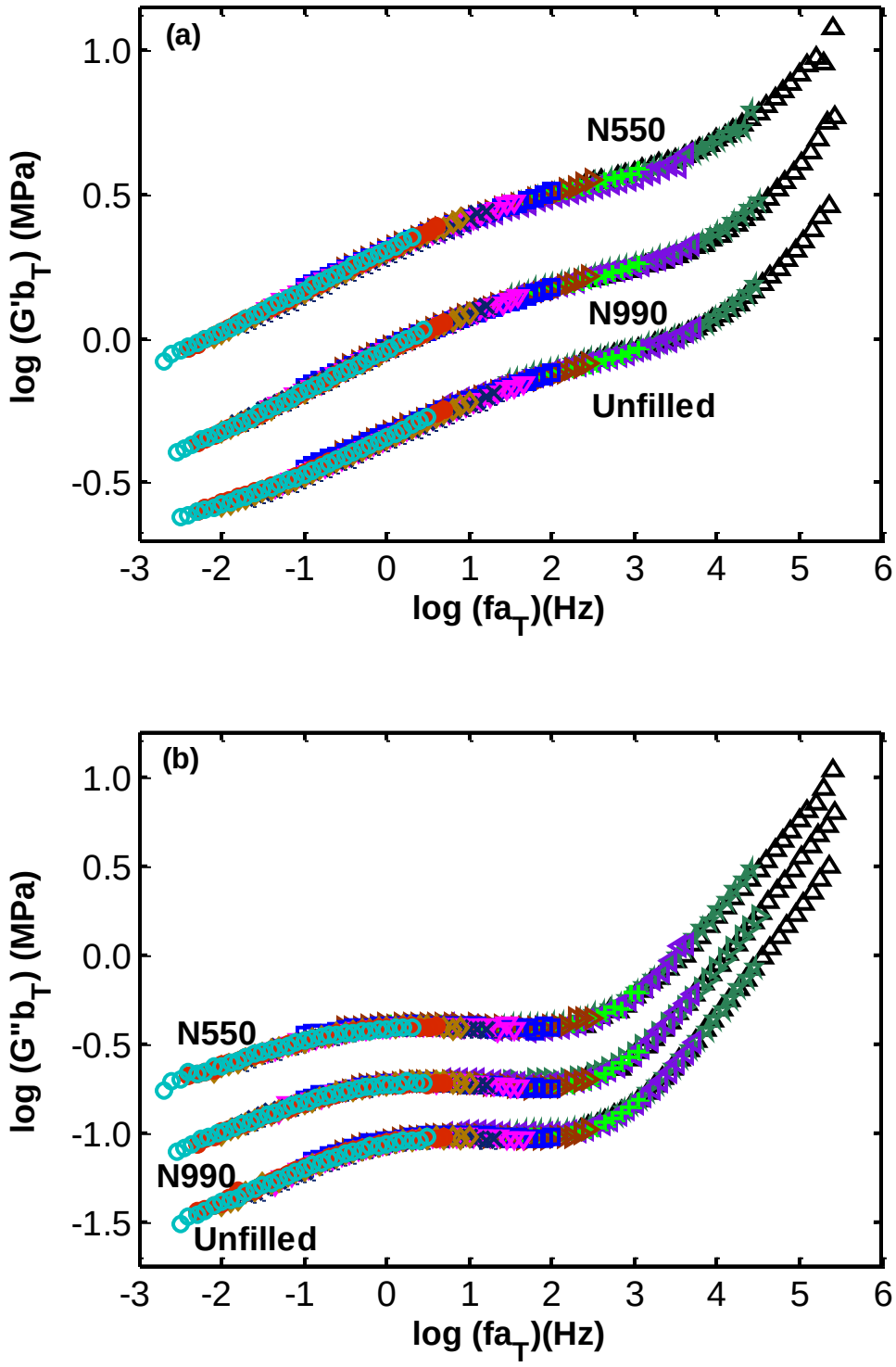

Figure 2.9: Storage (a) and loss modulus (b) master curves for unfilled SBR[126] and SBR filled with 40phr of N550 and N990 carbon black. Symbols are same as in Fig. 2.2.

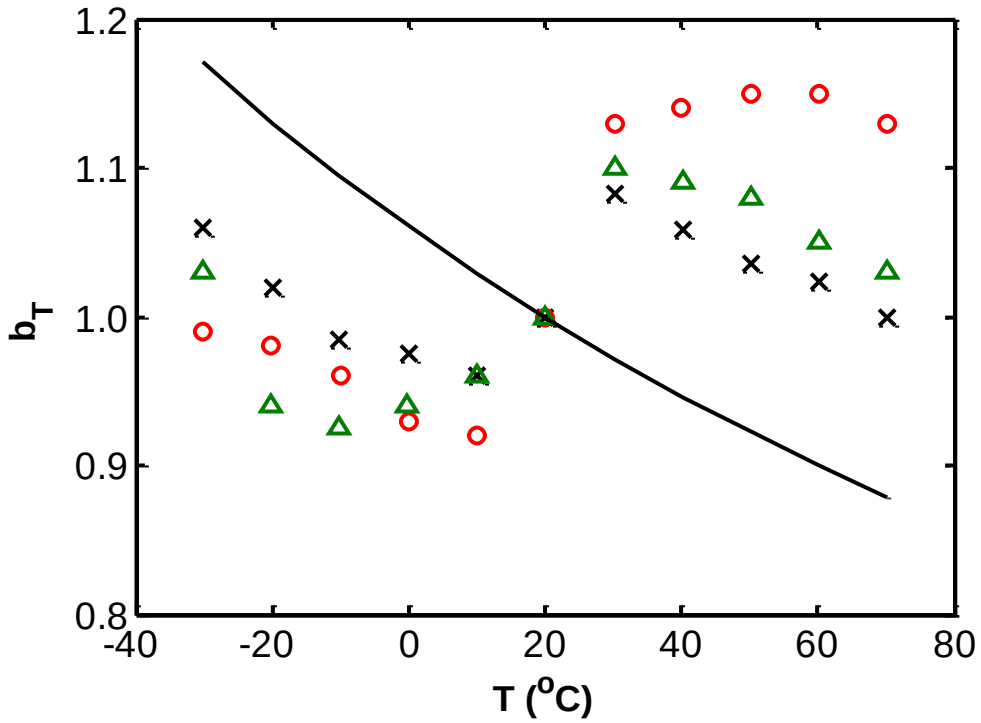

Figure 2.10: Temperature dependence of b_T for unfilled SBR[126] (×) and SBR filled with 40phr of N990 (△) and N550 (○) carbon black, The solid line is the standard $\rho_0 T_0/\rho T$ vertical shift from rubber elasticity.

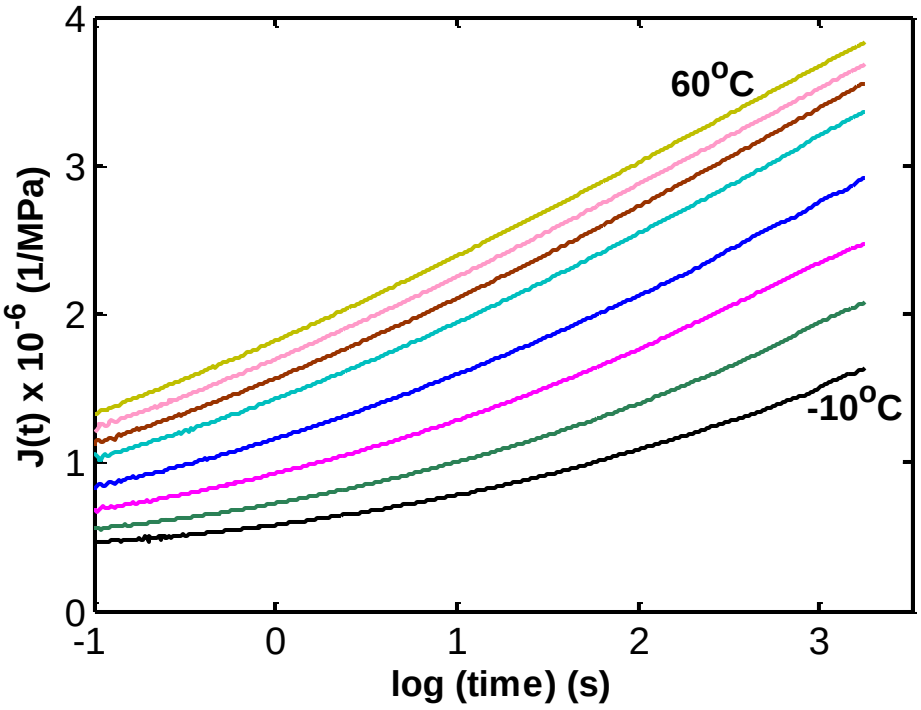

Figure 2.11: Creep isotherms for SBR filled with 40phr of N990 carbon black. Temperatures are in 10°C increments from -10°C to 60°C.

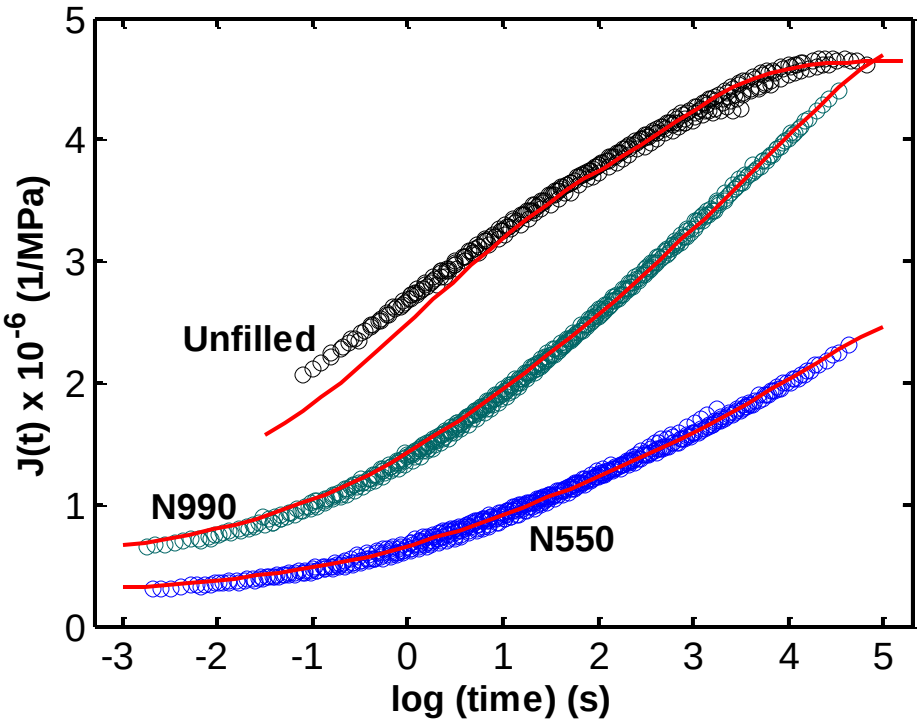

Figure 2.12: Creep compliance master curves for unfilled SBR[126] and SBR filled with 40phr of N550 and N990 carbon black. The predictions from Eqn. 2-2 are indicated by red lines.

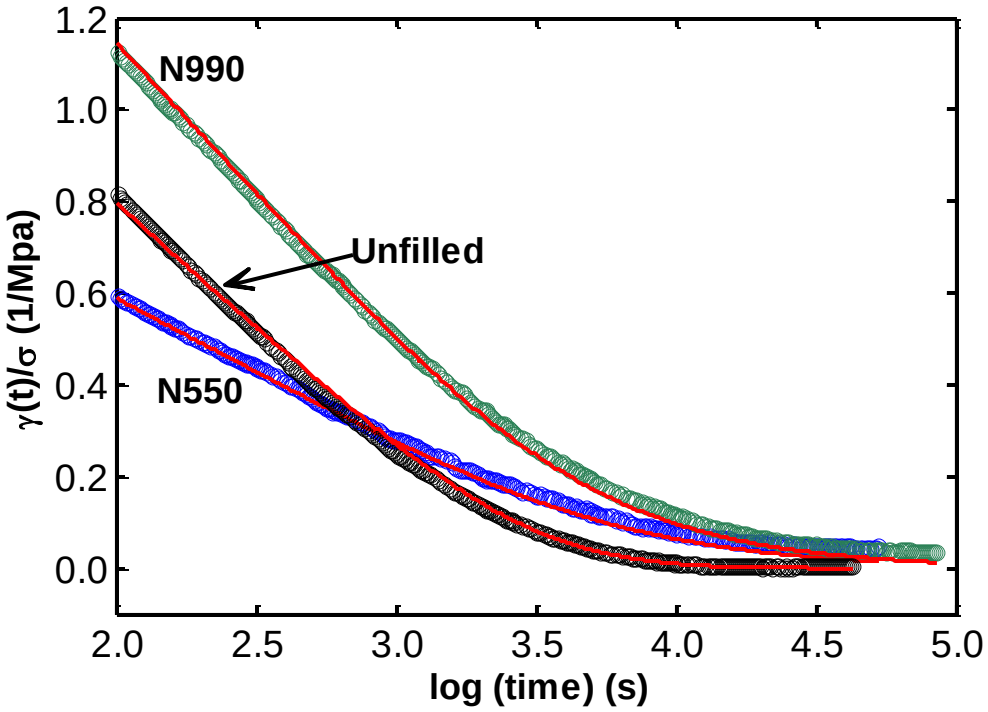

Figure 2.13: Creep-recovery response at 30°C for unfilled SBR[126] and SBR filled with 40phr of N550 and N990 carbon black. The predictions from the {Ji} spectrum using Eqn. 2-2 are indicated by red lines.

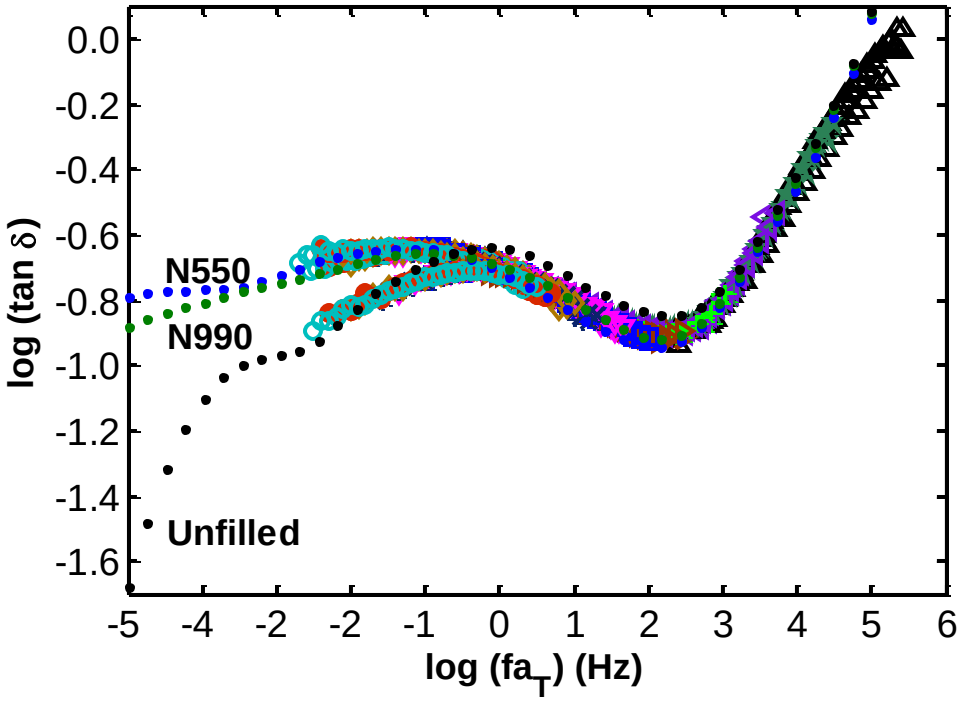

Figure 2.14: Tanδ master curves for SBR filled with 40phr of N550 and N990 carbon black. Extension of the tanδ response to lower frequencies (dotted lines) from {Ji} spectra determined using creep and creep recovery data (see text for explanation).

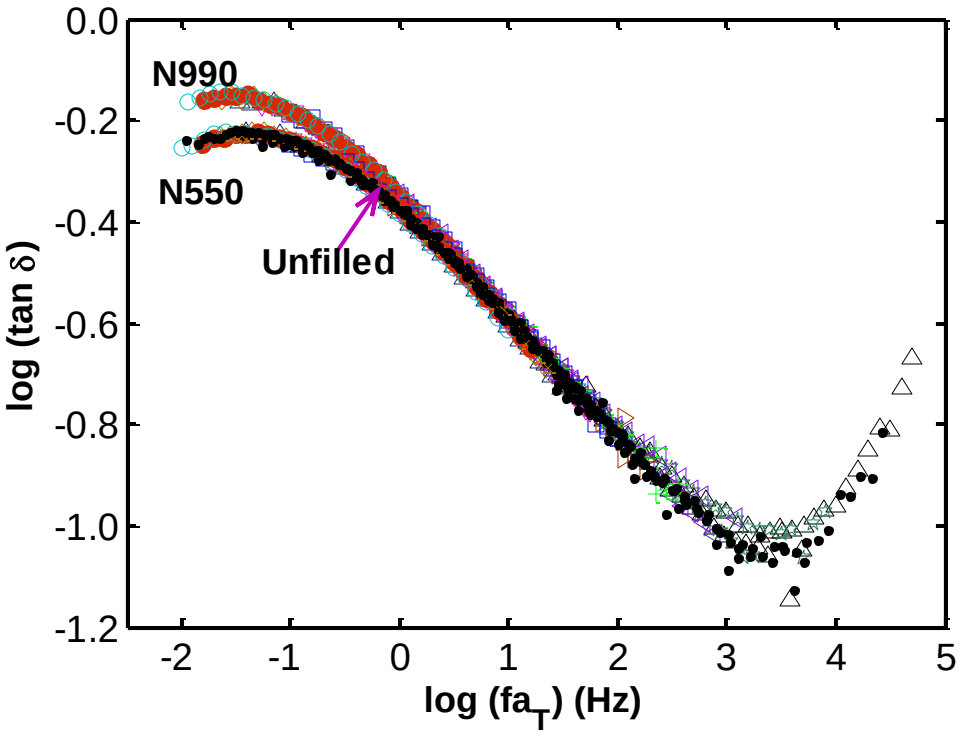

Figure 2.15: Tanδ master curve curves for polybutadiene filled with 36phr on N990 and N550 carbon black. The tanδ master curve for the unfilled polybutadiene[126] is shown by the black symbols, where it lies on top of the N550 master curve.

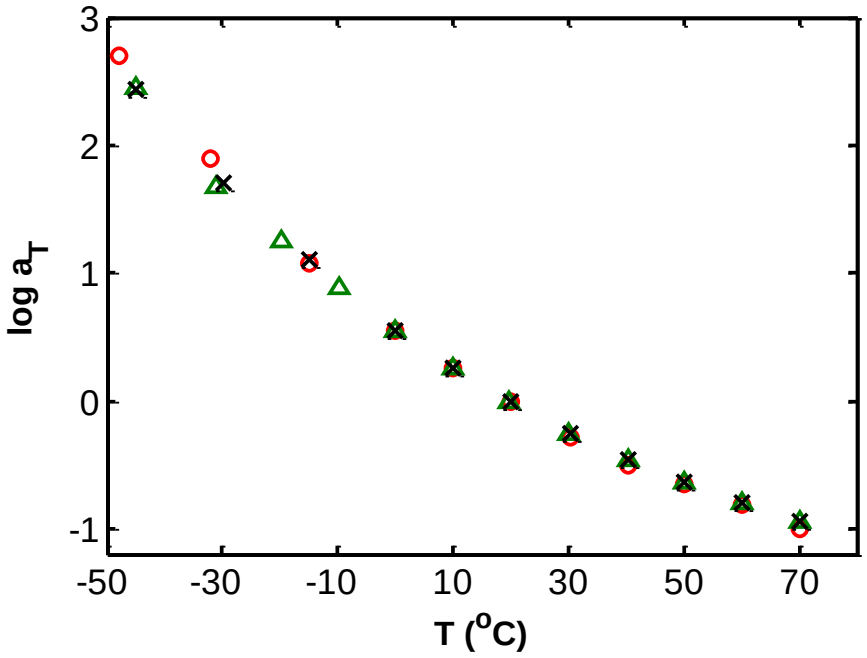

Figure 2.16: Temperature dependence of loga_T for unfilled polybutadiene[126] (×) and polybutadiene filled with 36phr of N990 (△) and N550 (○) carbon black.

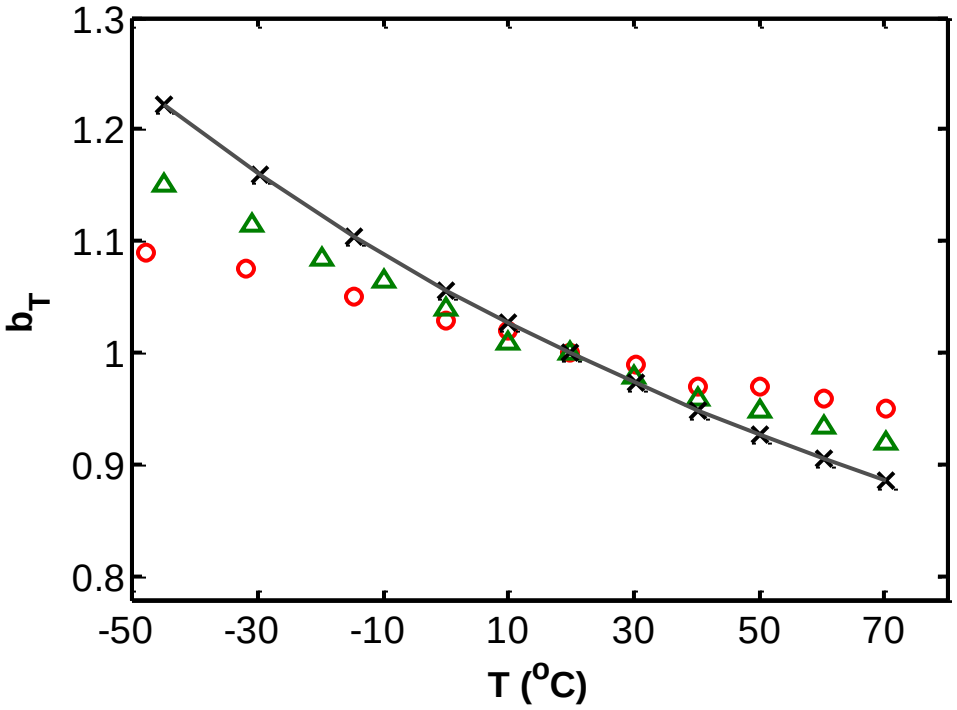

Figure 2.17: Temperature dependence of b_T vertical shift factors for unfilled polybutadiene[126] (×) and polybutadiene filled with 36phr of N990 (△) and N550 (○) carbon black. The line is the standard $\rho_0 T_0/\rho T$ vertical shift from rubber elasticity.

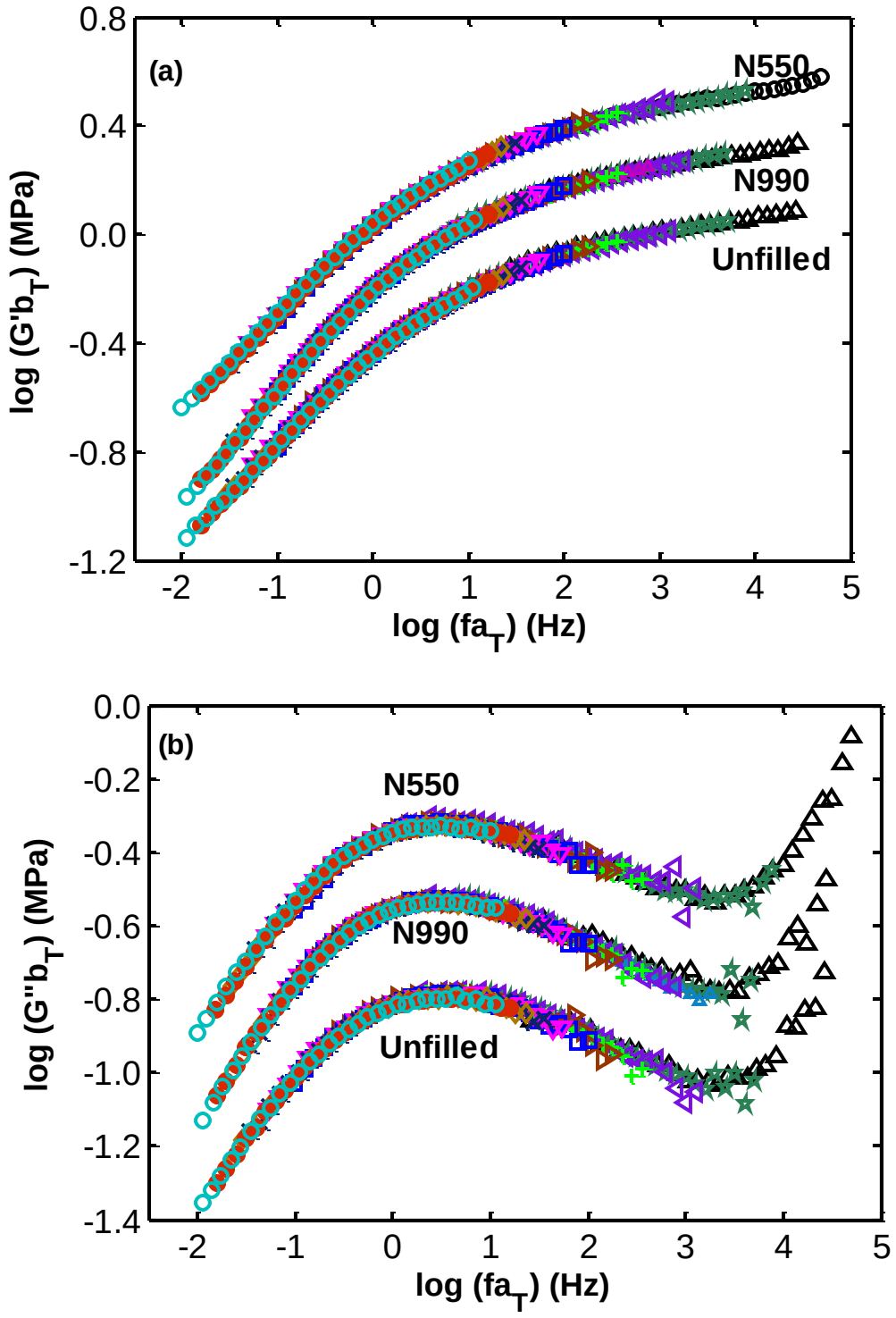

Figure 2.18: G' (a) and G" (b) master curves for unfilled polybutadiene[126] and polybutadiene filled with 36phr of N550 and N990 carbon black: Symbols indicate same temperatures as in Fig. 2.2.

CHAPTER 3. CRITICAL ANALYSIS OF DYNAMIC BEHAVIOR OF CARBON BLACK FILLED ELASTOMERS: PART I. LINEAR VISCOELASTIC MASTER CURVES

This Chapter is Derived from a Manuscript in Preparation with Co-authors G.A. Medvedev and J.M. Caruthers.

3.1 Introduction

Carbon black filled elastomers are by far the most studied materials in the area of rubber viscoelasticity. Establishing a relationship between their composition and their macroscopic response to deformation has been an ongoing challenge for the rubber industry. The principle of time-temperature superposition (TTS) allows obtaining the full spectrum of relaxation processes that characterizes the material. Although several authors [9,126]have reported the success of TTS for unfilled elastomers, this has not been the case for filled elastomers. Recently, Prabhu and co-workers have shown that TTS can be successfully applied to carbon black filled SBR as long as the applied strain is in the linear viscoelastic region[4]. It was demonstrated that for SBR loaded with a high and low structure carbon black, a strain amplitude independent region can be measured by dynamic tests and only within that region will the material obey the TTS principle. In the present study, the data has been extended to systematically study the effect of filler loadings and structures. The objective of this study is two-fold: (1) to demonstrate the effect of filler composition on the relaxation times spectrum as obtained by successful TTS (2) and to determine correlations (if any) between viscoelastic properties and filler parameters. We will address the first part in this communication.

Establishing viscoelastic linearity is key to success of the TTS procedure for filled rubber as demonstrated by recently.[4]. Dynamic measurements have long been an

important tool in identifying the Payne effect for filled elastomers, i.e. the point at which the storage modulus becomes strain amplitude dependent[16]. The critical strain amplitude, ε_c, at which this occurs (at given temperature and frequency), varies as a function of composition shifting to lower strains as filler loading is increased[16,24]. As a function of structure, several authors have shown that the critical strain ε_c is also translated to lower values with an increase in filler structure[2]

As stated by Prabhu *et al.*, some previous works on TTS of filled elastomers have not established a linear region before using TTS and other works have attempted to apply the TTS to analyzing the data in the nonlinear region[114,116,119-121]. The shifting procedures have also varied from no vertical shift[111-113] needed to one whereby different vertical shifts were applied to the storage and loss moduli from the same dataset[19,20].

Using the same shifting procedure as Prabhu and co-workers[4] , we report the effect of compositional variations on the linear viscoelastic response of carbon black filled elastomers using the TTS principle. This chapter is organized as follows: In the Experimental Section the filled elastomer synthesis and the mechanical testing setups are described. In the Results Section the TTS principle is illustrated for carbon black fillers of varying structure for different filler loadings. The extension of the viscoelastic master curves by creep recovery is also demonstrated. Finally, in the Discussion section we analyze the effect of composition on viscoelastic master curves setting the stage for the Part II, continued in the next chapter.

3.2 Experimental

The elastomer used was a random copolymer of styrene-butadiene rubber (SBR) (23.5 wt.% styrene) provided by the Goodyear Rubber Company (Plioflex 1502). High, moderate and low structure carbon black were the fillers used to reinforce the SBR. Cabot Corp. provided the various types carbon black as described in Table 3.1. The mixing procedure was initiated by masticating the SBR in a Brabender internal mixer at room temperature for 5 minutes at a rate of 20rpm. Carbon black was added to the SBR and allowed to incorporate for an additional 10 minutes. The amount of carbon black was

varied in order to create batches of 40, 20 and 10 phr (parts per hundred rubber) for the carbon black types utilized in this study. Mixing was continued in the Brabender two-roll mill where the cross-linking agent Dicumyl Peroxide (DCP) (Sigma-Aldrich) was added to the carbon black-SBR mixture. The amount of cross-linking agent was fixed for all batches i.e. 0.1 phr DCP. The carbon black-SBR-DCP mixture went through 20 passes in the two-roll mill at a temperature of 45ºC and at 10rpm. The mixture was then molded in a hot press (Carver Inc.) at 170°C under a pressure of 15,000lbs for 30 minutes to produce a square sheet (100mm x 100mm x 3mm) of cross-linked carbon filled SBR. A specimen without carbon black (unfilled) was also investigated. The control specimen were 0.1phr Unfilled SBR and 0.3phr unfilled SBR from previous work[4]. The mixing procedure for the unfilled SBR was similar to that of the filled case minus the internal mixer step. All cured rubber sheets were stored in a refrigerator (4ºC) until testing.

Dynamic experiments were performed in a Dyanstat dynamic mechanical tester [131] using a double shear sandwich test fixture. Two rectangular specimens of average dimensions 25mm x 14mm x 3mm were cut out from the rubber sheet for testing. The length to thickness ratio was kept at 8 as recommended by Sternstein [124] in order to prevent bending modes that would interfere with the desired simple shear deformation in the testing direction. The linear viscoelastic region was determined by carrying out room temperature Payne experiments at strain amplitudes 0.01 to 10% at a constant frequency of 1Hz. Once the linear regime was established, frequency sweep experiments (0.1 to 100Hz) was performed for every decade between 30ºC to 80ºC at constant strain amplitude. This temperature range was used for all experiments except 40phr N550 and N990 where 70ºC was the maximum test temperature.

The shifting procedure used for the time-temperature superposition is as described in the incipient work by Prabhu *et al.* [4]. In summary, the horizontal shift factors (a_T) is applied first to the tan δ isotherms. For the high temperature isotherms studied in this report, the horizontal shift factors were applied for all specimen tested for each filler type regardless of the volume fraction of filler for that batch. Once superposition is achieved for the tan δ case, the same shift factors are applied to the G' and G'' data. The log a_T temperature dependence was characterized by a WLF fit for all compositions of filled

SBR. In addition to horizontal shifting, vertical shift factors, b_T is applied to the G' and G'' data for superposition to occur.

Creep and Creep recovery experiments were conducted as previously described[4] in an AR-G2 rheometer (TA Instrument) for carbon black filled SBR. Tests were performed using cylindrical samples between parallel plates. Cylindrical cured elastomer specimens with a length 19mm and diameter 25mm were glued onto disposable aluminum plates using a quick curing epoxy (Loctite®). Care was taken to ensure that the applied torque produced strains within the linear viscoelastic regime. Creep recovery tests were performed at 30ºC, where the materials were first allowed to creep for 1 hour followed by recovery for 24 hrs.

3.3 Results

Dynamic Behavior of SBR Filled Elastomers

Figure 3.1 shows the shear storage modulus, G', loss modulus, G" and tan δ isotherms for 40phr N762 cured with 0.1phr DCP, which is representative of the systems studied here. The temperature range was 30ºC to 80ºC. At constant strain amplitude (and linear with respect to the linear viscoelastic region), frequency sweeps were performed from 0.1 to 100Hz. The viscoelastic isotherms for all the compositions tested are shown in Appendix B. As described in the Experimental section, TTS was applied by first shifting the tan δ isotherms horizontally using the a_T shift factor with respect to a reference temperature, 30ºC in this case. Once tan δ has been successfully shifted to give a master curve, the G' and G'' isotherms are shifted horizontally using the same shift factor a_T and then shifted vertically using the shift factor b_T to the reference temperature. The master curves are presented in Figure 3.3a-c for the N762 system and in Figures 3.2 and 3.4 for the N550 and N990 systems, respectively. Figure 3.2 shows a systematic increase in G', G'' and tan δ master curves for 40, 20, and 10phr N550-SBR. The reference material [4] (0.1phr unfilled SBR) master curves are also shown for comparison.

The tan δ master curves show a systematic response with filler concentration at low frequencies[132]. At higher frequencies (>10^0 Hz), all master curves merge since higher

frequency responses are dominated by the polymer matrix. This is consistent with previous work showing that for a given polymer, the higher frequency tan δ response is unaffected by the presence of fillers[4]. Each master curve also exhibits a maximum in tan δ that shifts to lower frequencies as the loading is increased. As expected, the terminal relaxation (low frequencies) appears to decelerate as filler loading is increased. It has been postulated that the tan δ response with respect to filler loading can be explained by a "slippage" dissipative process[132]. This will be discussed further in the next chapter.

For the N762-SBR material, the viscoelastic master curves (Figure 3.3) show similar features to the N550-SBR system. The terminal relaxation portion i.e. tan δ at low frequencies (Figure 3.3c) appears more compact than the N550-SBR. The merging of the master curves at high frequencies and the characteristic tan δ peak is also present. The G' and G'' master curves are also lower on the log scale (Figure 3.3a, 3.3b). As for the lowest structure carbon black system, N990-SBR, tan δ peak appears at higher frequencies than for N550-SBR and N762-SBR. The terminal relaxation is even more compact and is also reflected in the G' and G'' master curves (Figure 3.3a, 3.3b).

Figure 3.5 shows the a_T shift factors used to effect superposition for all structure blacks-SBR at various filler loadings. The unfilled shift factors for the base (0.1phr DCP) and the high crosslink density (0.3phr DCP) unfilled SBR are also shown for comparison. Although the difference is not significant, there is a systematic change in the temperature dependence of the loga_T shift factor with loading. The effect of carbon black structure is weak as seen by the similarities in all 3 figures (Figure 3.5a, 3.5b, and 3.5c). The loga_T shift function varied slightly (within experimental error) across volume fractions and filler types. At the same loading (phr), the larger structure blacks had slightly greater horizontal shift factors than the lower structure blacks. This is consistent with the fact that the higher structure blacks are affected more by temperature than lower structure blacks due to their interaction with the polymer (more bound rubber is formed)[133] Despite this subtle difference, the loga_T are all within experimental error about the same. The temperature dependence of the relaxation times is unaffected by filler addition [110].

Very little vertical shifting, b_T, (Figure 3.6) was needed to effect superposition. The vertical shift factors for the N550-SBR system (Figure 3.6a) show that higher

vertical shifts were required for the highest loading material. The b_T response to temperature is also systematic with higher loading requiring higher b_T than the base material. The effect of structure is apparent especially in the high structure, N550 material. A decrease in filler structure shows that the b_T utilized are much similar to the base elastomer than for high structure blacks. However, it does show that higher b_T was needed to implement superposition at higher filler loadings.

Creep Recovery

The viscoelastic response can be extended to lower frequencies than physically accessible through dynamic tests. The procedures employed using creep recovery are described in the previous chapter. The caveat in this procedure is the mismatch of creep to dynamic data by a factor of 1.3 for the instruments used. Creep and Creep recovery experiments were performed for 20phr and 40phr carbon black-SBR. Figure 3.7 shows the creep and creep recovery data for 20phr carbon black filled SBR of the three structures studied here. In Figure 3.7a, the creep recovery portion for all blacks appear to overlap but a closer look as given in Figure 3.7b shows that the long term recovery behavior is different for all structure blacks. While the N990 material appears almost flat at the end of the time window indicating that the recovery has completed, the N550 material appears to not level off over the observation time of 24hrs. To examine this difference, the rate of recovery is calculated via numerical differentiation of the data, where the results for two systems – N990 and N550 are shown in Figure 3.8. Figure 3.8 confirms the conclusion gleaned from Figure 3.7b, specifically that the rate of recovery for the N990 material has reached zero within the experimental scatter, but the rate of recovery for the N550 material has not. This implies that slower recovery processes are active in the higher structure systems.

The procedure for obtaining combined relaxation spectra using (and matching) the dynamic data and the creep recovery data is described in the previous chapter. The resulting combined master curves in the frequency domain for the storage and loss shear

moduli as well as the tanδ are shown in Figures 3.9 and 3.10 for the filler loadings of 20phr and 40phr, respectively.

As illustrated in Figures 3.9, the systematic difference in structure at a fixed loading extends into the lower frequency region. The deceleration of the relaxation processes is evident from the tan δ master curves (Fig 3.5c). The highest structure, N990 filled SBR has distinguishing features at low frequencies suggesting slower relaxation processes. At a higher filler loading, i.e. 40phr (Figure 3.10), the systematic difference in structure is also present, however; for the tan δ master curves, the long-term extension from creep does not follow the same ordered sequence as for the 20phr materials. However, we can deduce from Fig 3.10c that the rate of relaxation is slower for filled elastomers than for the unfilled elastomer.

3.4 Discussion

The successful application of TTS to filled elastomers has been extended for a wider range of filler loadings and structures. In addition to amplifying the storage and loss moduli responses, the effect of filler addition on the TTS at low frequencies is systematic for the tan δ master curves. Even in the presence of fillers, the loga_T shift function for the filled elastomers is similar to that of the unfilled polymer. Thus, the temperature dependence of the horizontal shift factors in the temperature region 80ºC or more above T_g of the rubber is essentially unaffected by the addition of fillers[25,127].

Looking at Figs. 3.2a,b through 3.4a,b, it appears that all filled storage and loss modulus master curves are parallel to those for the base material, in other words, the addition of filler into the base matrix simply amplifies the G’ and G” values of the unfilled material by the same factor and equally at all frequencies. However, examining Figs. 3.2c-3.4c, this only strictly holds for the lowest filler loading of 10phr, where the tanδ =G’/G” curves for this loading coincide with the tanδ curve for the unfilled material. At the higher filler loadings of 20phr and 40phr there is not a single tanδ curve, especially at lower frequencies, which would have been the case if the proportionality of G’ to G’ (unfilled) and of G” to G”(unfilled) was perfect. The “spraying” of the tanδ curves at

lower frequencies seems to become more pronounced at higher CB structures (compare N550 (Fig. 3.2c) and N990 (Fig. 3.4c).

Overlooking in the first approximation the subtle effects revealed by examination of the tanδ behavior, the effect of filler on the storage modulus G' appears to be captured remarkably well by a simple multiplication factor applied to the storage modulus of the unfilled material. This somewhat unexpected finding will be further explored in the Part II. Here we note that it should not be interpreted as an increase in the effective degree of crosslinking due to the presence of fillers. To stress this point the master curves for the unfilled material with a higher degree of crosslinking are shown in Figs. 3.2-3.4. Clearly, increase in the degree of crosslinking does lead to increase in the storage modulus G', but only at lower frequencies, where the transition zone modulus is unaffected. Also increase in the degree of crosslinking results in decrease in the loss modulus G" and the tanδ i.e. opposite of what addition of filler does.

Although the increase in the effective degree of crosslinking does not appear to be the dominant effect, there may be some effects due to the filler-curing agent interactions or formation of a bound layer, which is thought to hamper the crosslinking. Gent and co-workers studied the effect of carbon black on crosslinking[134]. Using swelling experiments, they confirm the results of earlier work by Lorenz and Parks[135] that in the swollen state, the volume fraction of filled rubber to that of its unfilled counterpart are directly proportional. This relationship suggests the actual degree of crosslinking in the matrix is unaffected by filler addition [134,135]. However, the restriction in swelling is due to an effective (not actual) degree of crosslinking as a result of filler addition. This is attributed to the formation of a bound rubber layer and verified by the lack of complete dissolution of rubber in swelling experiments [134]. Chodak and co-workers argued that as filler volume fraction is decreased, more rubber is available for crosslinking and thus, the crosslink density is increased[136]. While it is possible that the process and the efficiency of crosslinking may be affected by the presence of filler, within the curing timeframe, the effect (if any) is not evident in the viscoelastic master curves presented here.

Although the difference in $\log a_T$ can be said to be minimal (within experimental error of the unfilled), the subtle differences can explain tan δ behavior at low frequencies.

At low temperatures (higher frequencies), the polymer matrix dominates the viscoelastic effects, hence the loga_T for filled rubber should be the same as that of the unfilled material[112,117]. Although we do not probe low temperature effects in this chapter, previous work shows that the tan δ master curves merge at lower temperatures regardless of the filler structure[4]. Looking at Figure 3.5, at a temperature of 40ºC, all compositions appear to have the exact same loga_T temperature dependence as the unfilled SBR. This proves that the effect at higher frequencies (low temperatures) is polymer dominated.

In the previous work[4], we ascribed this structure dependence of viscoelastic properties to a filler-filler dissociation that much readily occurs for higher structure blacks. The effect of temperature is therefore more pronounced on the abundant filler-filler points of contact in high structure blacks. Song and co-workers suggest that the use of b_T in superposition is telling of the changes in the polymer-filler interaction[11]. The use of b_T implies that the polymer filler interaction varies as a function of structure and composition.

The differences in tan δ has been attributed to the presence of entanglements formed between bound rubber and the bulk rubber[112]. The interaction of the carbon black with the polymer and the surface area available for bound rubber formation will control the amount of entanglements. Since higher structure blacks (in this case) have higher surface area (and more void for rubber entrapment) than the rest of the carbon black tested here, it is expected that more entanglements are present resulting in an increase in the diameter of the bound rubber layer [133]. In order to account for the mechanisms for the loss processes, several theories have been put forth. Dissipative processes such as absorbed layer/bound rubber theory[7,19,133,137], interfacial chain slippage[99,138], bond cleavage[132] or any combination of all are speculated to play a role in the difference in tan δ behavior[132]. These and other mechanisms will be discussed in detail in the Part II of this communication.

Onogi. *et al.*[121] postulated that an increase in b_T with temperature had to do with a filler volume fraction effect. Specifically, the temperature dependence of b_T is attributed to differences in thermal expansion coefficients, α, of polymer-carbon black. Work done by Haong and co-workers[139] reported a decrease in α with increase in filler loading for

the temperature range of this report. This decrease in α with volume fraction increase has been ascribed to restricted mobility of polymer chains by the filler network created[139]. However, Kraus argued that in the rubbery region (high frequencies) α is unchanged so the difference in hysteresis (or tan δ) is not due to segmental mobility but to other mechanisms [127]. The effective volume concept as put forth by Medalia[140] is likely to play a role in the b_T behavior.

Using the creep recovery experiments the viscoelastic storage and loss moduli as well as tanδ master curves in the frequency domain have been extended to lower frequency, where the procedure was described in details in the previous chapter. The most important feature of Figs. 9c and 10c is the appearance of the low frequency relaxation processes in case of the filled systems that are not present in case of the unfilled material. This has been attributed to the adsorption of the polymer on the filler, reminiscent of the bound rubber theory[31] This long time response indicates that the time scale of the relaxation is related to the size of the molecular/mesoscopic unit undergoing relaxation. Consequently, the unfilled polymer will not exhibit relaxation times longer than that determined by the distance between crosslinks, which is clearly seen in the dependence of the loss peak on the crosslink density for the unfilled SBR[126] where the peak shifts to higher frequencies for higher crosslink densities. In contrast, in the presence of filler the longest relaxation processes stem from the cooperative movements that involve a number of chains attached to a given filler particle. The characteristic length of the particulate-polymer structure will be much larger than the distance between crosslinks, and consequently the time scale of the relaxation will be significantly longer.

In this work, we have investigated the effect of filler loading and structure on the linear viscoelastic behavior carbon black filled SBR. The implications and the correlations of the viscoelastic properties to filler parameters will be the focus of the second part of this communication continued in the next chapter.

Table 3.1: Properties of carbon black

Carbon black	Filler loading, phr	DBPA # (ml/100g)*	Surface Area (m^2/g)	Typical Ave. Particle Size (nm)+
N990	40, 20, 10	40	7-9	280
N762	40, 20, 10	67	27	80
N550	40, 20, 10	121	38-46	40-48

*Data supplied by the manufacturer; +Data from Basic Rubber Technology[141]

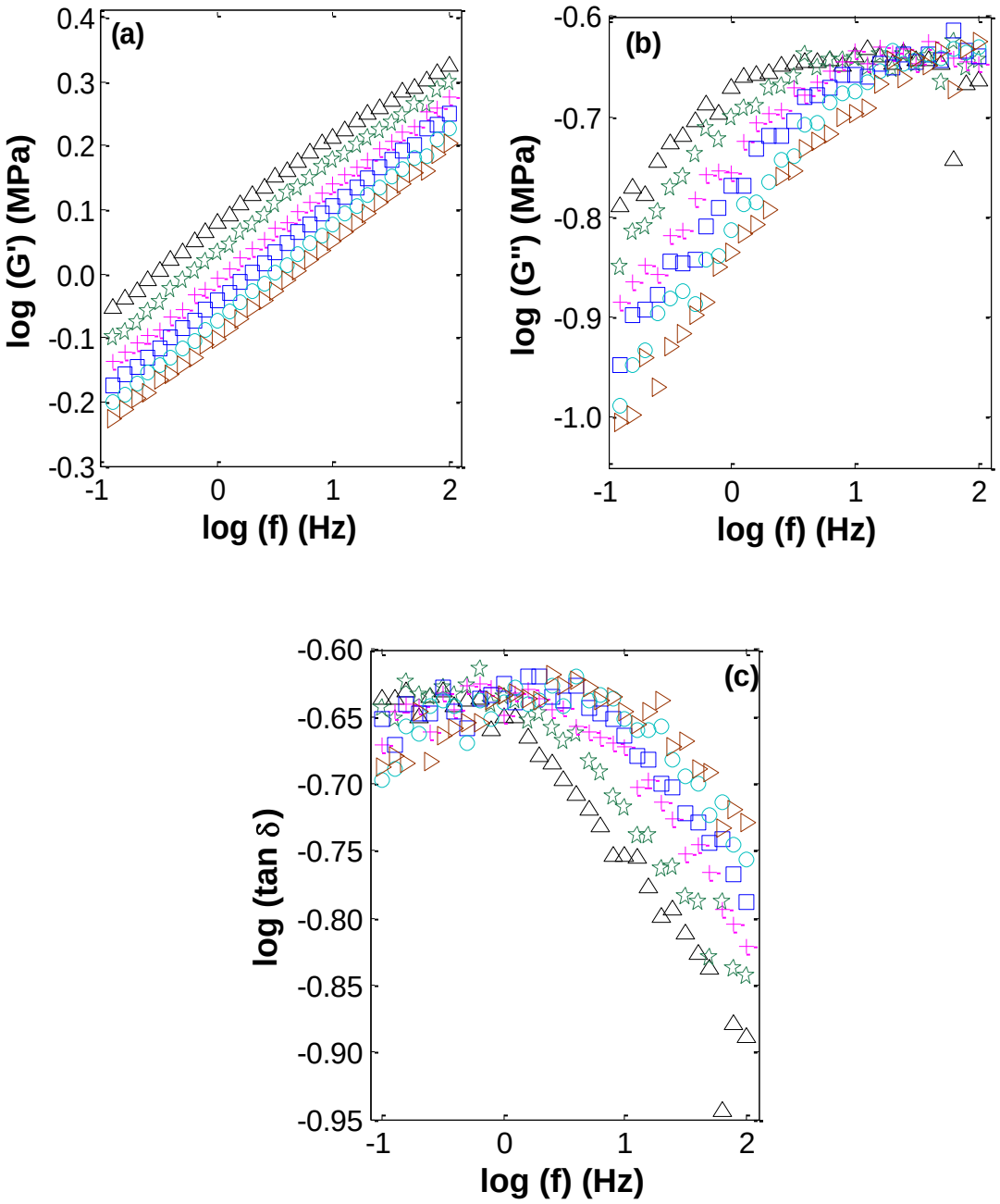

Figure 3.1: Storage modulus (a), loss modulus (b) and tan δ (c) isotherms for SBR with 40 phr of N762 cured with 0.1 phr of DCP. Temperatures (in ^{o}C) are as follows: △ 30, ☆ 40, + 50, □ 60, ○ 70, ▷ 80.

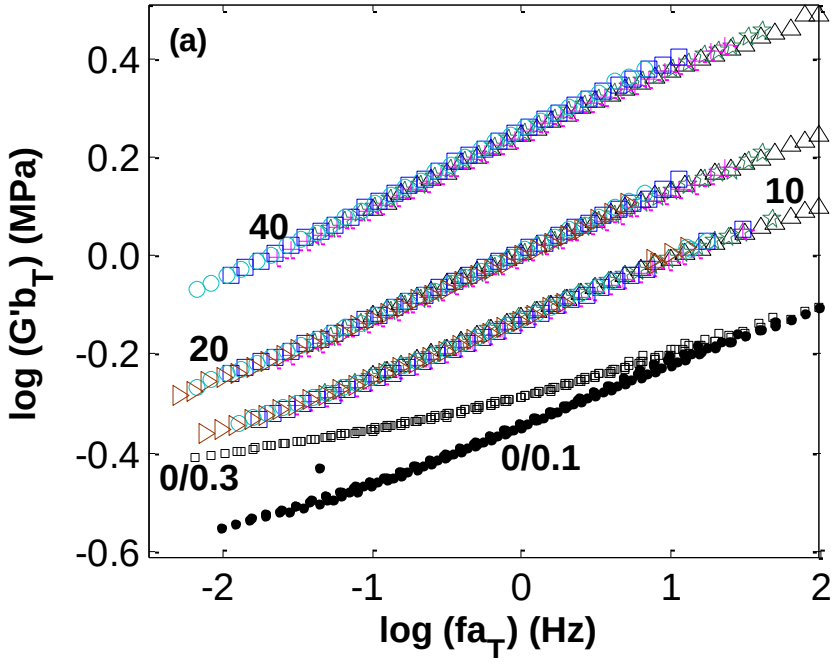
(a)
0.4
0.2
0.0
-0.2
-0.4
-0.6
log (G'b_T) (MPa)
40
20
10
0/0.3
0/0.1
-2
-1
0
1
2
log (fa_T) (Hz)

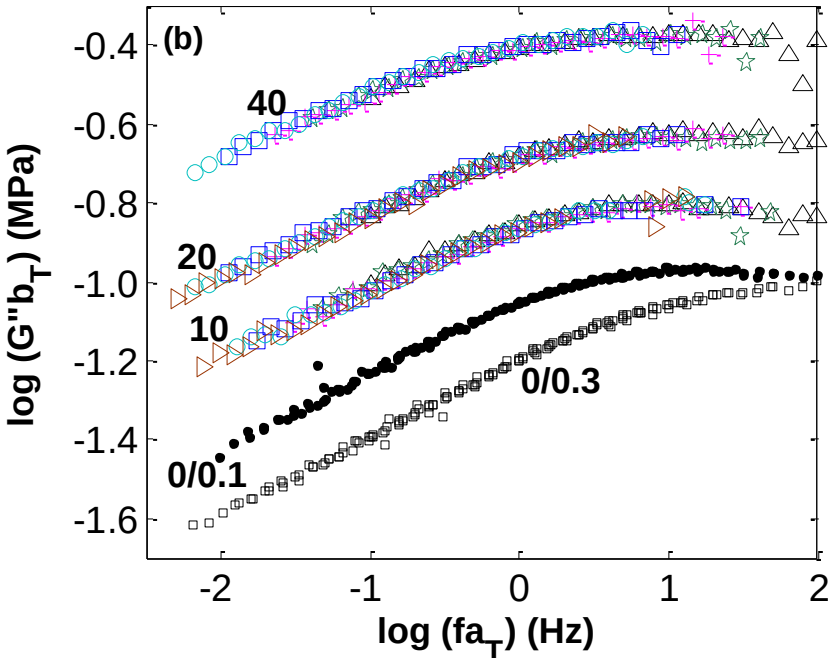
(b)
-0.4
-0.6
-0.8
-1.0
-1.2
-1.4
-1.6
log (G"b_T) (MPa)
40
20
10
0/0.3
0/0.1
-2
-1
0
1
2
log (fa_T) (Hz)

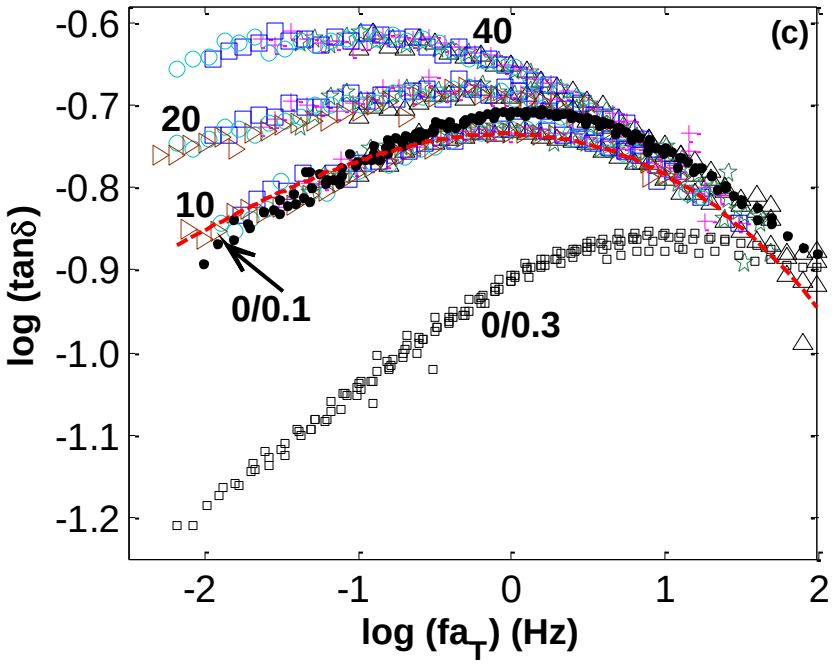

Figure 3.2: Storage modulus (a),loss modulus (b) and tan δ (c) master curves for SBR filled with 40phr, 20phr, and 10phr of N550 carbon black cured with 0.1phr DCP. The reference unfilled SBR[126] with 0.1 phr DCP (●) and 0.3 phr DCP (□) are also plotted for comparison. Temperature symbols are same as in Figure 3.1 Filler loading is indicated on curves in phr. The red dashed line in (c) is a guide to the eye for the 10phr material.

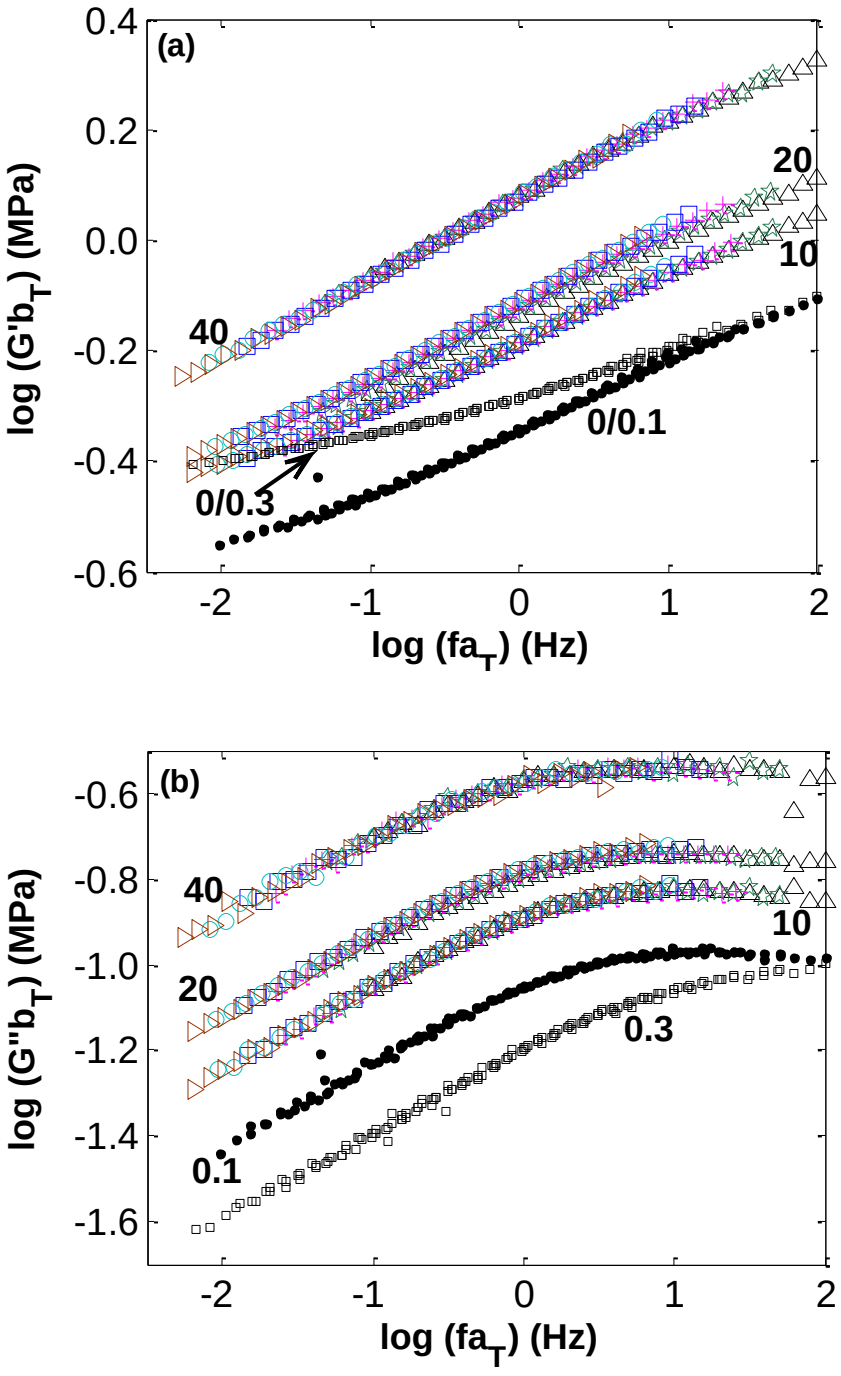
(a)
log (G'b_T) (MPa)
log (fa_T) (Hz)
40
20
10
0/0.1
0/0.3
(b)
log (G"b_T) (MPa)
log (fa_T) (Hz)
40
20
10
0.3
0.1

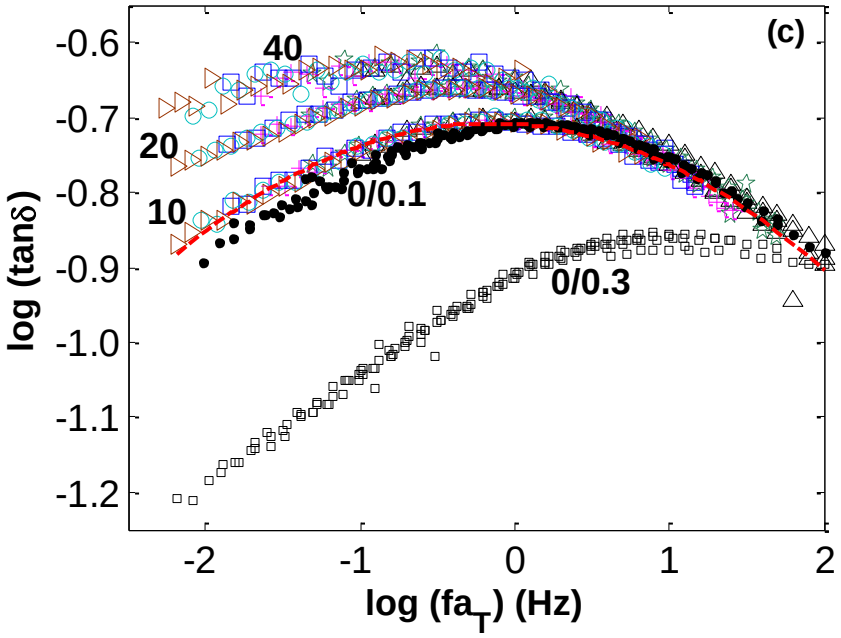

Figure 3.3: Storage modulus (a),loss modulus (b) and tan δ (c) master curves for SBR filled with 40phr, 20phr, and 10phr of N762 carbon black cured with 0.1phr DCP. Also included is the reference unfilled SBR[126] with 0.1 phr DCP and 0.3 phr DCP. Symbols are same as in Fig. 3.2

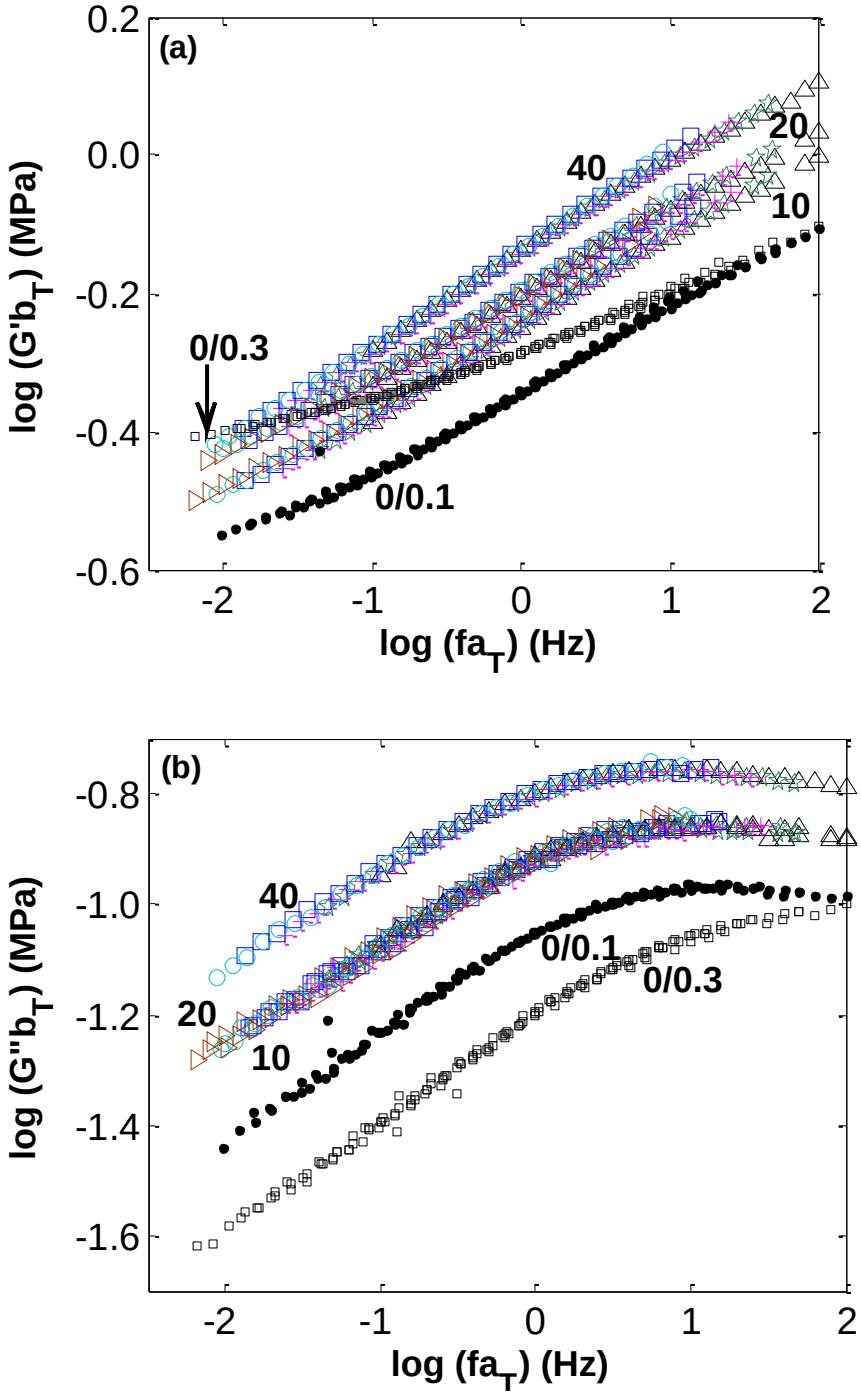
(a)
0.2
0.0
-0.2
-0.4
-0.6
-2
-1
0
1
2
log (G'b$_T$) (MPa)
log (fa$_T$) (Hz)
40
20
10
0/0.3
0/0.1
(b)
-0.8
-1.0
-1.2
-1.4
-1.6
log (G"b$_T$) (MPa)
40
20
10
0/0.1
0/0.3

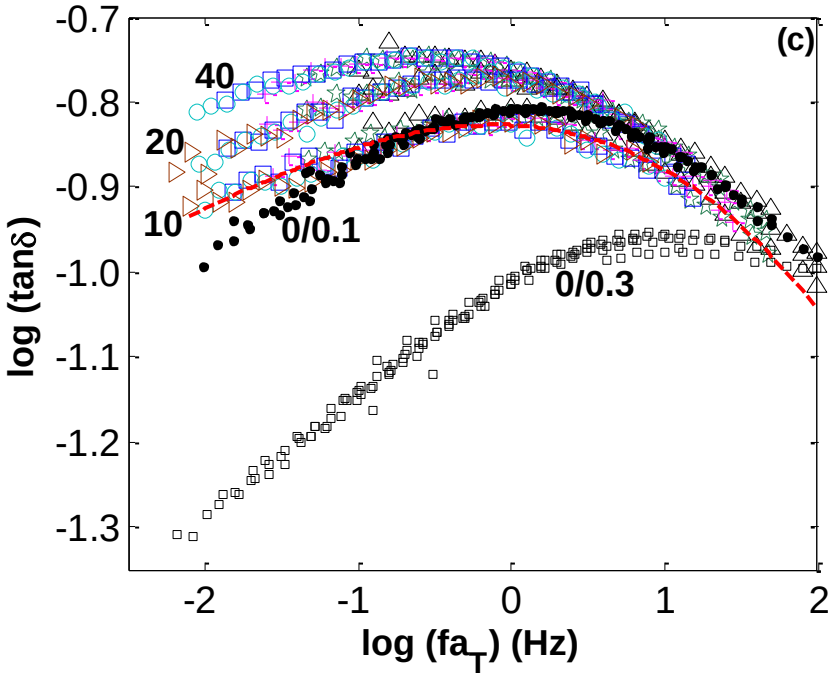

Figure 3.4: Storage modulus (a),loss modulus (b) and tan δ (c) master curves for SBR filled with 40phr, 20phr, and 10phr of N762 carbon black cured with 0.1phr DCP. Also included is the reference unfilled SBR[126] with 0.1 phr DCP and 0.3 phr DCP. Symbols are same as in Fig. 3.2.

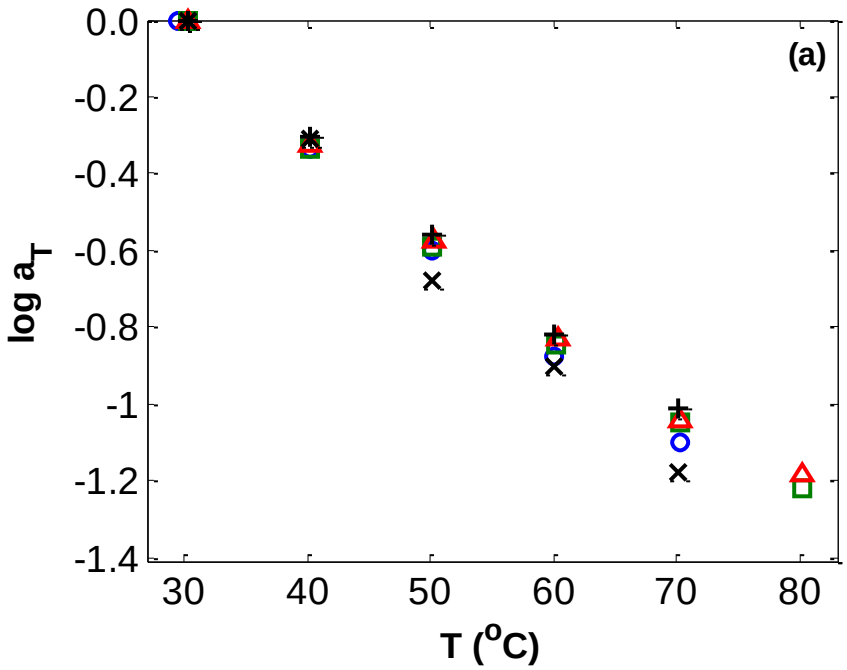
(a)
0.0
-0.2
-0.4
-0.6
-0.8
-1
-1.2
-1.4
log a_T
30
40
50
60
70
80
T (^{o}C)

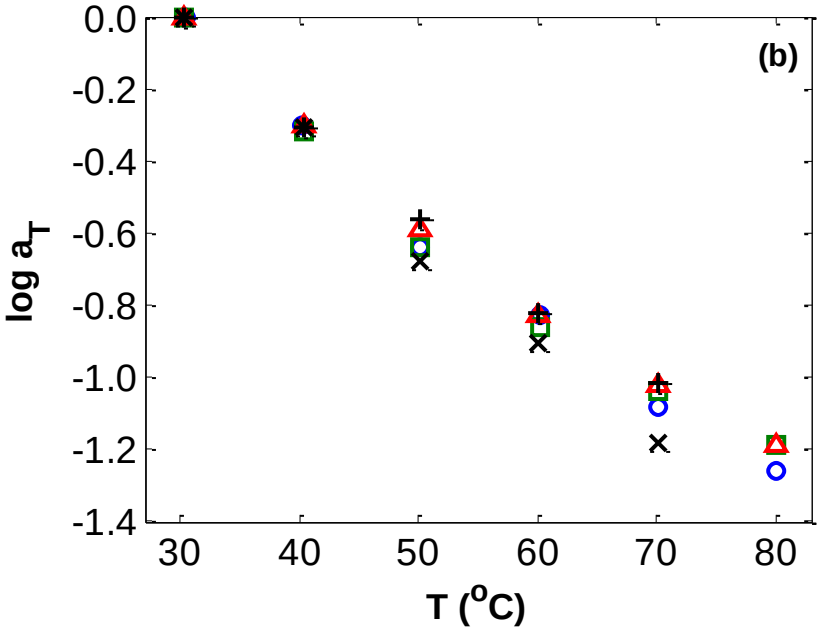
(b)
0.0
-0.2
-0.4
-0.6
-0.8
-1.0
-1.2
-1.4
log a_T
30
40
50
60
70
80
T (^{o}C)

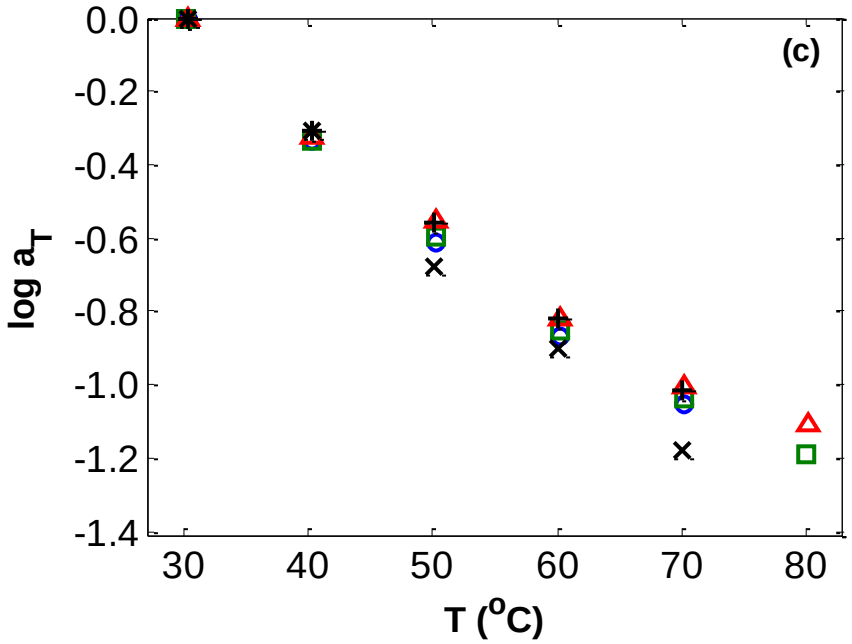

Figure 3.5: Temperature dependence of log a_T for SBR with 40 phr of (a) N550 (b) N762 and (c) N990 carbon black cured with 0.1 phr DCP at various filler concentrations: ○ 40phr, □ 20phr, △ 10phr. Log a_T for the reference unfilled SBR[126] with 0.1 phr DCP (+) and 0.3 phr DCP (×) are also plotted.

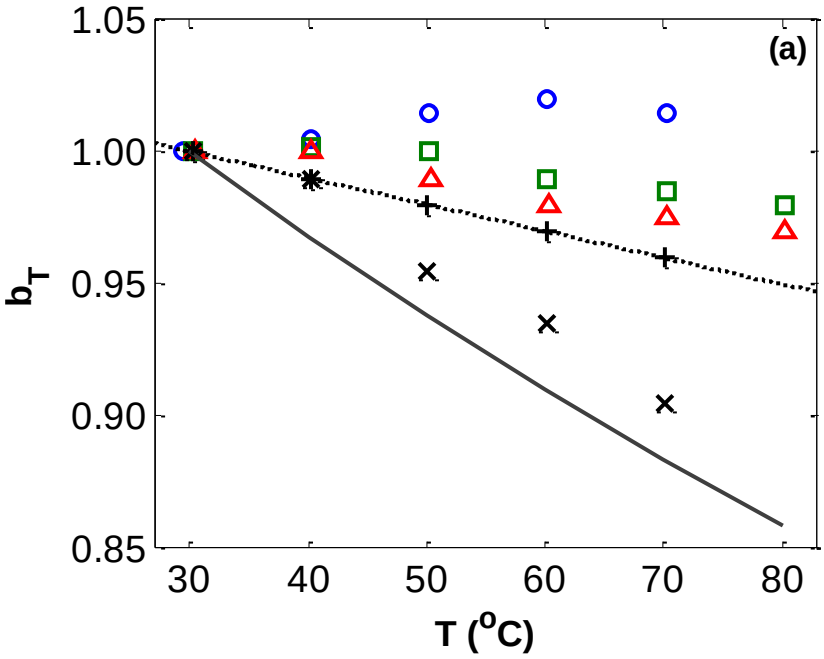
(a)
1.05
1.00
0.95
0.90
0.85
b_T
30
40
50
60
70
80
T (^{o}C)

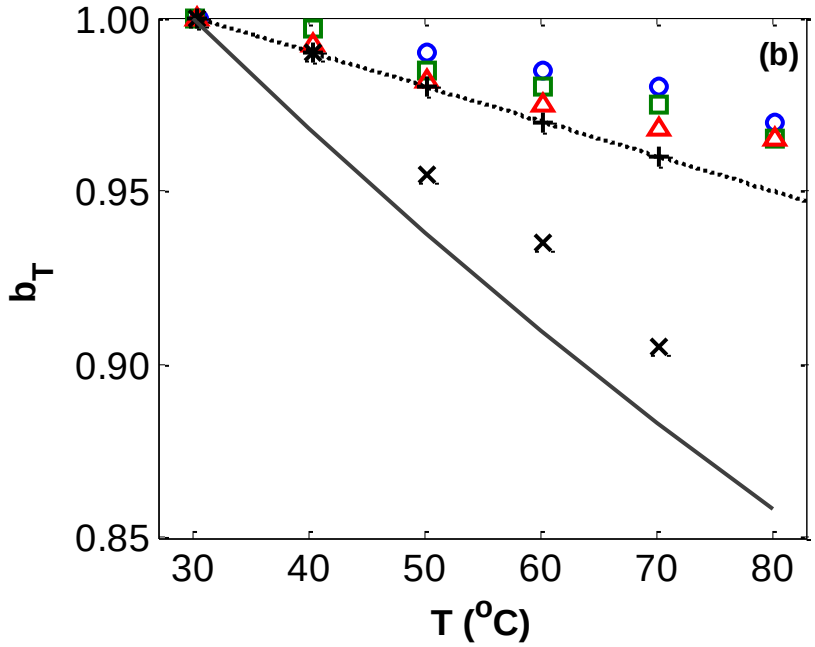
(b)
1.00
0.95
0.90
0.85
b_T
30
40
50
60
70
80
T (^{o}C)

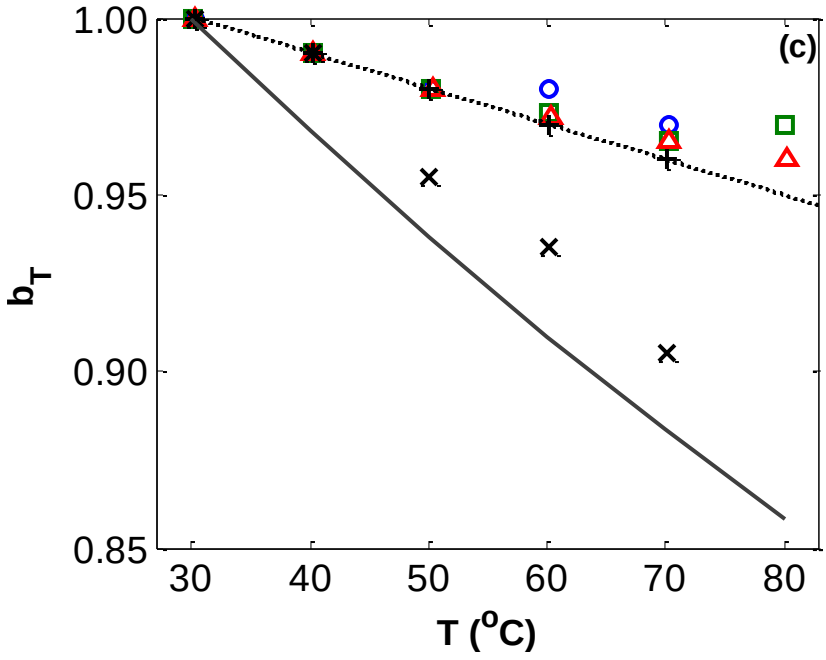

Figure 3.6: Temperature dependence of b_T for SBR with 40 phr of (a) N550 (b) N762 and (c) N990 carbon black cured with 0.1 phr DCP at various filler concentrations: ○ 40phr, □ 20phr, △ 10phr. b_T for the reference unfilled SBR[126] with 0.1 phr DCP (+) and 0.3 phr DCP (×) are also plotted. The solid line is the standard $\rho_0 T_0/\rho T$ vertical shift from rubber elasticity.

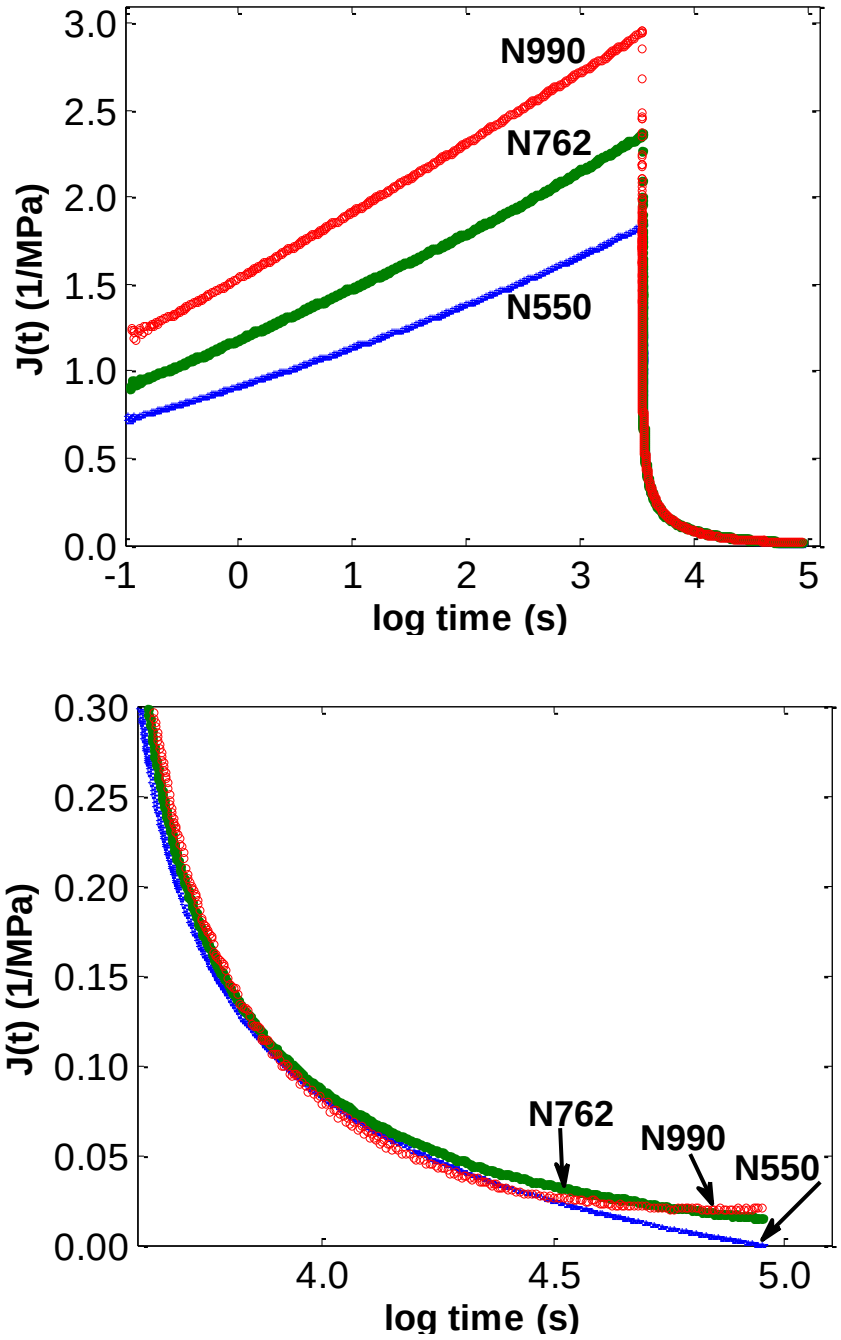

Figure 3.7: Creep and Creep recovery response SBR filled with 20phr of N990, N762, and N550. (a)Creep and creep recovery (b) Long term creep recovery response.

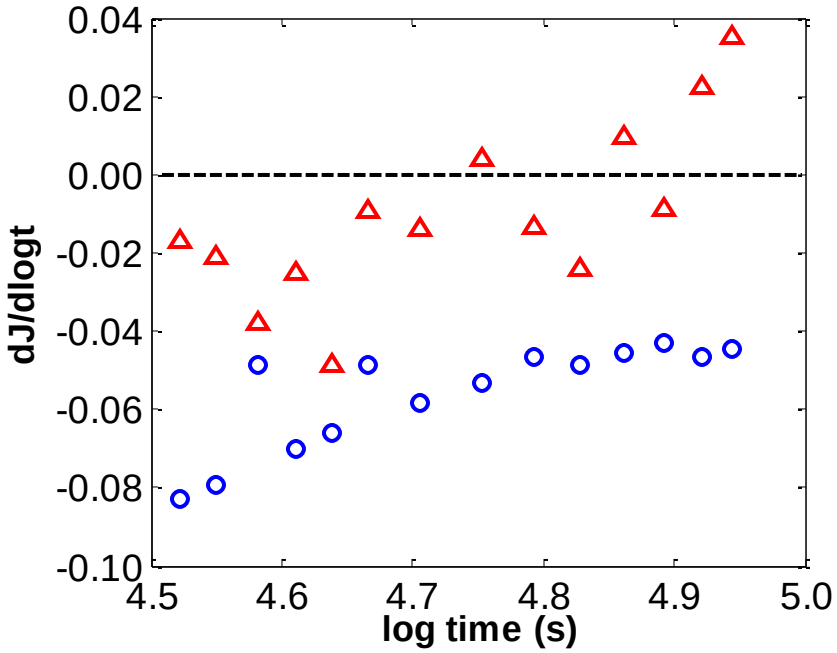

Figure 3.8: Long term rate of recovery from creep for SBR with 20phr of N550 (○) and N990 (△) carbon black cured with 0.1phr DCP.

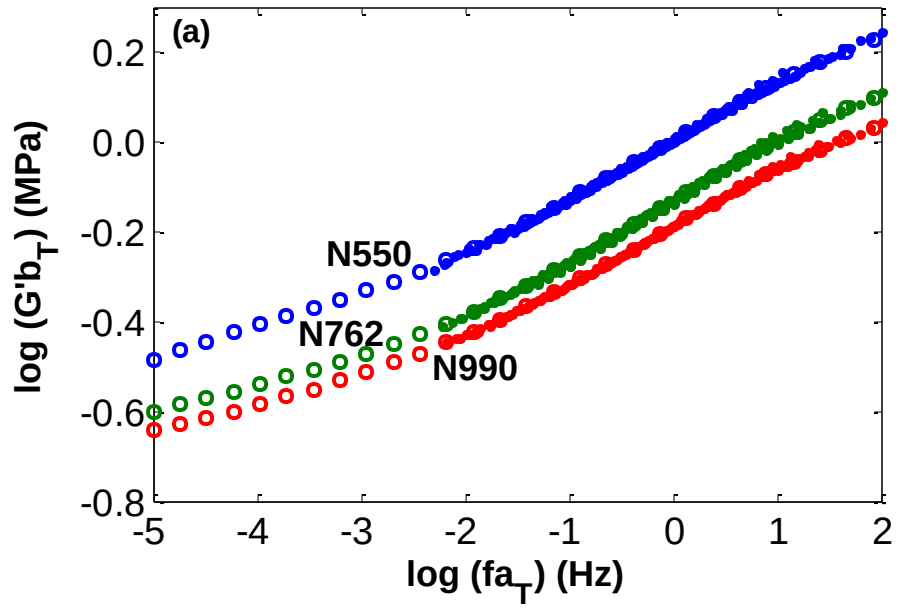
(a)
0.2
0.0
-0.2
-0.4
-0.6
-0.8
-5
-4
-3
-2
-1
0
1
2
log (G'b$_T$) (MPa)
log (fa$_T$) (Hz)
N550
N762
N990

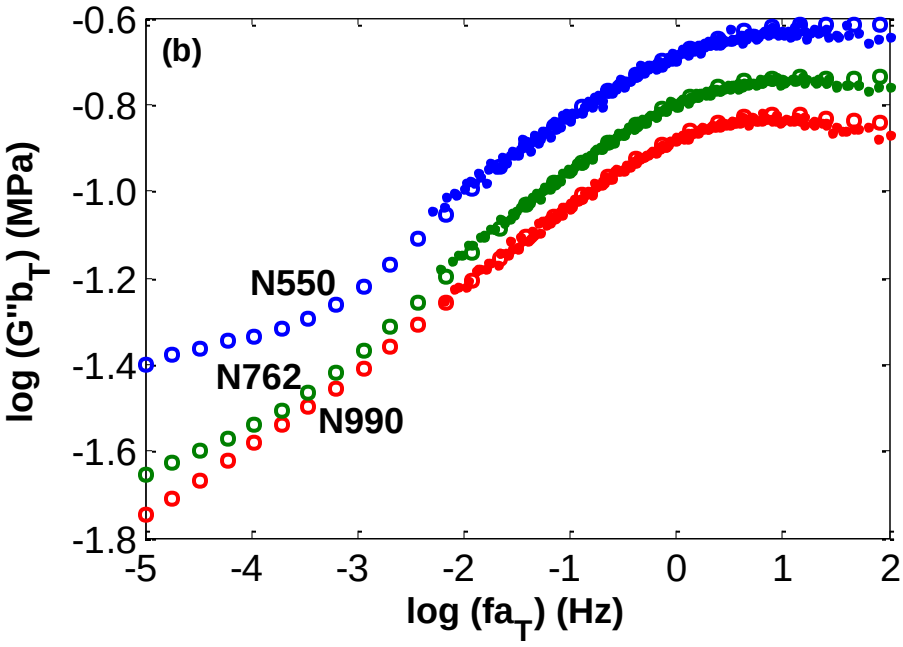
(b)
-0.6
-0.8
-1.0
-1.2
-1.4
-1.6
-1.8
-5
-4
-3
-2
-1
0
1
2
log (G''b$_T$) (MPa)
log (fa$_T$) (Hz)
N550
N762
N990

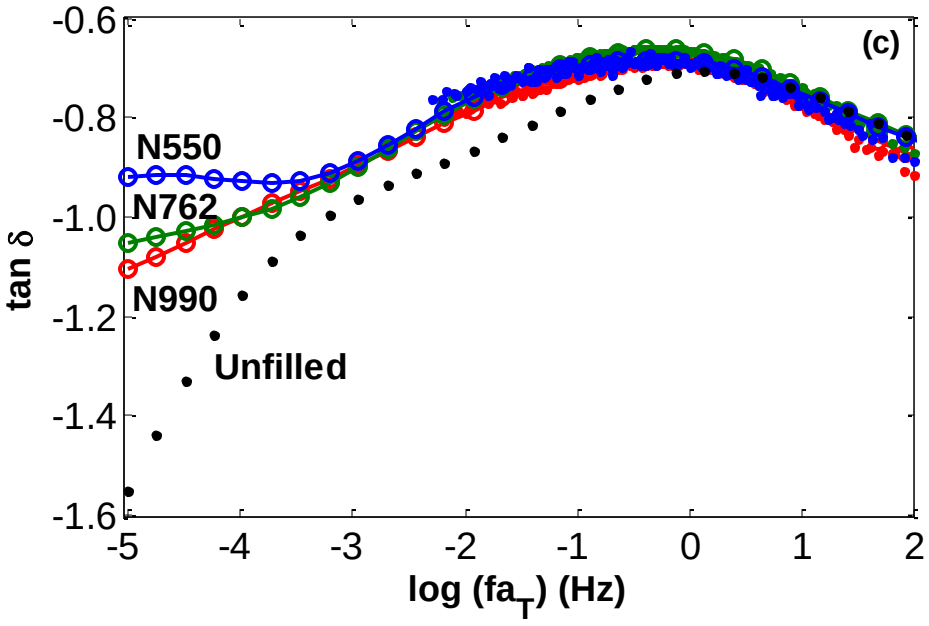

Figure 3.9: Storage modulus (a), loss modulus (b) and tanδ (c) master curves for SBR filled with 20 phr of N550, N762 and N990 carbon black. Extension of the viscoelastic response to lower frequencies (open circles) from $\{J_i\}$ spectra determined using creep recovery data. The extension for the reference unfilled SBR[126] is also plotted for comparison in (c).

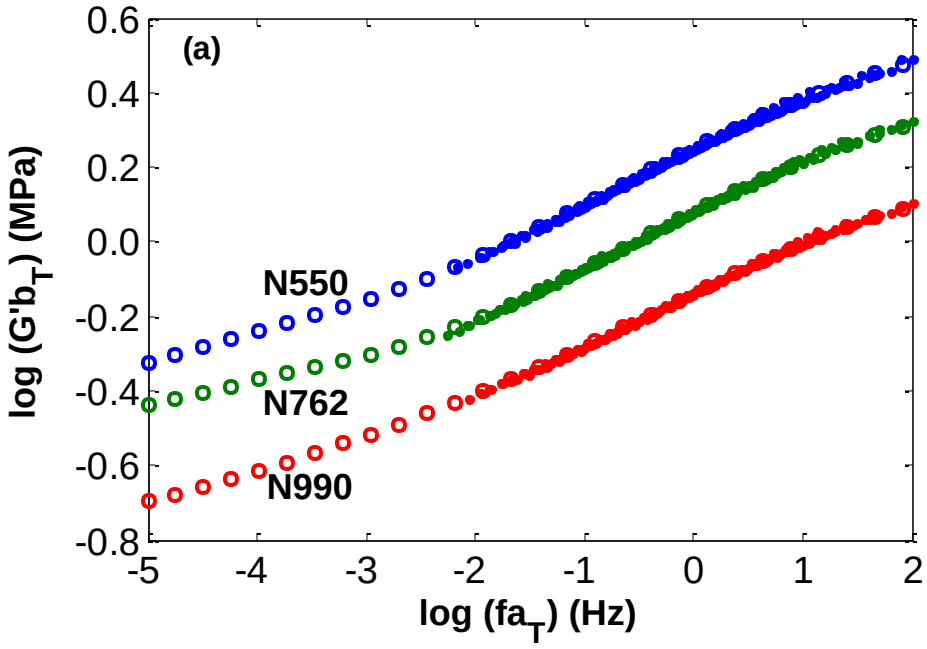
(a)
N550
N762
N990
log (G'b_T) (MPa)
log (fa_T) (Hz)
0.6
0.4
0.2
0.0
-0.2
-0.4
-0.6
-0.8
-5
-4
-3
-2
-1
0
1
2

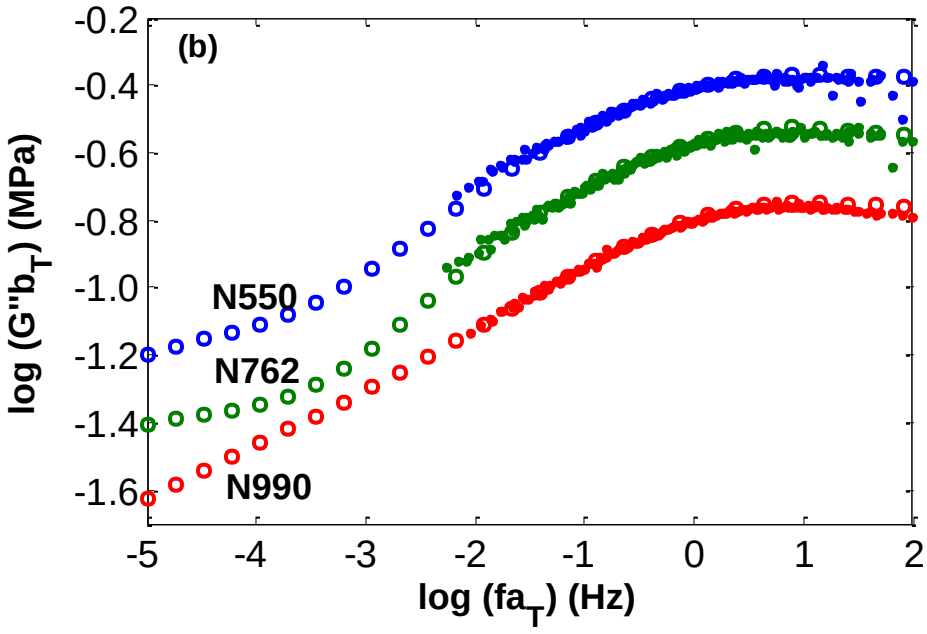
(b)
N550
N762
N990
log (G"b_T) (MPa)
log (fa_T) (Hz)
-0.2
-0.4
-0.6
-0.8
-1.0
-1.2
-1.4
-1.6
-5
-4
-3
-2
-1
0
1
2

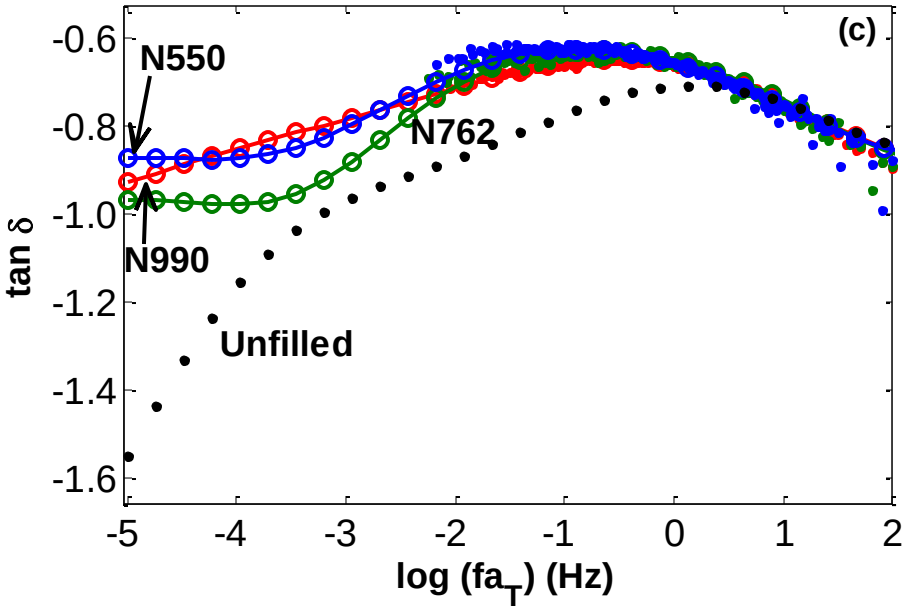

Figure 3.10: Storage Modulus (a), loss modulus (b) and tan δ (c) master curves for SBR filled with 40 phr of N550, N762 and N990 carbon black. Extension of the viscoelastic response to lower frequencies (open circles) from $\{J_i\}$ spectra determined using creep recovery data. The extension for the reference unfilled SBR[126] is also plotted for comparison in (c).

CHAPTER 4. CRITICAL ANALYSIS OF DYNAMIC BEHAVIOR OF CARBON BLACK FILLED ELASTOMERS: PART II. CORRELATION OF MECHANICAL RESPONSE TO COMPOSITION

This Chapter is Derived from a Manuscript in Preparation with Co-authors G.A. Medvedev and J.M. Caruthers.

4.1 Introduction

Most elastomers are utilized in their filled state, i.e. they contain particulate fillers that reinforce the elastomers' mechanical properties. Filled elastomers exhibit interesting nonlinear phenomena such as the Payne and Mullins effects. A unified perspective regarding the underlying physics of rubber reinforcement remains elusive. One classic contribution is the work by Medalia and co-workers that utilized a remarkably straightforward concept of effective volume ϕ_{eff}[140]. Specifically, they were able to demonstrate that the high amplitude modulus (HAM) observed in the Payne experiment for various filler structures can be captured using the effective volume as a single parameter, where the dependence of HAM on ϕ_{eff} was given by $G'_{HAM} = G'_o(1+2.5\phi_{eff}+14.1\phi_{eff}^2)$. Other works by Caruthers and co-workers pursued similar ideas and found a correlation between the loss tangent also at high strain amplitudes and the loading-interfacial area parameter[142]. At the same time, the low amplitude behavior as a function of filler composition was not systematically studied with a few exceptions notably by Ferry and some others[109,110]. Ferry and others have shown that the principle of TTS works in a limited number of cases. However, there have even been reports that mentioned TTS doesn't work for filled elastomers[114-116]. In Part 1 (the previous chapter), we studied the effect of particulate fillers in the linear range. We

have amassed a wealth of data with primary focus on successful application of TTS for filled elastomers. With the exception of the lowest frequency regions ($<10^{-1}$ Hz), there was a remarkable similarity in the shape of the viscoelastic response especially for G'. This gives us the idea that the data can be unified using the effective volume concept similar to Medalia's work at the high strain amplitude region.

Several theories have been put forth to quantify the extent of reinforcement in an elastomer that results from the addition of particulate fillers[22,61]. The very first concept that eventually led up to many current postulates was Einstein's derivation of the hydrodynamic effect (viscosity) caused by the addition of spherical particles in a liquid[143]. This viscosity law was adapted to rubber research replacing viscosity with the modulus of the rubber[144,145]. The effect of spherical fillers on the storage modulus in an elastomer is taken into account by the Einstein-Guth-Gold equation (Eq. 1) [130,143,144] given by the expression

$$G' = G'_o(1 + 2.5\phi + 14.1\phi^2) \qquad (4\text{-}1)$$

where G'_0 is the modulus of the matrix and φ is the volume fraction of filler. The second order term accounts for the interaction between the fillers that was not in the original Einstein equation. For a fixed amount (volume fraction) of carbon black in an elastomer, the equation predicts that the reinforcement effect without taking into account other factors such as structure. In some instances, especially at low strains, the Guth-Gold equation works despite its limitations. Another form of the Guth-Gold equation considers a shape factor with the underlying assumption resting on the fact that not all filler particles will be spherical in nature [130]. But even with shape considerations, the reinforcing capability of the filler is usually underestimated and is best suited for predicting the stress-strain relationships of filled elastomers that contain a small amount of spherical fillers[35,146]. To counter the problem of predictions based simply on filler loading, Medalia extended the Guth-Gold equation by assuming the presence of trapped, unperturbed rubber which effectively increased the modulus [147,148]. This is made possible by the structure of carbon black which contains volume that can occupy rubber (occluded rubber). A measure of this structure is provided by its DBPA number[112]. Occluded rubber

is not subject to deformation and as such, it effectively becomes part of the filler[140,147]. Hence, the expression for the effective volume fraction is given by,

$$\frac{\phi_{eff}}{\phi} = \frac{1 + 0.02139 * DBPA}{1.46} \tag{4-2}$$

where ϕ_{eff} is the effective volume fraction of filler taking into account the presence of occluded rubber[140]. Medalia's version of the Guth-Gold equation then becomes,

$$G' = G'_o(1 + 2.5\phi_{eff} + 14.1\phi_{eff}^{\ 2}) \tag{4-3}$$

Similar equations for predicting the loss modulus, G'', aren't as common. The assumptions and expressions used in G' determination cannot be presumed upon the loss modulus, G'' and consequently it cannot represent the ratio of G'' to G' - the loss tangent, tan δ. In studying the tan δ behavior of several elastomers, Caruthers and co-workers[149] established a correlation between carbon black properties and tan δ for experiments conducted in the nonlinear viscoelastic region. The filler parameters used were, ψ, the interfacial area of carbon black and φψ, the loading-interfacial area given by

$$\psi = \phi \text{ x} S \text{ x } \rho \tag{4-4}$$

$$\phi\psi = \phi(\phi \text{ x} S \text{ x } \rho) \tag{4-5}$$

where ρ is the density and S is the surface area of carbon black. For SBR and Natural Rubber (NR) filled elastomers, a relationship between the tan δ and φψ was determined for a wide range of carbon blacks. [149]. Medalia & Laube extended this work to NR and Butyl rubber (IIR) carbon black systems and established (through regression analysis) tan δ correlations to the φψ parameter [150]. They concluded that the tan δ is more dependent on loading than interfacial area for carbon black filled butyl rubber systems. It is worth noting that both works (Caruthers, Medalia) performed measurements at high strain amplitudes. However, we have investigated the use of these concepts in the linear viscoelastic region to ascertain if any correlations exist.

The purpose of this work is to critically analyze the data in Part I (the previous chapter) to determine if ideas of Medalia, Caruthers and others that served well to describe the effect of filler composition on the high strain amplitude properties can be

applied to low amplitude properties. If successful, we will determine if the entire range of viscoelastic deformation (Payne) can be unified. The chapter is organized as follows. Table 4.1 contains all the data from Part I. The rest of the chapter presents a critical analysis of data from Table 4.1. First we will start with the effective volume idea followed by the interfacial area concepts. We will demonstrate that some of these descriptors can be unified with the viscoelastic response at low strain amplitudes.

4.2 Results

From the data gathered in Part I, we have tabulated (Table 4.1) the viscoelastic properties and filler parameters in an attempt to find meaningful structure-property correlations. All the properties are systematically ordered with loading for each filler structure. A select few will be discussed here.

The viscoelastic master curves for the storage modulus in Figure 4.1 are all parallel relative to the mater curve of the unfilled elastomer regardless of the amount of filler present. Using the entire unfilled master curve, the factor needed to effect superposition with the filled master curve was determined. This ratio of the G' of the filled rubber to the G' of the unfilled rubber is given by the multiplicative factor $C_\phi = G'/G'_o$. Figure 4.1 shows the master curves with the approximation by multiplying the unfilled master curve by C_ϕ. At low filler concentration, the use of C_ϕ on the unfilled SBR predicts the filled master curves well for the entire log frequency scale (Figure 4.1). However, at the highest filler loading, 40phr, C_ϕ overestimates the filled mater curves at the low frequency regime. This deviation is present in all structure carbon blacks. Its absence at lower filler loading is suggestive of a critical volume fraction (percolation threshold) at which the underlying processes differ. Percolation theory invokes the concept of filler networking stating that a critical volume fraction exists at which all the filler in the matrix will be connected to each other. This critical volume, the percolation threshold, suggests the formation of a secondary network in addition to the cross linked rubber matrix.

In Figure 4.2, C_ϕ was plotted against the volume fraction of filler, φ, and compared with the prediction from the Guth-Gold equation. C_ϕ increases with structure with enhanced effects at high ϕ. As expected, the prediction from Guth-Gold underestimates the reinforcement capability of carbon black primarily because filler structure is not a consideration in the equation. It does appear that perhaps the lowest structure blacks utilized C_ϕ close enough to the Guth-Gold equation. We applied the C_ϕ determined from the storage modulus master curves to the loss modulus master curves to see if the G'' filled was a factor of the unfilled response. In Figure 4.3a, the use of C_ϕ on the unfilled master curves to predict $b_T G''$ of 10phr N990 works well. However, for $b_T G''$ in the 40phr N550 system (Figure 4.3b) fails for most of the frequency region.

Using the definition of effective volume fraction, ϕ_{eff}, derived from occluded rubber by Medalia and co-workers, the ϕ_{eff} was calculated for all carbon black used (shown in Table 1). In Figure 4.4a, we see that C_ϕ collapses onto a quadratic line with respect to ϕ_{eff} described $C_\phi = 1 + 2.8969\varphi_{eff} + 8.6854\varphi_{eff}^2$. Medalia's version of the Guth-Gold equation works well with our data at small effective volumes but deviates thereafter. Using Caruthers' equation for the loading-interfacial area, ϕψ was calculated for all filled SBR. Figure 4.4b shows that ϕψ varies linearly with C_ϕ

We investigated the horizontal and vertical shift data with respect to the effective volume concept. At a select temperature of 70ºC, the $\log a_T$ for all structure carbon blacks is plotted against ϕ_{eff} in Figure 4.5. A linear correlation exists with ϕ_{eff} where at a fixed temperature, higher structures systems require smaller shift factors. This again indicates the importance of structure rather that loading in a filled rubber and the influence of polymer-filler interactions. The b_T correlation to ϕ_{eff} also shows linear correspondence with effective volume fraction at a fixed temperature of 70ºC (Figure 4.6). The vertical shift factors all collapse on a straight line. As the amount of occluded rubber increases (higher structure and loading carbon black) the b_T gets closer to unity.

We now turn our focus to the dissipation behavior as expressed by G''. From dynamic experiments, the energy loss per cycle of strain is defined as, $\Delta E = \pi\gamma_o^2 G''$,

where γ_o is the strain amplitude[7,22]. Since the loss modulus is proportional to the energy loss, the area under the G'' master curve represents the total energy loss, or dissipation. Thus, the dissipation can be calculated by the area under the area under the loss modulus master curve, $A_{G''}$. Figure 4.7 shows this representation schematically. It is worth noting that only the dissipation in the specified region is investigated. With respect to $\phi_{eff,}$ ψ, φ ψ, the $A_{G''}$ collapses onto a straight line as seen in Figure 4.8. The correlation works best with ψ and φ ψ, which are parameters that take the area between the interfacial area between polymer and filler into consideration. Another parameter that describes the interfacial area per unit volume is $\psi / (1-\phi)$. The correlation with this parameter to dissipation is very good (Figure 4.8d).

The possibility of obtaining a unified description of both linear and nonlinear responses from the Payne effect is a question that requires addressing. Room temperature Payne experiments were performed on all materials studied (refer to Table 4.1) at a frequency of 1Hz. The G' was then normalized according to the expression below (Equation 4-6). As the high amplitude modulus (HAM) could not be directly measured, they were determined using Medalia's modified Guth-Gold equation, $G'_{Medalia} = G'_o(1+2.5\phi_{eff}+14.1\phi_{eff}^2)$. The normalized storage modulus was calculated thus,

$$G'_{normalized} = \frac{G'(\varepsilon) - G'_{Medalia}}{G'_{\varepsilon\to 0} - G'_{Medalia}} \tag{4-6}$$

Figure 4.9 shows that the normalized G' exhibits a systematic effect across filler structures and filler loadings. Kraus proposed an empirical expression for the normalized G' [45]. Expression for the G' is given by

$$\frac{G' - G'_{Medalia}}{G'_{\varepsilon\to 0} - G'_{Medalia}} = \frac{1}{1+(\varepsilon_0 / \varepsilon_c)^a} \tag{4-7}$$

where ε_0 is the strain amplitude and the critical strain amplitude halfway between the low amplitude modulus and the high amplitude modulus, ε_c, and *a* are model parameters. Utilizing Kraus definition, the prediction from the expression was derived for the carbon-black SBR systems and the constants are provided in Table 4.2. The prediction from Kraus along with the original data is shown in Figure 4.9. ε_c and a are said to be filler

independent quantities with *a* said to be between 1 and 1.2 as determined by Heinrich & Kluppel for a wide variety of NR and SBR carbon black materials[22]. The Kraus equation predicts the normalized G' behavior very well (Figure 4.9); however, ε_c and *a* varied significantly. (Table 4.2). The ε_c and *a* are plotted against filler effective volume in Figure 4.10a and 4.10b where generally both parameters decrease nearly linearly with the effective volume fraction, however the points do not collapse on a single curve reflecting either experimental uncertainty (primarily the fact that the HAM values were inaccessible and, hence, were extrapolated from the Medalia equation) or the empirical nature of Kraus equation

4.3 Discussion

The main conclusion of Chapters 2 and 3is the applicability of the TTS to filled materials allowing for the first time searching of the pattern in the linear viscoelastic behavior as expressed in the master curves as a function of filler loading and structure. On examining the storage and loss master curves for the filled system they appear remarkably parallel to those for the unfilled material giving an impression that they may be superposed by simple scaling. Indeed, when the storage modulus master curve of the unfilled material G' is multiplied by a factor it overlaps within experimental uncertainty with the corresponding master curve of the filled material in case of the filler loading of 10phr and 20phr, as shown in Figs. 4.1. In case of the highest loading of 40phr for all structures there is a distinct discrepancy at the frequencies below 0.1Hz, where the actual G' value is under-predicted by the multiplication procedure. This low frequency discrepancy notwithstanding, the simple idea of the G' (filled) being proportional to G' (unfilled) appears to work remarkably (even unexpectedly) well. This opens a possibility of unifying the diversity of the linear viscoelastic data for various filler compositions provided an appropriate descriptor can be found. Figs. 4a and 4b demonstrate that at least two such descriptors, namely the effective volume fraction $\phi_{eff,}$ and the loading-interfacial area parameter $\varphi\ \psi$ are capable of collapsing the entire data set onto a single curve/straight line.

Originally the effective volume fraction[140] and the interfacial area[149] parameters were used to unify the non-linear data, specifically the HAM obtained in the Payne experiment[124]. It is unanticipated that the same descriptors have been shown here to work on the linear viscoelastic properties i.e. LAM. Thus, the findings of this chapter suggest a possibility that the entire Payne effect response including the transient behavior can be unified across filler compositions. Pursuing this idea the Payne tests were carried out on all the systems studied here where the resulting normalized curves are shown in Figs. 4.9. The curves were fit to the phenomenological Krauss equation where the parameters are given in the Table 4.2 and also plotted versus the effective volume fraction in Figs. 4.10. Although the collapse of the data for various filler composition was not achieved (at least of the quality seen in Fig. 4.4) the strong correlation was demonstrated warranting future fruitful research.

G" behavior

The multiplication of the master curve for the unfilled material to obtain the master curve for the filled material does not work nearly as well for the loss modulus G" even for the lowest loading of 10phr as illustrated in Fig. 4.3a. For the highest loading it does not produce any overlap at all (see Fig. 4.3b), provided the multiplicative factor is used that resulted in the overlap of the storage modulus. An alternative idea to the multiplicative factor is the amount of dissipation, which is evaluated as the total area of the G" peak in the frequency domain. Figs. 8 demonstrate that the total dissipation does correlate with the interfacial area of the filler.

loga_T and logb_T

Although the effect of adding the filler on the TTS shift factors is weak overall as was reported in Part I, the systematic changes in both a_T and b_T with the filler composition are captured by the effective volume fraction as illustrated in Figs. 4.5 and 4.6. As we commented in Part I, the behavior of the G' and G" master curve for filled

materials vis-à-vis the unfilled cannot be readily explained by a simple increase in the effective crosslink density. This is because while increase in the crosslink density does result in an increase in the low frequency values of G', it also (i) does not affect high frequency values of G' and (ii) causes a decrease in the low frequency G". Both of these predictions contradict the experimental observations in Figs. 4.1 and 4.3.

It follows that more complicated explanations must be sought. The dissipative processes could be a result of filler-filler contacts, polymer-filler contacts, or likely a combination of both. There have been several schools of thoughts in the literature on the possible dissipative processes occurring in filled elastomers.

Filler network

At high temperatures (corresponding to low frequency on the logfa_T axis), Wang suggests that the main cause of dissipation in a filled rubber is due to the filler network. Percolation theory asserts that a critical loading exists whereby a filler network is formed. This has been probed via dielectric experiments by several authors[151-153]. Although the exact percolation threshold is system specific, it is generally accepted that high volume fraction filler are beyond the percolation threshold, in our case, the 40phr systems. For carbon black, Wang suggest that this filler network is created via a "joint rubber shell mechanism" and the rubber in the joint shell would affect the temperature dependence[7]. The joint shell layer adsorbs more energy resulting in higher hysteresis hence the difference between carbon black structures as seen in the b_TG' behavior at low frequencies and the b_TG'' at high frequencies.

Among other authors, Payne, Kraus and Sternstein have attributed the Payne effect to the breakage and reformation of filler networks[16,45,124] . Hence, the dramatic drop in storage modulus with strain amplitude is a measure of filler networking. The temperature dependence of filler-filler networking can be deduced from the shift factors (Figure 5, 6). As for the large deformation response (Payne), the constants from the Kraus equation ε_c and a were no match to those proposed in the literature. The explanation for ε_c is that it is system specific and depends on the crosslink density of the

polymer. However, the *a* constant has been reported to vary between 1 and 1.32[22,37,45,124] As there was no apparent trend in our findings of these constants with respect to effective volume fraction, this warrants further investigation on our materials.

Polymer filler interaction - Adsorption- desorption

The effect of the interaction between an elastomer and a reinforcing filler produces a filler-polymer gel also known as bound rubber. The idea of bound rubber as part of the filler was first proposed by Brennan *et al.*[154]. An approach to probing the nature of the polymer-filler interaction is through bound rubber measurements usually done by swelling the filled rubber in solvent [155,156]. Hamed & Hatfield proposed that the bound rubber is formed from polymer chains absorbed on different filler particles or trapped polymer entanglements adsorbed on adjacent particles [157]. Hence, bound rubber is more reactive to change in filler structure than surface area as evidenced in carbon black filled SBR studies [158]. The processes that result in creation of bound rubber is believed to have been formed even before crosslinking [159]. Evidence for this is taken from Gent *et al.* who reported no difference in swelling ratio of carbon-black filled cis-polyisoprene or polybutadiene before and after crosslinking[134].

To explain the contribution of bound rubber in viscoelasticity, several theories have been put forth[155,160]. The two-phase model asserts that bound rubber is comprised of two phases with different molecular mobility[159,161-164]. NMR studies by Fukahori identified the polymer layer closest to the filler with a thickness of roughly 0.5-2nm as the Glassy Hard (GH) layer which has restricted polymer mobility [54]. It was shown via NMR experiments that the polymer near the vicinity of the filler experiences lower mobility in comparison to the rest of the bulk polymer and can be said to be in a "glassy state"[162,165-167]. The GH layer effectively increases the diameter of the filler resulting in an increase in the effective volume fraction of filler. In Madelia terms, the GH layer is the occluded rubber, shielded from deformation. The second layer with a thickness of 3-8nm was identified as the Sticky Hard (SH) layer and is the portion of bound rubber that experiences some molecular mobility that increases as the distance from the filler

increases [159]. Evidence for the restricted mobility in the SH layer is illustrated by its inability to completely dissolve in solution. Clearly, the portion closest to the bulk rubber is more mobile which is what dissolves upon swelling. Evidence of an increased GH layer or immobile polymer phase (as some of the SH layer lack mobility) is given by results from bound rubber measurements by Dannenberg [133]. According to Wang[7], the rubber in the GH layer with restricted chain mobility results in a Tg shift to higher temperatures. At low frequency (corresponding to data obtained at high temperatures), the bound rubber content that can be extracted reduces for 70ºC and 80ºC by roughly 8% according to experiments by Wolff *et al.* for carbon back in SBR [155]. This implies a higher amount of extractable rubber at high temperatures, enhanced mobility in the SH layer. Effectively, any mechanical phenomena in the reinforcement by carbon black results from changes to the SH layer since the GH layer is considered as part of the filler. In cases where the GH layer is a small fraction of the filler diameter. e.g. at low filler volumes and structures, the dissipative processes are minimal [54]. This explains why the multiplicative constant works on G'' at low loadings behavior (refer to Figure 3a). The bound rubber content, hence the GH layer is higher for higher structure blacks [168]. For example, in a 50phr loaded carbon black SBR, the difference in bound rubber content for N762 versus N550 is about 54% in favor of the latter (the higher structure) [155]. At larger volume fractions, the contribution from the GH layer is more significant, approximately 10% of the filler diameter. Therefore, dissipative processes are more difficult to predict. The linear proportion of bound rubber to carbon black loading has been observed by several authors[133,155,157,168].

The effective volume concept works well with linear viscoelastic behavior. It is worth noting that Medalia's derivation of the effective volume fraction, [169]does not take into the account the nature of the rubber. Also, the shape of the filler aggregates and the polymer-filler interactions cannot be fully accounted for at high loading despite the fact that experiments were conducted in the linear viscoelastic regime. An additional set back as pointed out by Funt is that the differentiation between filler structures in their G' behavior is not observed if the rubber were to be uncured[112]. Despite this setback, for filled elastomers, the effective volume concept correlates well with $A_{G''}$ (Figure4.8).

Table 4.1: Filler and viscoelasticic properties of carbon black filled SBR

Carbon Black	Loading, phr	ϕ	$\phi_{effective}$	ψ, m^2/cm^3	$\phi\psi$, m^2/cm^3	$1/(1-\phi)$, m^2/cm^3	$A_{G''}$	C_ϕ	$fa_T = 10^{-2}$ Hz		
									Tan δ	$G''b_T$ (MPa)	$G'b_T$ (MPa)
N550	40	0.17	0.42	12.92	2.20	15.57	2.56	3.78	0.23	0.91	0.21
	20	0.09	0.23	6.84	0.62	7.52	1.46	2.16	0.18	0.57	0.10
	10	0.05	0.12	3.80	0.19	4.00	0.86	1.64	0.14	0.43	0.06
N762	40	0.17	0.29	8.31	1.41	10.01	1.66	2.61	0.20	0.62	0.13
	20	0.09	0.16	4.40	0.40	4.83	1.03	1.64	0.18	0.43	0.08
	10	0.05	0.09	2.44	0.12	2.57	0.84	1.42	0.15	0.39	0.06
N990	40	0.17	0.22	2.77	0.47	3.33	0.99	1.81	0.20	0.39	0.08
	20	0.09	0.12	1.47	0.13	1.61	0.81	1.41	0.16	0.33	0.05
	10	0.05	0.06	0.82	0.04	0.86	0.80	1.36	0.15	0.38	0.06
Unfilled	0	0	0	0	0	0	0.58	1.00	0.13	0.28	0.04

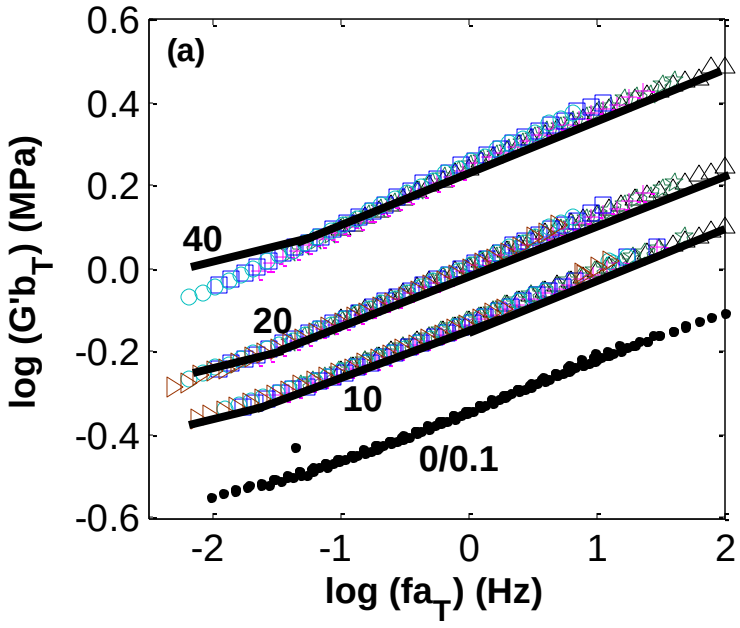
(a)
40
20
10
0/0.1
log (G'b$_T$) (MPa)
log (fa$_T$) (Hz)
0.6
0.4
0.2
0.0
-0.2
-0.4
-0.6
-2
-1
0
1
2

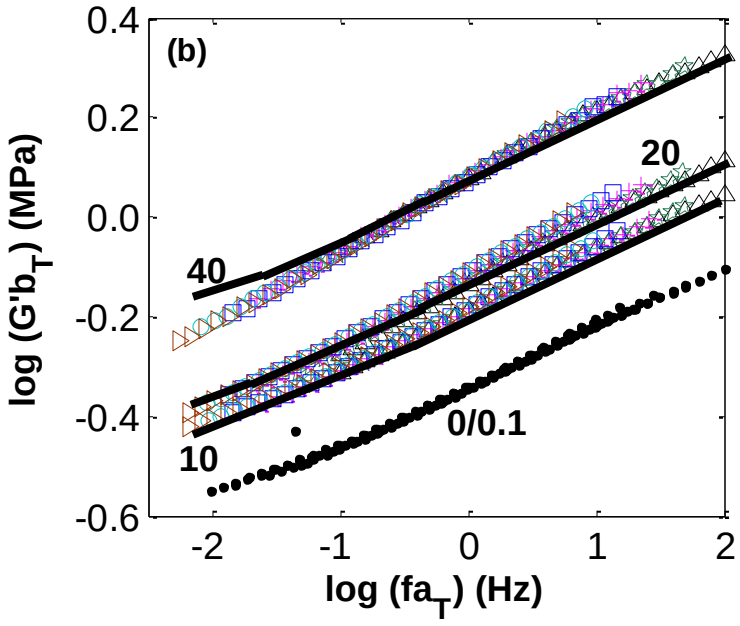
(b)
40
20
10
0/0.1
log (G'b$_T$) (MPa)
log (fa$_T$) (Hz)
0.4
0.2
0.0
-0.2
-0.4
-0.6
-2
-1
0
1
2

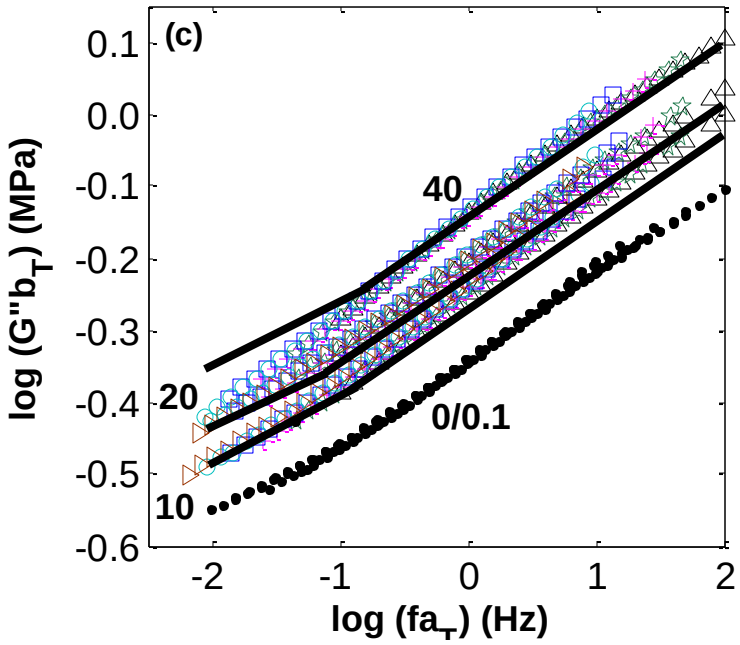

Figure 4.1: Storage modulus prediction of filled master curves from using multiplicative factor,C_{φ} on the reference unfilled elasomer (solid lines). Master curves for (a) N550 (b) N762 and (c) N990 carbon black filled SBR cured with 0.1phr DCP. The reference unfilled SBR[126] with 0.1 phr DCP (●) is also plotted for comparison. Filler loading is indicated on figure in phr. Temperatures (in ^{o}C) are as follows: △ 30, ☆ 40, + 50, □ 60, ○ 70, ▷ 80.

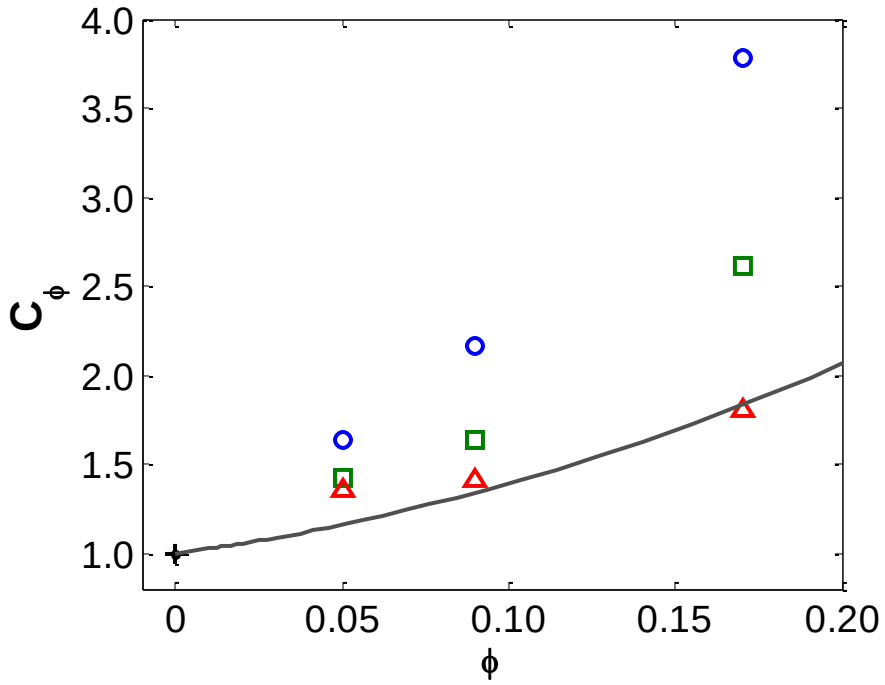

Figure 4.2: Correlation of C_φ to volume fraction for 0.1 phr DCP cured SBR with N990 (△), N762 (□), and N550 (○) carbon blacks. The unfilled SBR[126] with 0.1 phr DCP) (+) and the Guth-Gold prediction (solid line) are also plotted.

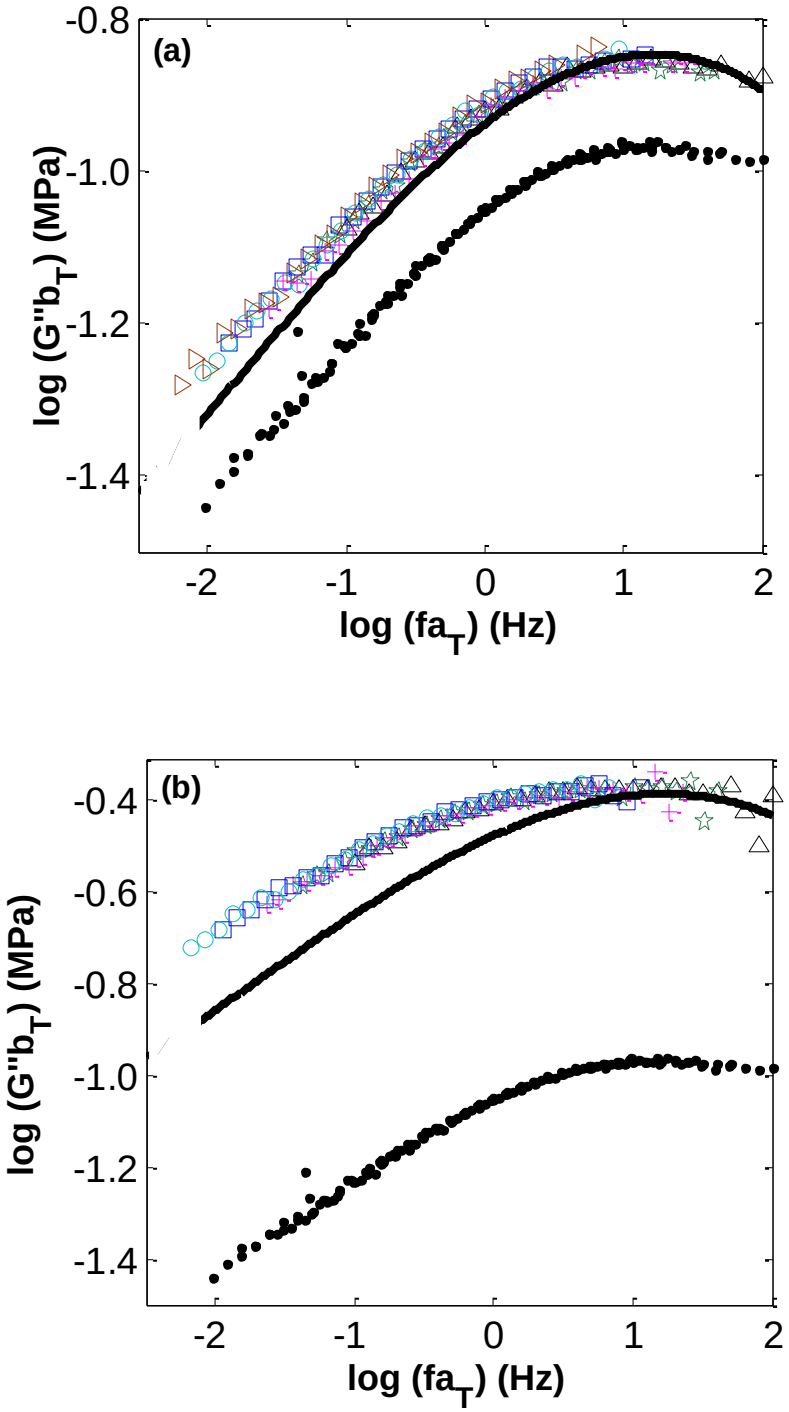

Figure 4.3: Loss modulus prediction of filled master curves using multiplicative factor, C_φ on the reference unfilled elasomer (solid line). Master curves for 0.1 phr DCP cured SBR with (a) 10phr N990 and (b) 40phr of N550 carbon blacks. The reference unfilled SBR[126] with 0.1 phr DCP (●) is also plotted for comparison. Symbols for the temperatures (in ^oC) are provided in Figure 4.1.

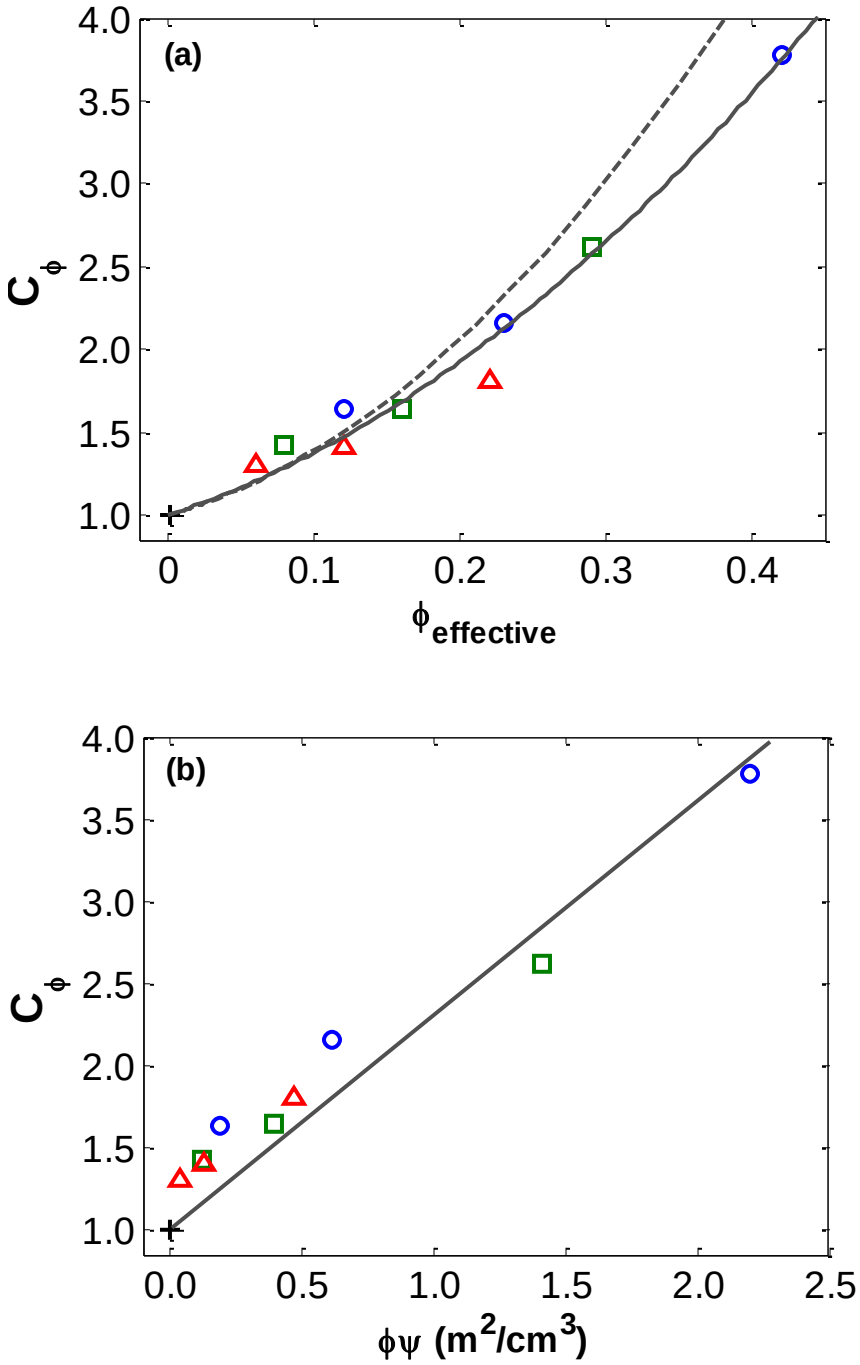

Figure 4.4: Correlation of C_φ to (a) effective volume fraction and to (b) loading-interfacial area for 0.1 phr DCP cured SBR with N990 (△), N762 (□), and N550 (○) carbon blacks and the unfilled SBR[126] with 0.1 phr DCP) (+). In (a) our fit to the data (solid line) and Medalia's modified Guth-Gold equation (dashed line) are also plotted. In (b) the line of best fit (solid line) is plotted.

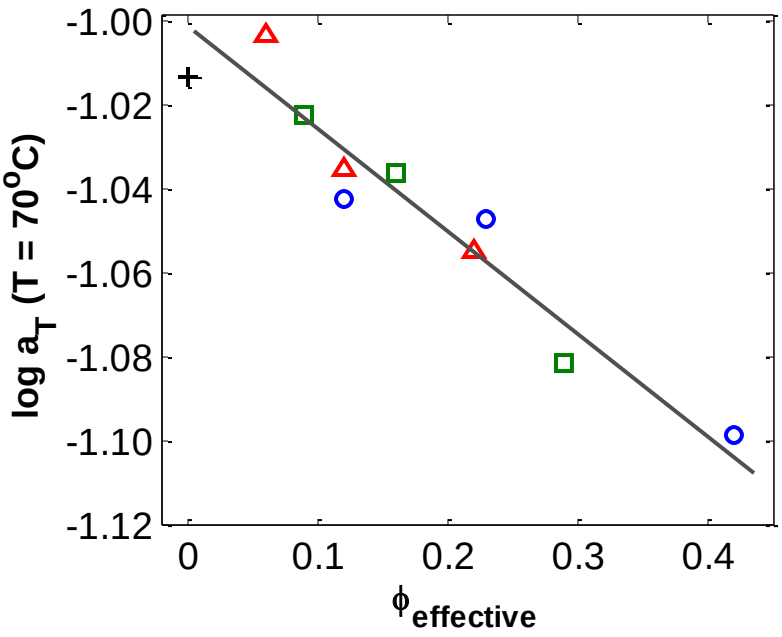

Figure 4.5: Log a_T dependence on the effective volume fraction at 70ºC for 0.1 phr DCP cured SBR with N990 (△), N762 (□), and N550 (○) carbon blacks. The reference unfilled SBR with 0.1 phr DCP[126] (+) is also plotted. The solid line is the fit to the data.

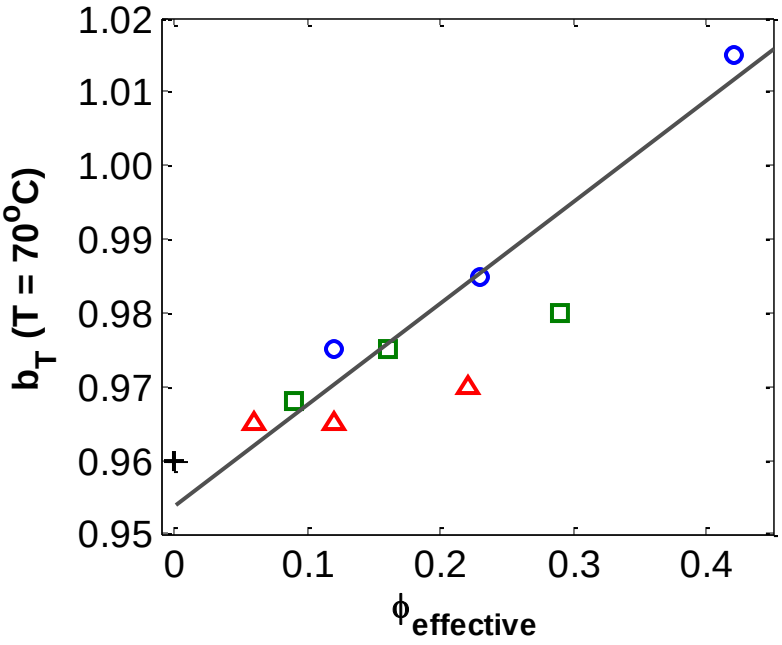

Figure 4.6: b_T dependence on the effective volume fraction at 70ºC for 0.1 phr DCP cured SBR with N990 (△), N762 (□), and N550 (○) carbon blacks. The reference unfilled SBR[126] with 0.1 phr DCP (+) is also plotted. The solid line is the fit to the data.

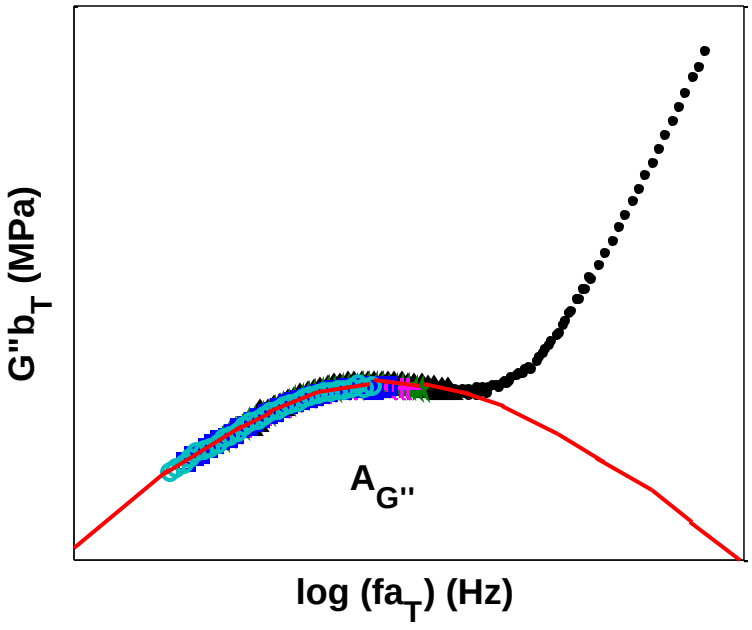

Figure 4.7: Schematic showing dissipation, $A_{G''}$ total area under the G'' mastercurve.

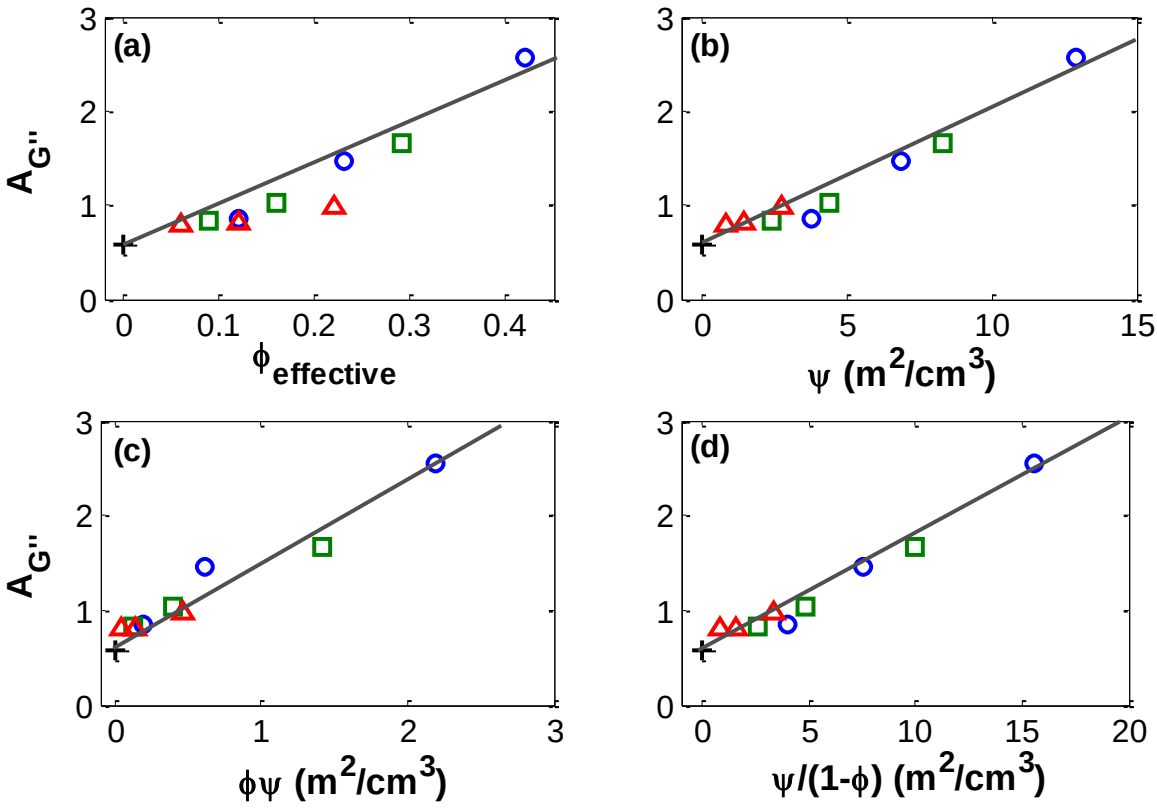

Figure 4.8: Dissipation, $A_{G''}$, as a function of filler parameters for SBR cured with 0.1phr DCP and with either N990 (△), N762 (□) or (N550 (○) carbon black. The reference unfilled SBR[126] with 0.1 phr DCP is also shown (+).The correlation with respect to (a) effective volume fraction (b) interfacial area, (c) loading-interfacial area, and (d) ratio of interfacial area per polymer volume fraction is given.

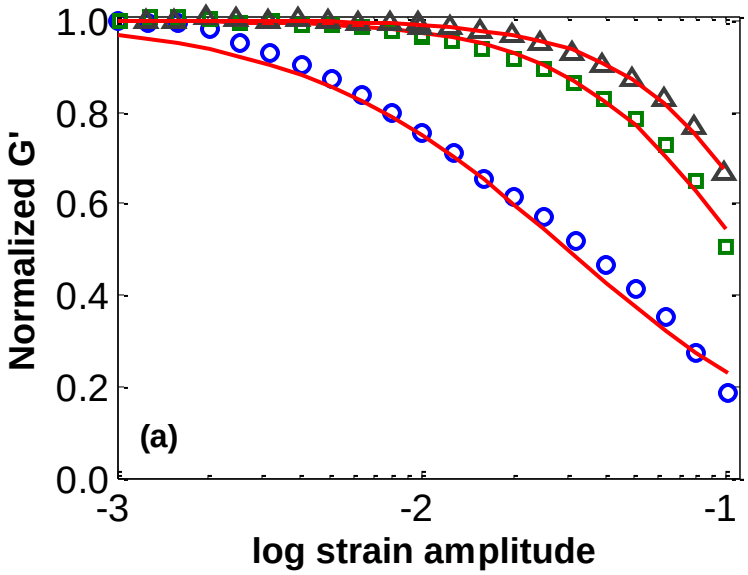
1.0
0.8
0.6
0.4
0.2
0.0
Normalized G'
(a)
-3
-2
-1
log strain amplitude

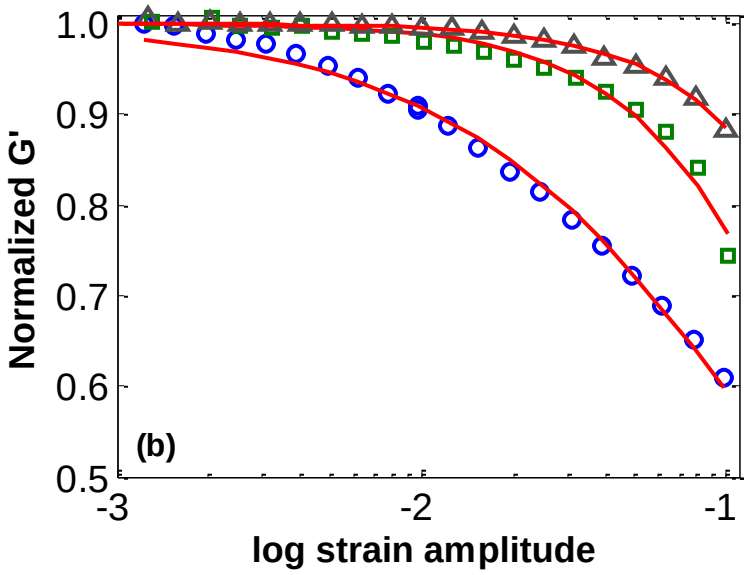
1.0
0.9
0.8
0.7
0.6
0.5
Normalized G'
(b)
-3
-2
-1
log strain amplitude

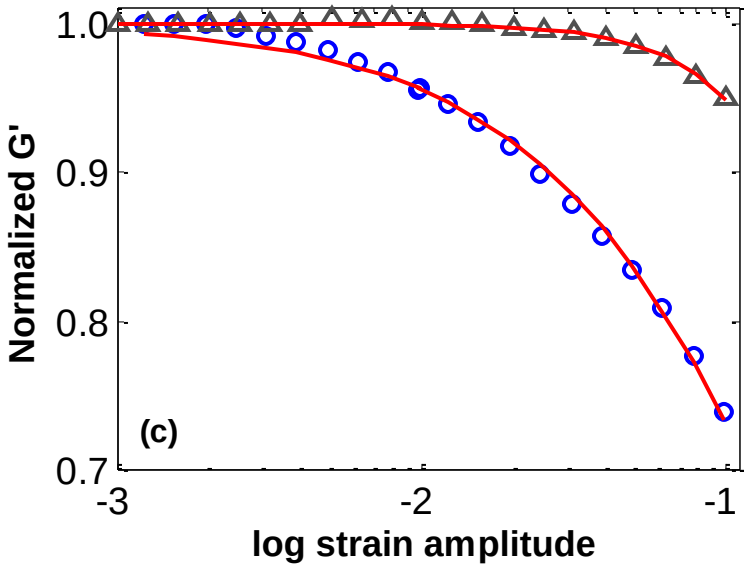

Figure 4.9: Normalized storage modulus with fit from Kraus equation (solid line) as a function of strain amplitude for 0.1 DCP cured SBR filled with (a) N550, (b) N762, and (c) N990 carbon blacks. Symbols are filler loadings in phr: 10 (△), 20 (□) and 40 (○).

Table 4.2: Kraus constants for normalized G' in Figure 4.9

Carbon Black	Loading, phr	a	γ_c
N550	40	1.0543	0.0322
	20	1.4836	0.1133
	10	1.6822	0.1531
N762	40	0.8281	0.1581
	20	1.3989	0.2387
	10	1.4536	0.4109
N990	40	0.9004	0.3036
	10	1.8943	0.4699

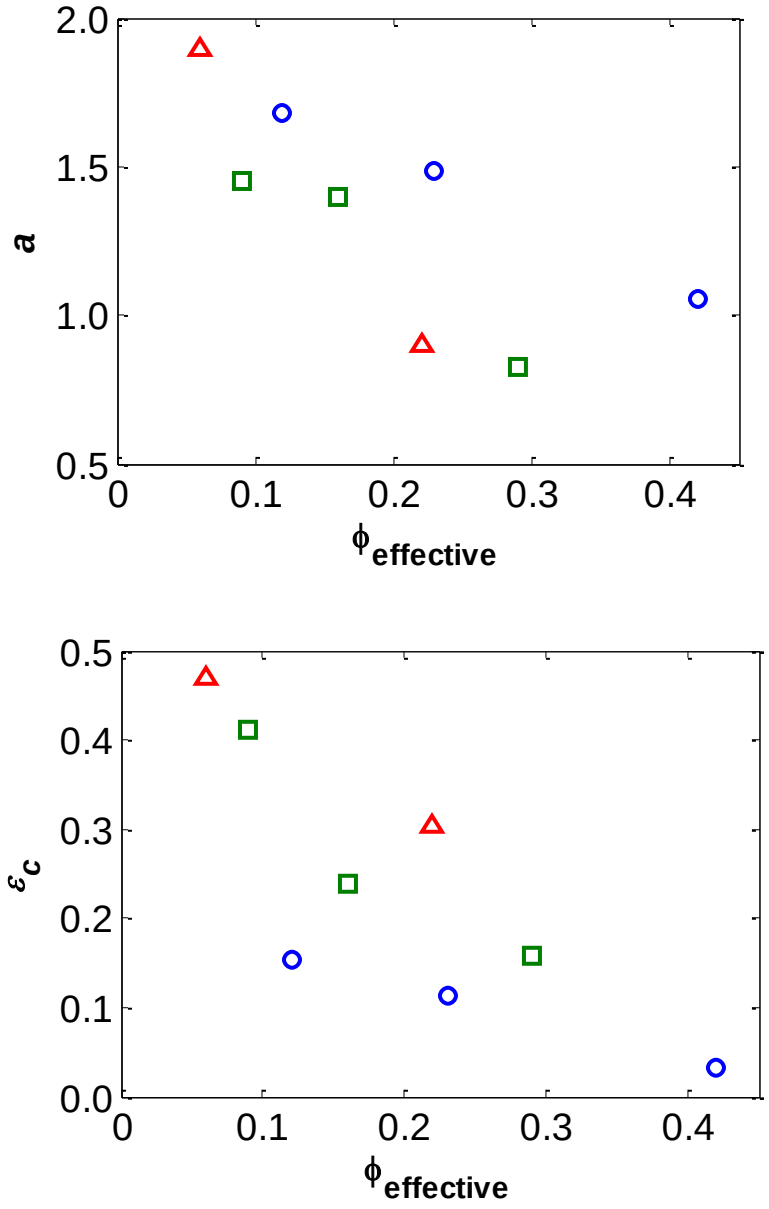

Figure 4.10: Kraus parameters showing the constants (a) *a* and (b) ε_c as a function of the effective volume fraction for 0.1phr DCP cured SBR filled with N990 (△), N762 (□) and N550 (○) carbon blacks.

CHAPTER 5. NECKING IN FUMED SILICA POLY (DIMETHYLSILOXANE) AND THE RESULTING PROPERTIES OF THE NECKED MATERIAL

This Chapter is Derived from a Manuscript Published with Co-authors G.A Medvedev and J.M. Caruthers in *Polymer* (Jan 2013).

5.1 Introduction

Filled elastomer systems are engineering materials with enhanced mechanical properties, including higher modulus, improved tensile strength, and greater tear resistance as compared to the unfilled elastomer. The nonlinear mechanical behavior of filled elastomers is quite complex exhibiting (i) stress-strain behavior with stress softening in cyclic uniaxial and shear deformations (i.e. the Mullins effect)[5,9,61,170], (ii) dynamic modulus that depends upon the strain amplitude and loading history (i.e. the Payne effect) [5,9,16,26], and (iii) a variety of other non-linear effects [5,9]. A number of mechanisms have been proposed to explain these effects as well as the primary effect of filler reinforcement [5,7,9,16,20,21,24,26,33,40,61,93]; however, a fundamental understanding remains incomplete. There have been numerous studies of the large deformation behavior of filled elastomers including fumed silica in PDMS systems [19,24,31,34,35,37,63,171-174], where the review articles by Diani *et al.*[61] and Heinrich *et al.*[40] contain extensive references to papers where the properties of polymer and filler were varied and the resulting mechanical response investigated.

The work in this chapter is part of a larger study of the mechanical properties of silica filled poly(dimethylsiloxane), PDMS, elastomer systems, where the time-dependent, nonlinear mechanical behavior is being investigated as a function of the composition of the filled elastomers. In the course of this study, an unanticipated necking

phenomenon was observed for specific fumed silica filled PDMS systems. The resulting mechanical properties and the composition requirement for necking in these elastomer systems are the focus of this communication. Although there have been numerous studies of the nonlinear mechanical properties of PDMS filled with both carbon black and fumed silica particulates [19,24,31,34,35,37,63,174], to the best of our knowledge this is the first time that necking has been reported for silica filled PDMS or, more generally, for any unfilled or filled elastomer system. As will be discussed in this chapter, the conditions for necking are (i) a high filler surface area (which is equivalent to small primary particles), (ii) filler aggregates with high structure and (iii) strong bonding between the filler surface and the polymer. We believe that this specific set of compositional requirement has not been met in previous studies of particulate elastomer systems.

In this chapter, we will report on fumed silica filled elastomers that can exhibit necking, including the nonlinear stress-strain behavior, dynamic mechanical response, tensile strength, and tear resistance of these filled elastomers. This chapter is organized as follows: In the Experimental Section, the filled elastomer synthesis and the mechanical testing setups are described. In the Results Section, the formation of a neck as the filled elastomer is subjected to uniaxial tension test is presented as well as the mechanical characterization of the necked material. Finally, in the Discussion section, a possible mechanism responsible for the necking behavior will be proposed.

5.2 Experimental

The elastomer was trimethylsiloxy-terminated PDMS (DMS-T72, Gelest Inc) with a kinematic viscosity of 2 million cSt and a weight average molecular weight of greater than 500,000 g/mol as reported by the manufacturer. Evonik, Inc provided hydrophilic, pyrogenic fumed silica with varying surface areas as given in Table 5.1, where the surface of the fumed silica is hydroxylated and consequently interacts with the PDMS primarily via hydrogen bonds. The surface area of the hydrophilic silica ranges from 50 to 380m^2/g. The PDMS was cured using Dicumyl Peroxide (DCP) at 1phr (parts of DCP per 100 parts by weight of rubber). The PDMS and silica were mixed in a

Brabender internal mixer for 10 minutes followed by several passes through a two-roll mill for an additional 10 minutes, during which time the DCP was added. The mixture was then molded in a hot press (Carver Inc.) at 170°C under a pressure of 15,000lbs for 90 minutes to produce a square sheet (100mm x 100mm x 3mm) of the silica filled PDMS. Test specimens were then cut from this sheet. Various compositions of fumed silica filled PDMS elastomers test specimens were manufactured using this procedure.

Room temperature tensile tests were performed at a constant extension rate of 50 mm/min (i.e. a strain rate of approximately $0.01s^{-1}$), using an Instron 5567 testing instrument with a ±1000 N load cell. The axial strains were determined using an Instron Advanced Video extensometer unless specified otherwise. This setup was also used to measure the (i) tensile strength and (ii) tear resistance using the trouser test geometry. The sample dimensions for the Instron testing were 57mm x 19.6mm x 3.3mm for the standard samples and 60mm x 4.4mm x 2.5mm for the necked samples.
Dynamic experiments were performed using a Dyanstat dynamic mechanical tester using a double shear sandwich test fixture. Payne experiments at strain amplitudes from 0.01 to 10% were carried out at room temperature at a constant frequency of 1Hz. The sample dimensions for the Dynastat shear testing are 15mm x 15mm x 3

5.3 Results

Stress-strain curves in uniaxial extension are shown in Fig. 5.1 for PDMS filled with 40phr of particulate silica for four different surface area fumed silica. The OX50 and A150 filled systems exhibit the well known stress-strain behavior of highly filled elastomers. Specifically, upon the first loading the stress-strain curve exhibits a tangent modulus that decreases from the initial value up through moderate deformations; subsequently, the modulus begins to exhibit strain hardening at large deformations. Upon unloading of the OX50 and A150 filled materials, there is a dramatic decrease in the stress, where the tangent modulus of the unloading curve can be an order-of-magnitude greater than the modulus just prior to unloading. The difference between the loading and

unloading stress-strain curves results in considerable hysteresis, and upon unloading to zero stress there is a significant 'permanent' set in the material, where most of the 'permanent' set can be recovered upon resting for sufficient time in the load free state. The deformation of the OX50 and A150 test specimens is spatially uniform. In contrast to the stress-strain behavior exhibited by the OX50 and A150 filled systems, both the A300 and A380 filled PDMS exhibit a pronounced decrease in local cross-section area when subjected to uniaxial tension, which gradually extended to the entire specimen length between the grips, i.e. a neck is formed and propagates. The stress-strain response for the A300 and A380 filled PDMS systems is characterized by three distinct regions: (i) an initial region of rapidly rising stress, (ii) a region where the axial force (or equivalently the engineering stress) is constant until the necking reaches the grips and (iii) a region where stress increases again corresponding to further deformation of the necked material. A specimen that undergoes necking does not recover its original shape upon resting in the load free state even when the material is allowed to relax for several days at 100^{o}C. For the A380 filled PDMS material, the strains in Fig. 5.1 were measured using the crosshead displacement as the video extensometer failed after the necking started; consequently, the post necking portion for A380 stress-strain curve may also include necking that is continuing to occur within the gripped parts of the specimen. Neck formation was only observed for fumed silica filled PDMS with particulates having 300 or 380 m^2/g specific surface area.

The stress-strain behavior of the necked material is shown in Fig. 5.2 for a 35phr A380 filled PDMS specimen, where the primary question is if any more necking on top of the original necking occurs. The procedure for testing of the necked material in uniaxial deformation involved: (i) releasing the original specimen that underwent necking from the grips, (ii) cutting a new test specimen from the neck region, and (iii) re-gripping this specimen in the Instron test instrument. The strain in the necked material shown in Fig. 5.2 is defined as $\varepsilon = \Delta l / l_o$, where Δl is the change in length and l_o is the initial specimen length, which is new for each specimen. The stress-strain curve of the virgin material (solid line) has a characteristic flat region corresponding to neck formation and growth similar to the one seen in Fig. 5.1. The stress-strain curve of the specimen cut

from the necked portion of the original sample does not have a flat region as shown in Fig. 5.2 (circles). When this specimen is released and re-gripped, the stress-strain curve is obtained shown in Fig 5.2 as triangles. With each re-gripping the material reaches higher tensile stress values for the same strains. However, the initial modulus appears to be decreasing from the highest value observed for the virgin material. The dimensions of the specimens in Fig. 2 are given in Table. 5.2. The significant decrease in the width and thickness, i.e. from specimen 1 (solid line) to specimen 2 (circles) shows the severity of the necking that occurs. There is still a reduction in the width and thickness of specimen 3 (triangles) as compared with specimen 2 but not as dramatic. Finally, comparison between specimens 4 and 3 demonstrates that virtually no more changes in the specimen dimensions are occurring.

The tensile strength of the necked material was tested in accordance to ASTM D412 using dogbone specimens cut from the neck region. Examining the stress-strain curve in Fig. 5.3, the necked material exhibited a lower initial elastic modulus as compared to the virgin material, no further necking and increased tensile strength. The 40phr A300 filled PDMS can be deformed by an additional 330% after the neck is formed with a tensile strength of 8.9 MPa. For comparison the stress-strain curve of PDMS filled with 30phr A150 fumed silica is also shown in Fig. 5.3, where it can be deformed to approximately 440% strain before failure with a tensile strength of 3.2 MPa. The necked A380 filled elastomer exhibits a tensile strength that is roughly 3 times that of the A150 filled elastomer, where both materials have 40 phr of the fumed silica. The tensile strength and elongation at break of the fumed silica filled PDMS elastomer systems examined in this study are given in Table 5.3.

The stress-strain behavior of the A300 filled PDMS systems at various filler volume fractions was investigated, where a filler loading of 30phr (i.e. a volume fraction of 12%) or higher is required for necking. A similar dependence on filler volume fraction was also observed for the A380 filled PDMS elastomers, where necking also requires at least 30phr silica loading. In an attempt to verify whether lower silica surface area composites would neck at higher filler volume fraction, the filler content in the OX50 and A150 filled PDMS systems was increased to 100phr and 60phr respectively, where the

specimens fractured at respective strains of 167% and 179% and there was no sign of necking for both materials. The stress-strain curves for the 100phr OX50, 60phrA150 and for 40phr filled materials are provided in Appendix C.

The effect of the aggregate size, i.e. the number of primary particles in a fumed silica particulate, on the nonlinear stress-strain behavior was studied using fumed silica - A300SP (Evonik, Inc.). A300SP has surface area of $300m^2/g$ just like the A300, but according to the manufacturer consists of smaller aggregates. Since the surface area is primarily a function of the size of the primary particles that comprise the aggregate, the primary particle size is essentially the same for the A300 and A300SP fillers. The stress-strain behavior for 30phr of the A300SP filled PDMS material is shown in Figure 5.4 as well as the stress-strain behavior for 30phr of the A300 material. The A300 filled PDMS exhibits necking from a strain of approximately 10% to 130%, which is clearly seen upon examining the tensile specimen, although the necking is not as pronounced as that seen in the necked region of stress-strain curve for A300 filled material shown in Fig. 5.1 (where filler loading is 40phr). In contrast, the A300SP filled PDMS does not exhibit necking. The initial modulus of the A300 and A300SP filled elastomers is nearly the same, where the initial high modulus response extends to a higher stress for the A300SP filled PDMS. However, at strains larger than 20% A300SP filled PDMS exhibits first a sharp decrease in the tangent modulus and then a steady increase in the tangent modulus with no necking vs. the necking exhibited by the A300 filled elastomer. Both materials exhibit significant hysteresis, although the permanent set in the necked A300 filled PDMS is larger. In summary, a requirement for necking is that the fumed silica aggregates have a large number of primary particles (and presumably a larger overall size).

The tear resistance was measured using the ASTM D624 trouser test method for a number of fumed silica filled PDMS elastomers and the results are reported in Table 5.3. For the A300 material that necked, the trouser test specimen was prepared by cutting out the necked portion and then cutting it in a trouser form. The tear resistance was determined to be 55 kN/m for the A300 filled PDMS material, the highest for all the materials tested. The tear resistance increases with the surface area of the silica, but there appears to be no clear correlation between tear resistance and necking.

The dynamic mechanical behavior of non-necked and necked silica filled PDMS systems was studied in a shear deformation, where the amplitude of the applied oscillatory shear strain was systematically increased from 10^{-4} to 10^{-1}, i.e. a Payne experiment. The frequency of oscillation was 1Hz and the experiments were carried out at room temperature. The specimens were allowed to rest for a minimum of 1hr after loading into the shear test fixture to ensure the relaxation of any effects due to loading into the apparatus. In Fig. 5.5a the typical Payne experiment results are shown for the A150 filled PDMS material, where the storage modulus starts decreasing at strain amplitude of approximately 0.3%. In Fig. 5.5b a similar result is shown for a virgin A300 filled material, where the modulus at small strain amplitudes is 3.7MPa and at a strain amplitude of 0.8% there begins a dramatic decrease in the modulus. When the deformation is stopped, the dynamic response recovers to 90% of the small amplitude storage modulus value within minutes, and the recovery is complete if the sample is allowed to rest (approximately 1 hour for A150 and 2 hours for A300). The initial modulus and magnitude of modulus decrease are larger for the A300 filled elastomer as compared to the A150 material, which is consistent with higher surface area of the A300 fumed silica. The results above for the filled elastomers not subjected to pre-deformation are consistent with what is typically observed in the dynamic response of particulate filled elastomers in a Payne experiment [24].

Also shown in Fig. 5.5a are the dynamic responses for an A150 filled elastomer that was subjected to the following deformation history: (i) a specimen was deformed in constant strain rate uniaxial extension to 300% strain, (ii) the strain was reversed until that tensile stress was zero (and there was 87% permanent set), (iii) shear test specimens were cut from the deformed specimen, and (iv) a Payne experiment was performed. Payne experiments were performed on two different shear specimens: one where the direction of the shear deformation was parallel to the axis of the uniaxial deformation and a second where the shear was perpendicular to the uniaxial deformation. The dynamic modulus is shown in Fig. 5.5a, where the deformed material has a lower storage modulus as compared to that of the virgin material, where again G' begins to decrease at approximately 0.3% strain. There is essentially no difference in the Payne experiment

when the shear deformation is parallel vs. perpendicular to the direction of the 300% tensile deformation. The data show that once unloaded, the A150 filled PDMS elastomer is isotropic at least for strains of 10% or less and for times greater than 5 minutes needed to perform the Payne experiment.

The dynamic modulus is shown in Fig. 5.5b for the necked material of the A300 filled PDMS elastomer. A300 filled test specimens for the Payne experiment was prepared in a similar manner to that described above for the A150 filled PDMS. Similar to the A150-PDMS system, the deformed (necked) A300 filled PDMS elastomer exhibits lower storage modulus than that of the undeformed (i.e. non-necked) elastomer; however, the necked material exhibits considerable anisotropy. The necked material is almost 2 times stiffer in the direction of the original tensile deformation than in the direction perpendicular to the original tensile deformation. This anisotropy appears to be permanent, where waiting for two days did not change the anisotropic behavior.

Finally, a Mullins experiment was also performed on the necked material, where the results are shown in Fig. 5.6. The material is subjected to a series of loading and unloading cycles, where the maximum strain is increased for each cycle. The direction of deformation for the stress-strain response shown in Fig. 5.6 is the same as the uniaxial deformation that caused the necking. The typical features of the Mullins effect are observed for the necked 30phr A300 filled PDMS (i.e. large hysteresis, stress softening, and return to the stress-strain curve of the virgin material once previous maximum strain is reached). Thus, the necked material exhibit stress-strain behavior consistent with that typically observed for filled elastomers.

5.4 Discussion

In this work, we report on the necking of fumed silica filled PDMS. Although necking is well known in amorphous polymers below T_g as well as in semi-crystalline polymers [175,176], we believe that this is the first report of necking occurring in a filled amorphous polymer well above its T_g (the T_g of PDMS is -125°C) [177]. At room temperature PDMS does not exhibit crystallinity; thus, crystallinity can be ruled out as a

mechanistic explanation for the observed necking. Consequently, the observed necking behavior must be due to the presence of the particulate fillers and not due to the rubber matrix.

Necking only occurs over a narrow range of compositions for the fumed silica filled PDMS; specifically, (i) the volume fraction has to be 30phr (i.e. 12 volume percent) or greater, (ii) the fumed silica must have a surface area of 300 m^2/g or greater, (iii) the aggregate size must be large (see comparison between A300 and A300SP in Fig. 5.4), and (iv) there must be strong adhesion between the rubber matrix and the filler particles. The last point is supported by the observation that no necking was observed in the systems where the silica surface was treated/passivated in both this work and the literature[101,178,179].

Numerous studies of the mechanical properties of fumed silica filled PDMS elastomers have been reported in the literature, although none have reported necking. Cochrane and Lin [180] studied the mechanical properties of fumed silica filled PDMS and were able to achieve a high filler content of 55phr by employing a processing aid. They used the fumed silica with the surface area of $200m^2/g$; thus, based upon the results shown in this communication necking would not be anticipated, since a surface area of $300m^2/g$ or higher is needed for the necking. Additional studies on other fumed silica filled PDMS elastomers either used lower surface area silica [19] or surface treated silica [19,173], where the passivated silica surface is not expected to adhere strongly to the polymer matrix; consequently, necking would also not be expected for these systems. Finally, studies of Yatsuyanagi *et al.*[41] with fumed silica in SBR also did not exhibit necking, which is again consistent with weaker polymer-filler interactions as compared to the PDMS-silica interface. In summary, other silica-filled systems, in which necking was not observed, did not meet the requirements given above for the primary particulate size (as determined by specific surface area) and the mechanical strength of the particulate-polymer interface.

A mechanism for describing the necking of the fumed silica filled PDMS elastomer must take into account all the key observations reported in this study; specifically,

1. Necking requires particulate fillers with high structure, high surface area and strong polymer-filler adsorption;
2. Necking is not recoverable with time and temperature;
3. The tensile strength is higher for the necked materials as compared to filled elastomers that do not neck; and,
4. The dynamic shear modulus in the necked materials is anisotropic.

We will now critically examine several potential mechanisms that have been proposed to describe the large deformation behavior of filled rubbers[5,9,26,181] with respect to the four observations described above. It is clear that some type of deformation induced damage is occurring in the filler-polymer network, where the permanency of the damage and the microstructural origin of the damage remains a subject of debate [5,43]. Postulated damage mechanisms include (i) chains scission [38,39,50,79], (ii) chains desorption from the filler surface [99,100] and (iii) aggregates/agglomerates breakage[40,42]. In what follows we consider the plausibility for each of these mechanisms to be responsible for the necking phenomenon. Chains desorption is unlikely, since necking is not observed in the systems with weaker bonding between the fillers and the matrix, e.g. fumed silica with a passivated surface in PDMS or carbon black in SBR. Chains scission is unlikely to be responsible for the necking phenomenon for the following reasons: (i) aggregate size is the principle difference between the A300 filled PDMS that shows necking and A300SP filled PDMS that does not exhibit necking, where there is no reason why the chains scission would be occurring in the former but not the latter; also, (ii) in case of the chains scission the resulting unattached portions of the chains would likely retract into random coil configurations, where it is difficult to identify the source of the anisotropy in the modulus observed in the dynamic experiment. Breakage of agglomerates is likely to be reversible and, hence, is ruled out because the original state of the material before necking is irrecoverable. Thus, the breakage of filler aggregates emerges as a prime candidate as the mechanism of necking consistent with the experimentally observed phenomena. Aggregate breakage would be expected in the systems where (i) the size of the primary particles is small, i.e. for fillers with large surface area, and hence the fused area between particles is also small with less particle-to-particle strength, (ii) aggregate

structure has long branches so that under deformation an aggregate experiences large forces and torques due to local heterogeneities in the deformation field, and (iii) the coupling between the fillers and the polymer chains is strong, thereby ensuring that the aggregates break before the bonds at the filler-polymer interface. As reported in this chapter, these are same conditions that needed for the filled elastomer to exhibit necking.

A schematic representation of the postulated aggregate breaking mechanism during necking of fumed silica filled PDMS is shown in Fig. 5.7. Because of the random location and orientation of the particles in addition to the inherent size/shape distribution of the particulates, there will be a distribution in the magnitude and orientation of the local stresses, where the macroscopically observed stress is the average of these local stresses. As illustrated in Fig. 5.7a, when the material is deformed there is a broad distribution of local forces/torques acting on an aggregate, where there will be instances of very large forces shown in red. If the forces/torques are sufficiently large and the strength of the aggregate is small, the aggregate can break. Once the aggregate breaks the forces/torques will be redistributed in such a way that there is a more uniform sharing of the load. This is shown schematically in Fig. 5.7, where there are both large (i.e. red) and small (i.e. blue) forces in the deformed material just prior to formation of the neck in contrast to a more uniform distribution with only intermediate forces in the necked material. As a result of aggregate breaking during necking, the peak values of the forces are reduced by the re-arrangement of the pieces of the broken aggregates in order to re-equilibrate the total force and torque on the individual particulates. In a material undergoing necking the most ‘distressed’ aggregates break, where the level of aggregate ‘distress’ is a combination of the size of the aggregate (larger aggregates are more likely to experience disparate forces transferred by the matrix resin) and the inherent local non-uniformity of composition in a highly filled particulate system. Although not a mechanistic proof, the above picture is consistent with the experimental observations of necking reported in this communication. Specifically, A300 silica aggregates are made up of small 7nm diameter primary particles and have a high structure with more than eighty primary particles per aggregate[182]. Based upon the aggregate breakage postulate described above, this highly branched structure fragments during large deformation

causing the A300-PDMS material to neck. In contrast, in the low surface area (i.e. large primary particle) systems like A90, A150, A200 the contact area between the primary particles that make up the aggregate is larger, and hence particle-to-particle strength is greater. Consequently, when a large external stress is applied to these lower surface area particulate fillers, the polymer will detach from the particulate surface before the aggregates can break – thus, necking does not occur. Also, if the surface has been passivated, the polymer matrix will detach before aggregate breakage occurs, consistent with the observation that systems with weaker polymer particulate interactions due to passivation as well as carbon black filled systems do not exhibit necking.

The aggregate breakage mechanism provides an explanation for the high ultimate properties of the necked material. During necking the breakage of aggregates is not random, but at stress concentrations so that the deformed material moves towards a lower energy state. As a result, a more regular effective polymer-filler network is created as compared to the non-necking material where the particulate-polymer network remains random. It is well known in unfilled elastomers that a regular network has higher ultimate properties[183,184]. Specifically, in a random network the short chains support a disproportionate amount of the load and break first, followed by the breaking of chains of increasing length as the deformation continues. In contrast, in a regular network most of the chains reach their extensibility limit together, thus there are more active chains supporting the stress resulting in an increase in ultimate properties like tensile strength and to a lesser degree tear resistance. Aggregate breakage is a mechanism that results in the deformation induced formation of a more regular polymer-particulate network (at least more regular in the stress bearing sense) thereby increasing the tensile strength. As for the anisotropy exhibited in the dynamic storage modulus exhibited at low strain amplitudes (see Fig. 5.5), the breakage and realignment of aggregates during necking produces a configuration where the rubber chains are oriented in the direction of the stretch. The breakage of aggregates is permanent, which explains why the anisotropy in the Payne effect does not recover with time.

An interesting observation with the implications for understanding the nature of the stress softening is the Mullins behavior observed in the necked material. Some

authors [42] have speculated that the Mullins effect is caused by the breakage of aggregates/agglomerates; thus, if significant aggregate breakage has occurred in the necked material, the Mullins effect may be expected to be eliminated or at least significantly reduced. However, the Mullins effect was observed in the necked material. Thus, breaking of aggregates appears not to be the predominant mechanism behind the Mullins effect, at least for the highly branched silica in PDMS systems investigated in this study.

In summary, necking in fumed silica filled PDMS elastomers has been reported for the first time, where the conditions needed for necking are a surface area greater than $300m^2/g$, filler loading greater than 30phr and particulates with a high structure, i.e. untreated fumed silica with large aggregates. The ultimate properties of the necked material were superior to its un-necked counterpart and both the Mullins and Payne effects were present in the necked material. The dynamic modulus exhibited anisotropy with respect to the direction of the necking deformation, where the anisotropy was not found in fumed silica filled PDMS elastomers that did not neck although the materials were pre-stretched to similar strains. Based upon these experimental observations, it has been postulated that necking occurs due to the breakage of delicate highly branched aggregates at the points of local stress concentrations. The preferential breakage of the most mechanically distressed aggregates will result in a more regular filler-matrix network, giving rise to higher ultimate properties of the necked material.

Table 5.1: Properties of untreated fumed silica

Silica	Surface Area (m^2/g)	Ave. Particle Size (nm)
OX50	50	40
A90	90	20
A150	150	14
A200	200	12
A300	300	7
A300SP	300	7
A380	380	-

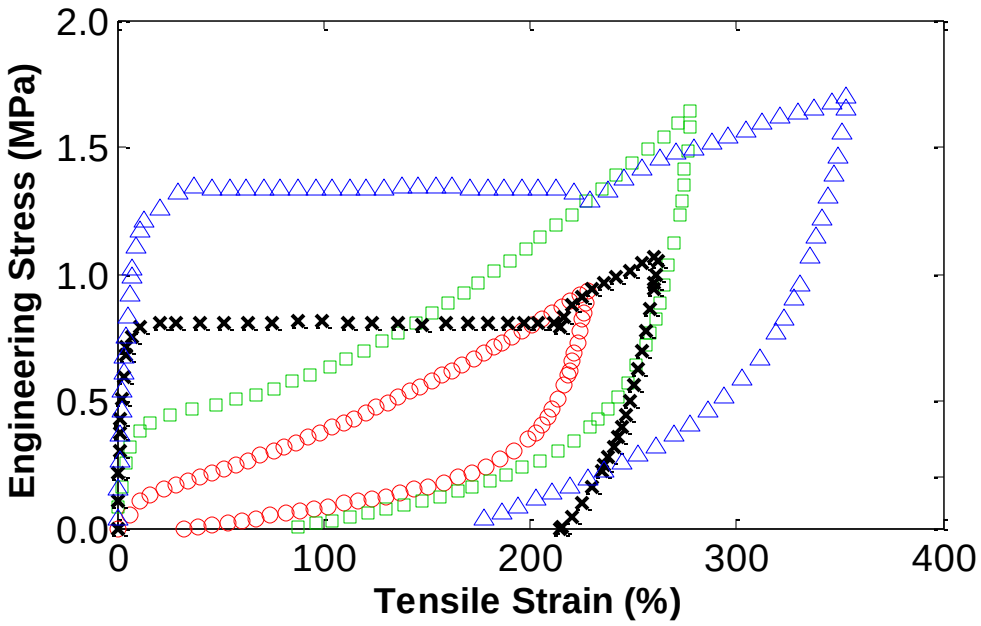

Figure 5.1: Stress-strain behavior for various surface area 40phr fumed silica filled PDMS elastomer systems: OX50 (○), A150 (□), A300 (x), and A380 (△).

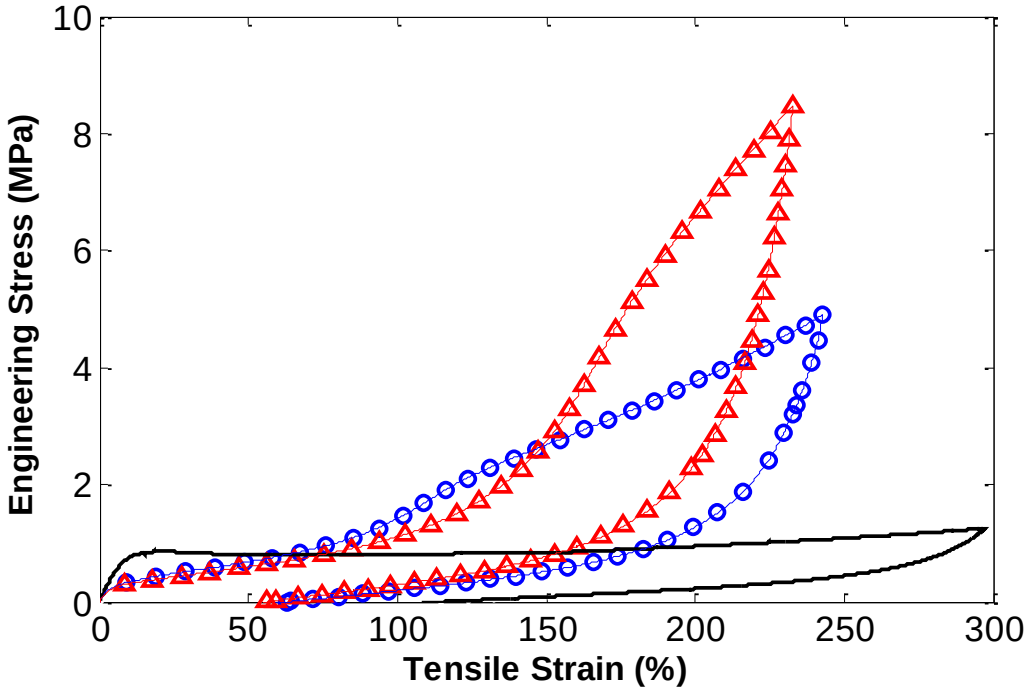

Figure 5.2: Stress-strain behavior of a necked material, 35phr of A380 fumed silica-PDMS. Original specimen 1 (solid line); specimen 2 -cut out of the necked portion of specimen 1 (○); and specimen 3 -re-gripped 2 (Δ). Initial sample dimensions are given in Table 5.2.

Table 5.2: Initial dimensions of specimens in Figure 5.2 prior to deformation

Specimen in Figure 5.2	1(-)	2(O)	3(Δ)	4*
Initial thickness (mm)	4.8	3.5	3.1	3.0
Initial width (mm)	6.4	4.7	4.4	4.3

*Specimen 4 stress-strain curve is not shown in Figure 5.2 as it failed in the grips at approximately 50% strain.

Table 5.3: Tensile strength, Elongation at break and tear resistance for fumed silica-PDMS composites

Material (surface area in bold)	Amount of silica (phr)	Tensile Strength ,MPa	Elongation at break, %	Tear Resistance, kN/m
Unfilled PDMS	0	0.1	62	1
OX**50**	40	1.9	434	11
	100	2.4	167	6
A**90**	40	4.2	408	8
A**150**	30	5.5	746	34
	35	5.6	688	36
	40	3.2	444	34
	60	2.2	179	16
A**200**	30	5.8	801	39
	35	4.6	732	43
	40	6.0	676	43
A**300**SP	30	5.1	658	45
A**300** necked	30	7.7	650	44
	35	11.1	476	55
	40	8.9	329	-
A**380** necked	30	8.9	462	48
	35	10.6	555	34
	40	10.1	533	-

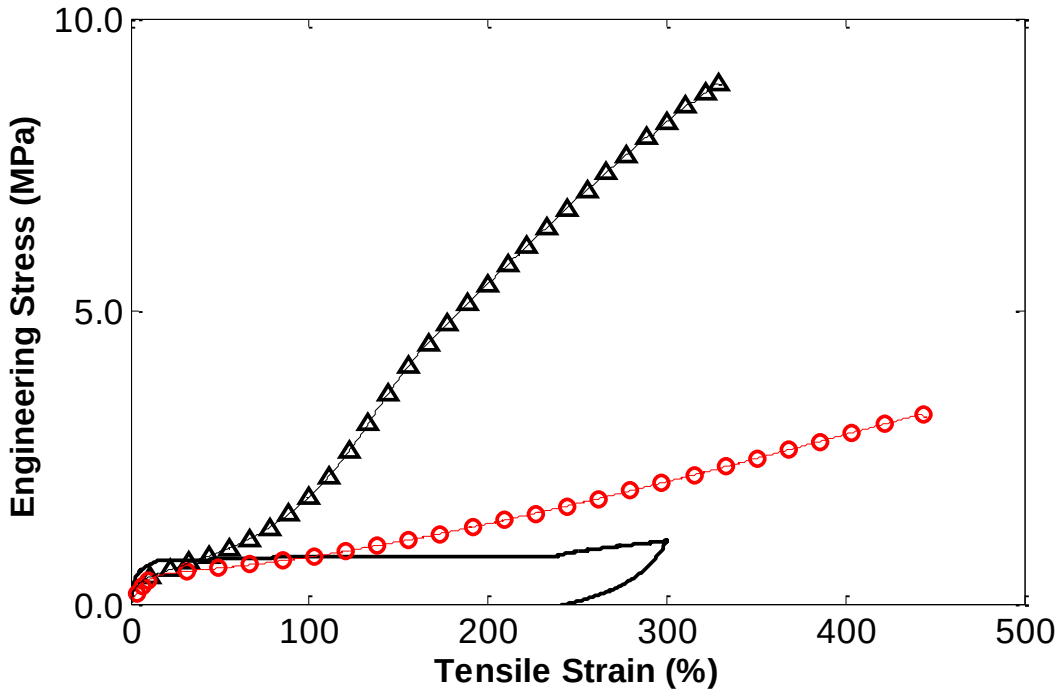

Figure 5.3: Stress-strain behavior to failure for different surface area 40phr fumed silica filled PDMS elastomers. A300 filled PDMS: original specimen (solid line); 2nd pull of the necked portion after re-gripping (△). For comparison, the stress-strain curve for the A150 filled PDMS that does not neck (○).

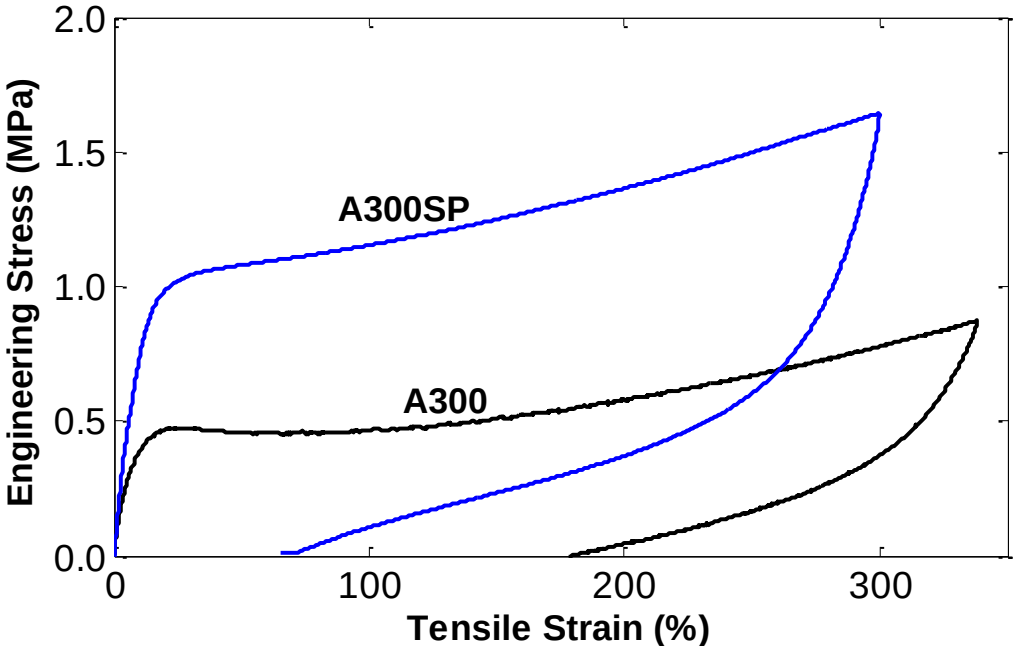

Figure 5.4: Stress-strain behavior for PDMS elastomers filled with 30phr of A300 and A300SP fumed silica.

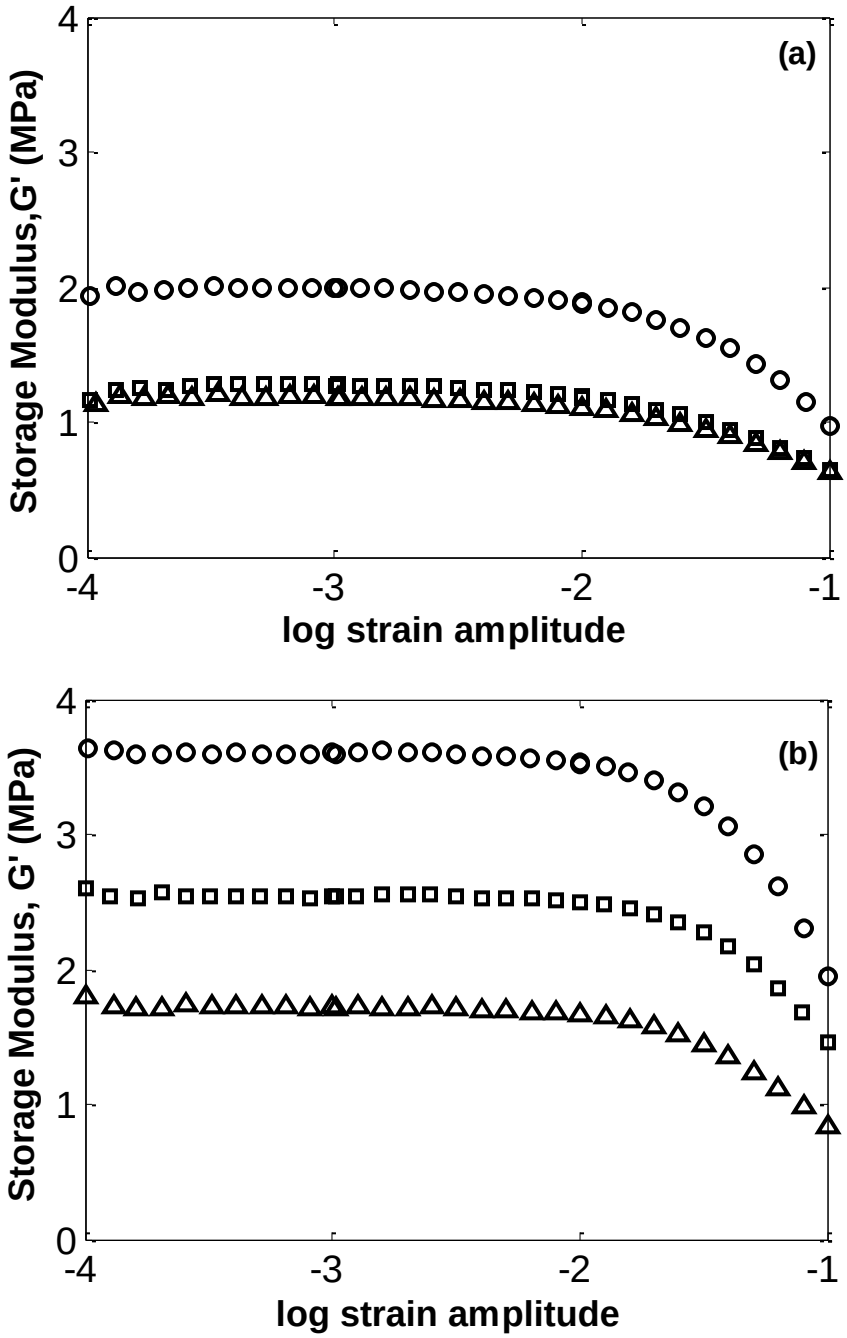

Figure 5.5: Storage modulus from Payne experiment in shear for 30phr of (a) A150 and (b) A300 in PDMS. The virgin materials (○) are shown in both figures**.** (a) Material stretched uniaxially to 300% strain, unloaded and then dynamically tested parallel (□) and perpendicular (△) to the direction of the uniaxial extension. (b) Material stretched uniaxially to induce necking, unloaded and then the cutouts from the necked portion are dynamically tested parallel (□) and perpendicular (△) to the direction of the uniaxial extension.

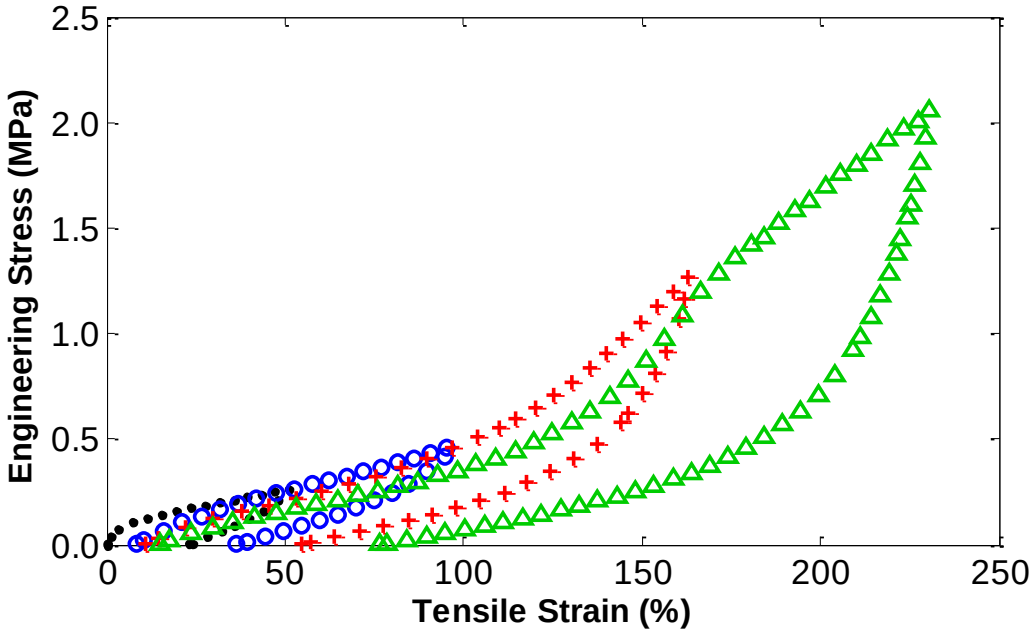

Figure 5.6: Mullins effect for the necked region of A300 PDMS filled with 30phr of A300 fumed silica. Sequential tensile strain cycles: 1st pull to 52% (●); 2nd pull to 94% (○); 3rd pull to 163% (+) and 4th pull 230% (△).

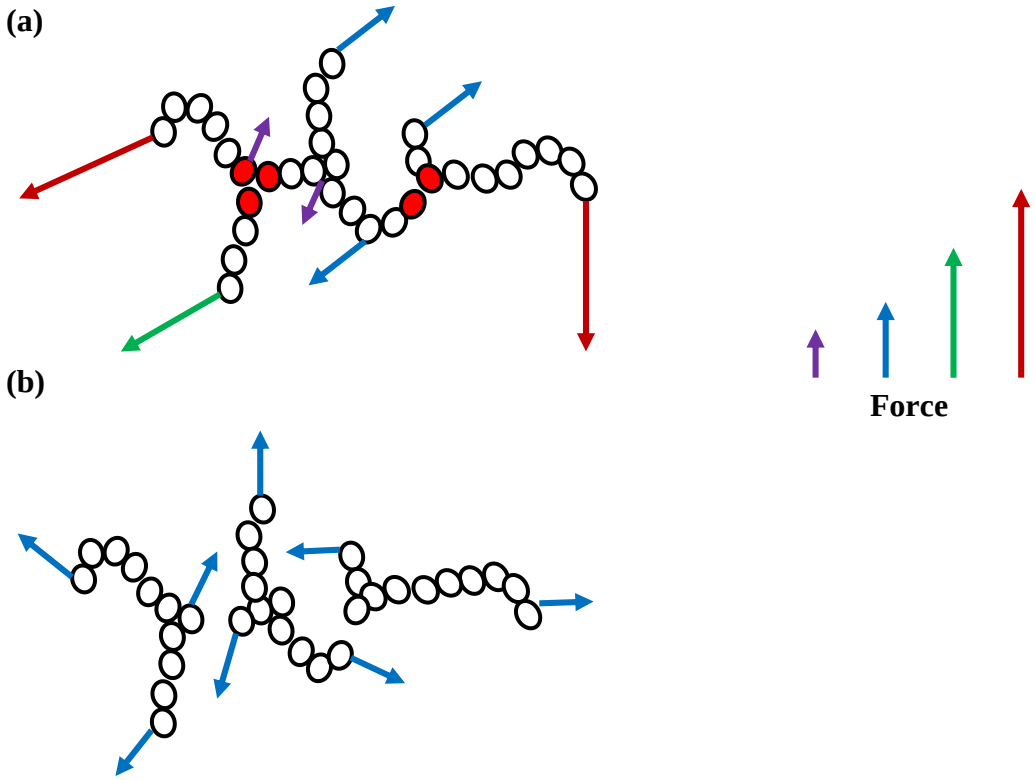

Figure 5.7: Schematic of the “wishbone” mechanism of aggregates breaking under deformation. (a) Prior to necking and (b) during necking. Forces are applied to filler by polymer matrix (not shown). The filled particles experience high stress/torque and when they break, the stress on both the particles and the surrounding rubber matrix is equalized

CHAPTER 6. CONCLUSIONS AND RECOMMENDATIONS

6.1 Linear Viscoelastic Behavior

6.1.1 Summary

The linear and nonlinear mechanical properties of filled elastomers were investigated as a function of composition for carbon black and fumed silica systems. In Chapter 2, the dynamic mechanical response was investigated for a series of carbon black filled SBR and carbon black filled polybutadiene rubber at extremely small strains using double sandwich shear geometry. Time-temperature superposition was shown to hold for both a low structure and a high structure carbon black provided the dynamic mechanical response is within the linear region. The loga_T horizontal shift for the filled elastomers were the same as that for the unfilled elastomer. However, the b_T vertical shift does change with the addition of filler, where a non-standard vertical shift factor was observed for both unfilled and filled SBR. The long-time/low-frequency behavior was further investigated using creep compliance and creep recovery responses, where overlap was achieved between the dynamic and creep data. Significant low frequency processes are evident in the relaxation spectra of the filled elastomers but are absent in the unfilled elastomer.

In Chapter 3, the linear viscoelastic behavior is investigated as a function of filler composition for carbon black filled SBR. To probe the low frequency i.e. long term behavior of the material, experiments were performed at temperatures 80ºC to 130 ºC above T_g (-50 ºC). Storage and loss isotherms are obtained in the dynamic mechanical tests for the temperatures from 30ºC to 80ºC in the double sandwich shear geometry and successfully superposed to form master curves. To probe the low frequency / long time behavior, creep and creep recovery experiments are performed in torsion at a temperature of 30ºC. The relaxation spectra of the filled elastomers exhibit significant low frequency

processes that are absent in the unfilled elastomer. Both storage and loss moduli appear to increase with filler structure at a given loading.

Chapter 4 presents the critical analysis of the filled master curves from the previous Chapter. A key observation is that the storage shear modulus master curves for all filler loadings and structures appear parallel to that for the unfilled material for the entire frequency range so that they may be superposed using appropriate scaling factors. The dependence of the scaling factor on filler parameters, including: volume fraction, effective volume fraction, interfacial area, loading-interfacial area, and an interfacial area per unit volume is investigated. The effective volume proposed by Medalia and co-workers[140,147,185] works best in unifying the viscoelastic storage modulus data for all compositions studied. Correlation of the energy dissipated/area under the loss modulus peak with the filler parameters is established. The Payne effect is studied as a function of the filler composition and it is shown that the parameterization using the effective volume is sufficient to capture most but not all of the filler loading and structure effect on the modulus versus strain magnitude behavior.

6.1.2 Recommendations

It is generally accepted that the polymer-filler interaction and/or the filler-filler interaction are the dominant factors in the mechanical response of filled elastomers. Quantification of the contribution of these interactions has not been thoroughly investigated. The best estimate for polymer and filler surface activity is their surface energy. The surface energy concept asserts that fillers such as carbon black have a tendency to attach better with the SBR than with other aggregates. Hence, the polymer-filler interaction in carbon black is greater than the filler-filler interaction. On the contrary, fillers such as fumed silica have very low surface energies. Within a polymer matrix, they have a tendency to dominate through filler-filler effects. A study on the TTS of fumed silica in SBR would provide additional insight on the influence of filler interactions. Fumed silica is preferred to other fillers because of its silanol groups that

can easily be modified to alter interactions with itself and the polymer. A full picture on the effect of filler and polymer interactions on TTS can thus be attained.

6.2 Nonlinear Mechanical Behavior

6.2.1 Summary

The last part of Chapter 4 shows the Payne effect for a series of carbon black filled elastomers. The Kraus function was used to fit the experimental data and the constants were generated. However, the effective volume concept did not correlate well with the constants ε_c and *a*. In Chapter 5, we present for the first time the necking for a lightly cross-linked poly(dimethylsiloxane) elastomer filled with 30phr or more of high surface area ($\geq$300m^2/g) fumed silica. Necking is a well-known phenomenon in uniaxial extension of filled and unfilled semi-crystalline polymers as well as amorphous polymers below their glass transition temperature; however, until now, necking has not been observed for elastomers. A series of linear and non-linear mechanical properties of the necked material were studied. The tensile strength of the necked material was found to be significantly higher than that for non-neck forming systems. Payne experiments show anisotropy in the G' behavior of the necked material and Mullins was still present in the system. The observed necking behavior is consistent with deformation induced aggregate breakage where a "wish-bone" mechanism was postulated.

6.2.2 Recommendations

Payne effect

Works by authors such as Kraus[45], Clement[37] and co-workers have showed that the constants derived from the Kraus agglomeration-deagglomeration expression were similar. The constant *a*, for our system (refer to Chapter 4) for some carbon black-SBR materials varied beyond the reported numbers in the literature of 1-1.3. An investigation as to why a deviation from the standard values needs to be carried out. Furthermore, an

assessment of the Payne experiment with measurable filler parameters is needed in the nonlinear Payne region. Perhaps the right parameter is the filler surface area and not structure in this region. This warrants further investigation.

To probe the structural character of the filler network deserves more attention. Wang *et al.* [186] discovered that a filled rubber system (carbon black – polybutadiene) under very small strains may display feature fluctuations that could be associated with a transition of the filler from an elastic solid state to a dispersed fluid state and that is reminiscent of critical phenomena. The experimental procedure involved dynamic oscillations at 0.01% strain amplitude for at least 30hours. It was observed that there was a critical strain γ_c at which a significant change in behaviour occurred. It appears that this experimental set-up probes the structural character of the underlying microstructure. Further analysis is needed and specifically, the correlation of γ_c to perhaps the Kraus constants, ε_c or a would be beneficial. In addition, any correlation of γ_c to filler parameters is necessary.

Mullins Effect

In studying the contribution of viscoelasticity via stress-strain experiments, .Bhattacharya *et al*.[60] were able to superpose the Mullins loading and unloading curves using the strain amplification theory proposed by Mullins and Tobin[58]. Recall from Chapter 1 that the strain amplification is the modification of the applied strain by the equation $\lambda = 1 + (\lambda - 1)X$, where λ is the strain shifted extension ratio, λ is the rescaled value, and X is the amplification factor. Bhattacharya *et al.* show perfect superposition as seen in Fig.6.1 and the inverse of X was directly proportional to the λmax. However, preliminary results using PDMS-A300SP show a lack of superposition especially for the loading curves (Figure 6.2). The curves superpose to a certain point, thereafter, they all deviate. On the other hand, the unloading curve data all superposes, the first unloading (purple) being the outlier. A complete study of strain amplification on all silica-filled PDMS is necessary.

Necking

To serve as evidence of the mechanism occurring during necking, a non-destructive means of investigating the structure of the filler within the matrix is needed. One potential technique involves a study by X-Ray scattering, specifically small-angle x-ray scattering (SAXS). Based on the contrast in electron density within a sample, information on the extent of x-ray deflection when a filled elastomer is subjected to an x-ray source is collected. This scattering intensity provides structural information on the particle size, number density, specific surface area, mass fractal dimension and aggregate size and number density of the sample[187]. It also provides an indication of the presence of agglomerates (clusters of aggregates) through a power-law tail of intensity in angle at the lowest angles. The minimum size for SAXS (correlation distance) is on the order of 0.05 nm depending on the wavelength used. Additionally, ultra small angle x-ray scattering (USAXS) can be used to further increase the scattering range. The scattering equation is: $q = (4\pi/\lambda \sin 2\theta)$ where q is the scattering range, λ is the wavelength of the X-ray and 2θ is the scattering angle. The Guinier and Porod approximations are used to relate the scattering intensity, q to specific dimensions and properties[188,189]. Recently, small-angle X-ray scattering (SAXS) measurements have been performed on several filled elastomers[182,190-193]. Specifically, several authors have determined aggregate, primary particle and agglomerate sizes by combining SAXS and USAXS techniques[182,192] The success of these works in characterize the morphology of the aggregates within a filled elastomer is promising and would be useful in supporting the “wish-bone” mechanism proposed for the necked material.

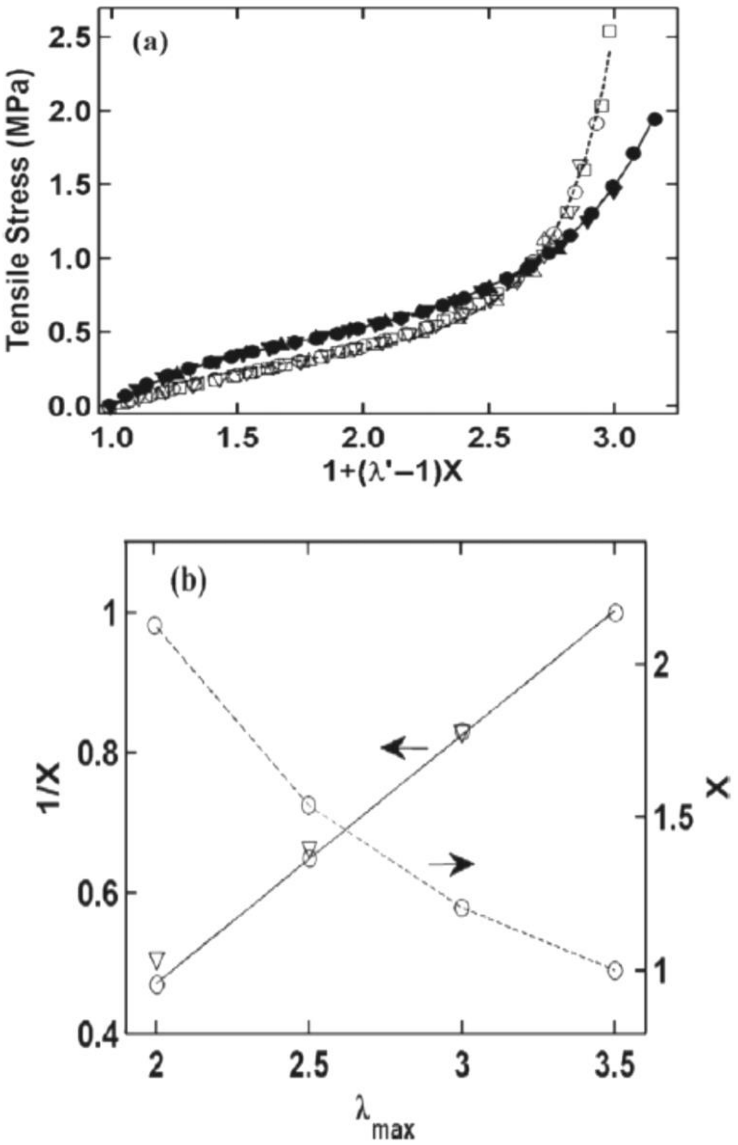

Figure 6.1: The superposition of Mullins for filled SBR using the strain amplification concept[60]. (a) The loading and unloading curves (b) The strain amplification factor, X

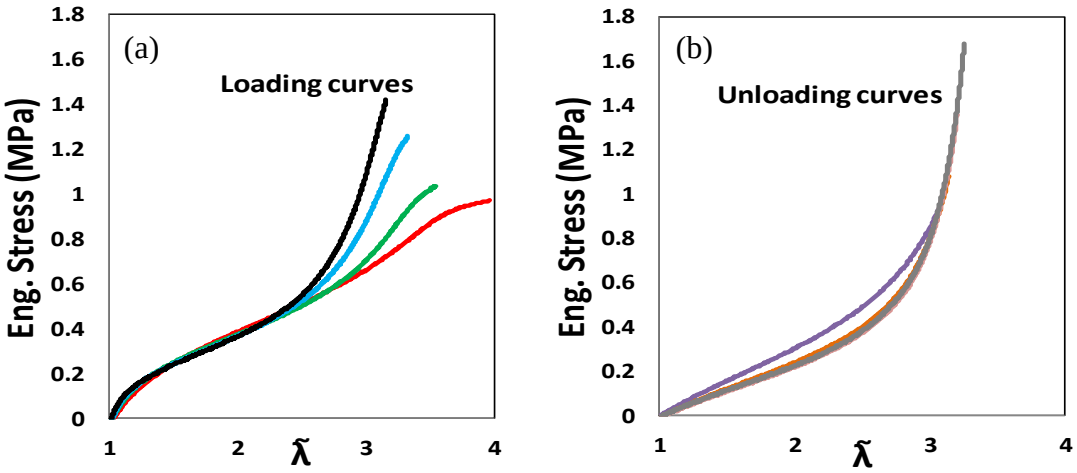

Figure 6.2: Strain amplification superposition for PDMS filled with A300SP silica (a) Loading curves (b) Unloading curves.

LIST OF REFERENCES

LIST OF REFERENCES

(1) Steinmann, P.; Hossain, M.; Possart, G. *Archive of Applied Mechanics* **2012**, *82*, 1183.

(2) Prabhu, R. Dissertation, Purdue University, 2012.

(3) Bhattacharya, A. PhD Thesis, Purdue University, 2010.

(4) Prabhu, R.; Ogebule, O.; Klitkou, R.; Medvedev, G. A.; Caruthers, J. M. *submitted* to Polymer 2013.

(5) Leblanc, J. L. *Filled polymers: science and industrial applications*; CRC, 2009.

(6) Brunauer, S.; Emmett, P. H.; Teller, E. *Journal of the American Chemical Society* **1938**, *60*, 309.

(7) Wang, M. J. *Rubber chemistry and technology* **1998**, *71*, 520.

(8) Nielsen, L. E.; Landel, R. F. *Mechanical Properties of Polymers Composites 2e*; Marcel Dekker Incorporated, 1994; Vol. 90.

(9) Ferry, J. D. *Viscoelastic properties of polymers*; 3d ed.; Wiley: New York, 1980.

(10) Shaw, M. T.; MacKnight, W. J. *Introduction to polymer viscoelasticity*; Wiley-Interscience, 2005.

(11) Song, Y.; Zheng, Q.; Cao, Q. *Journal of Rheology* **2009**, *53*, 1379.

(12) Plazek, D.; Chay, I.-C.; Ngai, K.; Roland, C. *Macromolecules* **1995**, *28*, 6432.

(13) Chung, G.-C.; Kornfield, J.; Smith, S. *Macromolecules* **1994**, *27*, 5729.

(14) Kaplan, D.; Tschoegl, N. In *Recent Advances in Polymer Blends, Grafts, and Blocks*; Springer: 1974, p 415.

(15) Payne, A. *Journal of Applied Polymer Science* **1962**, *6*, 57.

(16) Payne, A.; Whittaker, R. *Rubber chemistry and technology* **1971**, *44*, 440.

(17) Payne, A. R. *Journal of Applied Polymer Science* **1962**, *6*, 368.

(18) Aranguren, M. I.; Mora, E.; DeGroot Jr, J. V.; Macosko, C. W. *Journal of Rheology* **1992**, *36*, 1165.

(19) Aranguren, M. I.; Mora, E.; Macosko, C. W.; Saam, J. *Rubber chemistry and technology* **1994**, *67*, 820.

(20) Bokobza, L. *Macromolecular Materials and Engineering* **2004**, *289*, 607.

(21) Boonstra, B. *Polymer* **1979**, *20*, 691.

(22) Heinrich, G.; Klüppel, M. In *Filled Elastomers Drug Delivery Systems*; Springer Berlin Heidelberg: 2002; Vol. 160, p 1.

(23) Heinrich, G.; Klüppel, M.; Vilgis, T. *Current Opinion in Solid State and Materials Science* **2002**, *6*, 195

(24) Clément, F.; Bokobza, L.; Monnerie, L. *Rubber chemistry and technology* **2005**, *78*, 211.

(25) Medalia, A. I. *Rubber chemistry and technology* **1978**, *51*, 437.

(26) Payne, A.; Kraus, G., Ed.; Interscience: New York, 1965, p 69.

(27) Roland, C. M. *Journal of rheology* **1990**, *34*, 25.

(28) Rendek, M.; Lion, A. *ZAMM - Journal of Applied Mathematics and Mechanics / Zeitschrift für Angewandte Mathematik und Mechanik* **2010**, *90*, 436.

(29) Rendek, M.; Lion, A. *International Journal of Solids and Structures* **2010**, *47*, 2918.

(30) Chazeau, L.; Brown, J.; Yanyo, L.; Sternstein, S. *Polymer composites* **2000**, *21*, 202.

(31) Cassagnau, P.; Melis, F. *Polymer* **2003**, *44*, 6607.

(32) Payne, A.; Watson, W. *Rubber Chemistry and Technology* **1963**, *36*, 147.

(33) Fröhlich, J.; Niedermeier, W.; Luginsland, H. *Composites Part A: Applied Science and Manufacturing* **2005**, *36*, 449.

(34) Suzuki, N.; Yatsuyanagi, F.; Ito, M.; Kaidou, H. *Journal of applied polymer science* **2002**, *86*, 1622.

(35) Bokobza, L. *Journal of applied polymer science* **2004**, *93*, 2095.

(36) Ramier, J.; Gauthier, C.; Chazeau, L.; Stelandre, L.; Guy, L. *Journal of Polymer Science Part B: Polymer Physics* **2006**, *45*, 286.

(37) Clement, F.; Bokobza, L.; Monnerie, L. *Rubber chemistry and technology* **2005**, *78*, 232.

(38) Kraus, G.; Childers, C.; Rollmann, K. *Rubber Chemistry and Technology* **1966**, *39*, 1530.

(39) Bueche, F. *Journal of Applied Polymer Science* **1960**, *4*, 107.

(40) Heinrich, G.; Klüppel, M. *Filled Elastomers Drug Delivery Systems* **2002**, 1.

(41) Yatsuyanagi, F.; Suzuki, N.; Ito, M.; Kaidou, H. *Polymer* **2001**, *42*, 9523.

(42) Yamaguchi, K.; Busfield, J.; Thomas, A. *Journal of Polymer Science Part B: Polymer Physics* **2003**, *41*, 2079.

(43) Voet, A. *Journal of Polymer Science: macromolecular reviews* **2003**, *15*, 327.

(44) Voet, A. *Rubber Chemistry and Technology* **1981**, *54*, 42.

(45) Kraus, G. *Applied Polymer Symposia* **1984**, 75.

(46) Klüppel, M.; Schuster, R. H.; Heinrich, G. *Rubber chemistry and technology* **1997**, *70*, 243.

(47) Ulmer, J. *Rubber chemistry and technology* **1996**, *69*, 15.

(48) Huber, G.; Vilgis, T. A.; Heinrich, G. *Journal of Physics: Condensed Matter* **1996**, *8*, L409.

(49) Van de Walle, A.; Tricot, C.; Gerspacher, M. *Kautschuk und Gummi Kunststoffe* **1996**, *49*, 172.

(50) Maier, P. G.; Goritz, D. *Kautschuk Gummi Kunststoffe* **1996**, *49*, 18.

(51) Zhu, A.-J.; Sternstein, S. *Composites science and technology* **2003**, *63*, 1113.

(52) Smit, P. *Rheologica Acta* **1969**, *8*, 277.

(53) Levresse, P.; Feke, D.; Manas-Zloczower, I. *Polymer* **1998**, *39*, 3919.

(54) Fukahori, Y. *Rubber Chemistry and Technology* **2003**, *76*, 548.

(55) Bouasse, H.; Carrière, Z. In *Annales de la faculté des sciences de Toulouse*; Université Paul Sabatier: 1903; Vol. 5, p 257.

(56) Mullins, L. *Rubber Chemistry and Technology* **1948**, *21*, 281.

(57) Mullins, L.; Tobin, N. *Rubber chemistry and technology* **1957**, *30*, 555.

(58) Mullins, L.; Tobin, N. *Journal of Applied Polymer Science* **1965**, *9*, 2993.

(59) Mullins, L. *Rubber Chemistry and Technology* **1969**, *42*, 339.

(60) Bhattacharya, A.; Medvedev, G. A.; Caruthers, J. M. *Rubber chemistry and technology* **2011**, *84*, 296.

(61) Diani, J.; Fayolle, B.; Gilormini, P. *European Polymer Journal* **2009**, *45*, 601.

(62) Suzuki, N.; Ito, M.; Yatsuyanagi, F. *Polymer* **2005**, *46*, 193.

(63) Hanson, D. E.; Hawley, M.; Houlton, R.; Chitanvis, K.; Rae, P.; Orler, E. B.; Wrobleski, D. A. *Polymer* **2005**, *46*, 10989.

(64) Harwood, J.; Mullins, L.; Payne, A. *Journal of Applied Polymer Science* **1965**, *9*, 3011.

(65) Harwood, J. A. C.; Payne, A. R. *Journal of Applied Polymer Science* **1966**, *10*, 1203.

(66) Qi, H. J.; Boyce, M. C. *Mechanics of Materials* **2005**, *37*, 817.

(67) Speich, J. E.; Borgsmiller, L.; Call, C.; Mohr, R.; Ratz, P. H. *American Journal of Physiology-Cell Physiology* **2005**, *289*, C12.

(68) Harwood, J.; Payne, A. *Journal of Applied Polymer Science* **1966**, *10*, 315.

(69) Dorfmann, A.; Ogden, R. *International Journal of Solids and Structures* **2004**, *41*, 1855.

(70) Johnson, M. A.; Beatty, M. F. *Continuum Mechanics and Thermodynamics* **1993**, *5*, 301.

(71) Govindjee, S.; Simo, J. *International Journal of Solids and Structures* **1992**, *29*, 1737.

(72) Simo, J. *Computer methods in applied mechanics and engineering* **1987**, *60*, 153.

(73) McCrum, N.; Read, B. E.; Williams, G. *Anelastic and dielectric effects in polymeric solids*; John Wiley & Sons Ltd, 1967.

(74) Govindjee, S.; Simo, J. *Journal of the Mechanics and Physics of Solids* **1991**, *39*, 87.

(75) Ogden, R.; Roxburgh, D. *Proceedings of the Royal Society of London. Series A: Mathematical, Physical and Engineering Sciences* **1999**, *455*, 2861.

(76) Bergstrom, J.; Boyce, M. *Rubber chemistry and technology* **1999**, *72*, 633.

(77) Gent, A. *Rubber chemistry and technology* **1996**, *69*, 59.

(78) Mossi Idrissa, A.; Ahzi, S.; Patlazhan, S.; Rémond, Y.; Ruch, D. *Journal of Applied Polymer Science* **2012**, *125*, 4368.

(79) Blanchard, A.; Parkinson, D. *Rubber Chemistry and Technology* **1952**, *25*, 808.

(80) Bueche, F. *Journal of applied polymer Science* **1961**, *5*, 271.

(81) Qi, H. J.; Boyce, M. C. *Journal of the Mechanics and Physics of Solids* **2004**, *52*, 2187.

(82) De Tommasi, D.; Puglisi, G. *Journal of Elasticity* **2007**, *86*, 85.

(83) De Tommasi, D.; Puglisi, G.; Saccomandi, G. *Journal of Rheology* **2006**, *50*, 495.

(84) Wineman, A.; Rajagopal, K. *Archives of Mechanics* **1990**, *42*, 53.

(85) Miehe, C. *European journal of mechanics. A. Solids* **1995**, *14*, 697.

(86) Miehe, C.; Keck, J. *Journal of the Mechanics and Physics of Solids* **2000**, *48*, 323.

(87) Marckmann, G.; Verron, E.; Gornet, L.; Chagnon, G.; Charrier, P.; Fort, P. *Journal of the Mechanics and Physics of Solids* **2002**, *50*, 2011.

(88) Septanika, E.; Ernst, L. *Mechanics of materials* **1998**, *30*, 253.

(89) Chagnon, G.; Verron, E.; Marckmann, G.; Gornet, L. *International journal of solids and structures* **2006**, *43*, 6817.

(90) Arruda, E.; Boyce, M. *Journal of the Mechanics and Physics of Solids* **1993**, *41*, 389.

(91) Wolff, S.; Wang, M.-J. *Rubber chemistry and technology* **1992**, *65*, 329.

(92) Wu, S. *Polymer Handbook* **1999**, *4*, 521.

(93) Heinrich, G.; Klüppel, M.; Vilgis, T. A. *Current Opinion in Solid State and Materials Science* **2002**, *6*, 195.

(94) Huber, G.; Vilgis, T. *Kautschuk und Gummi, Kunststoffe* **1999**, *52*, 102.

(95) Sternstein, S. S.; Zhu, A.-J. *Macromolecules* **2002**, *35*, 7262.

(96) Lion, A. *Rubber Chemistry and Technology* **1999**, *72*, 410.

(97) Lion, A.; Kardelky, C.; Haupt, P. *Rubber Chemistry and Technology* **2003**, *76*, 533.

(98) Lion, A.; Kardelky, C. *International Journal of Plasticity* **2004**, *20*, 1313.

(99) Dannenberg, E. *Trans. Inst. Rubber, Ind* **1966**, *42*.

(100) Houwink, R. *Rubber Chemistry and Technology* **1956**, *29*, 888.

(101) Wolff, S.; Wang, M. J. *Rubber chemistry and technology* **1992**, *65*, 329.

(102) Wang, M.-J.; Wolff, S. *Rubber chemistry and technology* **1992**, *65*, 715.

(103) Lorenz, H.; Meier, J.; Klüppel, M. In *Elastomere Friction*; Besdo, D., Heimann, B., Klüppel, M., Kröger, M., Wriggers, P., Nackenhorst, U., Eds.; Springer Berlin Heidelberg: 2010; Vol. 51, p 27.

(104) Richter, S.; Saphiannikova, M.; Stöckelhuber, K. W.; Heinrich, G.; Wiley Online Library: 2010; Vol. 291, p 193.

(105) Boyce, M. C.; Arruda, E. M. *Rubber Chemistry and Technology* **2000**, *73*, 504.

(106) Haupt, P.; Sedlan, K. *Archive of Applied Mechanics* **2001**, *71*, 89.

(107) Roland, C.; Lee, G. *Rubber chemistry and technology* **1990**, *63*, 554.

(108) Treloar, L. *The physics of rubber elasticity*; 3rd ed.; Oxford University Press, 1975.

(109) Åredal, T. G. *Journal of Applied Polymer Science* **1973**, *17*, 2823.

(110) Ferry, J. D.; Fitzgerald, E. R. *Rubber chemistry and technology* **1982**, *55*, 1403.

(111) Fletcher, W. P.; Gent, A. N. *British Journal of Applied Physics* **1957**, *8*, 194.

(112) Funt, J. M. *Rubber chemistry and technology* **1988**, *61*, 842.

(113) Isono, Y.; Ferry, J. D. *Rubber chemistry and technology* **1984**, *57*, 925.

(114) Adicoff, A.; Lepie, A. H. *Journal of Applied Polymer Science* **1970**, *14*, 953.

(115) Stacer, R. G.; Husband, D. M. *Rheologica Acta* **1990**, *29*, 152.

(116) Stacer, R. G.; Husband, D. M.; Stacer, H. L. *Rubber chemistry and technology* **1987**, *60*, 227.

(117) Arai, K.; Ferry, J. D. *Rubber chemistry and technology* **1986**, *59*, 592.

(118) Fitzgerald, E. R.; Ferry, J. D. *Polymer Bulletin* **1982**, *8*, 339.

(119) Klüppel, M. *Journal of Physics: Condensed Matter* **2009**, *21*, 035104.

(120) Fritzsche, J.; Klüppel, M. *Journal of Physics: Condensed Matter* **2011**, *23*.

(121) Onogi, S.; Masuda, T.; Matsumoto, T. *Transactions of the Society of Rheology* **1970**, *14*, 275.

(122) Salgueiro, W.; Marzocca, A.; Somoza, A.; Consolati, G.; Cerveny, S.; Quasso, F.; Goyanes, S. *Polymer* **2004**, *45*, 6037.

(123) Sternstein S, S. In *Polymer Characterization*; American Chemical Society: 1983; Vol. 203, p 123.

(124) Chazeau, L.; Brown, J. D.; Yanyo, L. C.; Sternstein, S. S. *Polymer Composites* **2000**, *21*, 202.

(125) Ferry, J. D.; Grandine, L. D.; Fitzgerald, E. R. *Journal of Applied Physics* **1953**, *24*, 911.

(126) Prabhu, R.; Klitkou, R.; Medvedev, G. A.; Caruthers, J. M. *Journal of Polymer Science Part B: Polymer Physics* **2013**, *51*, 687.

(127) Kraus, G.; Gruver, J. T. *Journal of Polymer Science Part A-2: Polymer Physics* **1970**, *8*, 571.

(128) Gauthier, C.; Reynaud, E.; Vassoille, R.; Ladouce-Stelandre, L. *Polymer* **2004**, *45*, 2761.

(129) Doi, M.; Edwards, S. F. *The theory of polymer dynamics*; Oxford University Press, USA, 1986.

(130) Guth, E. *Journal of Applied Physics* **1945**, *16*, 20.

(131) Sternstein, S.; Craver, D. *Aduances in Chemistry* **1983**.

(132) Tunnicliffe, L.; Thomas, A.; Busfield, J. In *Constitutive Models for Rubber VII.*; Jerrams, S., Murphy, N., Eds.; CRC Press/Bakelma: 2012, p 63.

(133) Dannenberg, E. *Rubber chemistry and technology* **1986**, *59*, 512.

(134) Gent, A.; Hartwell, J.; Lee, G. *Rubber chemistry and technology* **2003**, *76*, 517.

(135) Lorenz, O.; Parks, C. *Journal of Polymer Science* **1961**, *50*, 299.

(136) Chodak, I.; Chorvath, I.; Novak, I.; Csomorova, K. *European Polymer Journal* **1992**, *28*, 107.

(137) Leblanc, J. L. *Journal of applied polymer science* **1997**, *66*, 2257.

(138) Jha, V.; Hon, A. A.; Thomas, A. G.; Busfield, J. J. *Journal of Applied Polymer Science* **2008**, *107*, 2572.

(139) Haong, G. C. N., L.; Gerspacher, M. *Journal of the Korean Physical Society* **2004**, *44*, 962.

(140) Medalia, A. *Rubber chemistry and technology* **1973**, *46*, 877.

(141) *Basic Elastomer Technology*; Rubber Division, 2001.

(142) Caruthers, J.; Cohen, R.; Medalia, A. *Rubber Chemistry and Technology* **1976**, *49*, 1076.

(143) Einstein, A. *Annalen der Physik* **1906**, *9*, 289.

(144) Guth, E.; Gold, O. *Phys. Rev* **1938**, *53*, 2.

(145) Guth, E.; Simha, R. *Kolloid-Zeitschrift* **1936**, *74*, 266.

(146) Sarkar, A., Purdue University, 2005.

(147) Medalia, A. *Rubber chemistry and technology* **1972**, *45*, 1171.

(148) Wolff, S.; Donnet, J.-B. *Rubber Chemistry and Technology* **1990**, *63*, 32.

(149) Caruthers, J. M.; Cohen, R. E.; Medalia, A. I. *Rubber Chemistry and Technology* **1976**, *49*, 1076.

(150) Medalia, A.; Laube, S. *Rubber Chem Technol* **1978**, *51*, 89.

(151) Medalia, A. I. *Rubber Chemistry and Technology* **1986**, *59*, 432.

(152) Mani, J.; Meier, J.; KLÜPPEL, M. *KGK. Kautschuk, Gummi, Kunststoffe* **2006**, *59*, 648.

(153) Fukahori, Y.; Hon, A.; Jha, V.; Busfield, J. *Rubber Chemistry and Technology* **2013**.

(154) Brennan, J.; Jermyn, T.; Boonstra, B. *Journal of Applied Polymer Science* **1964**, *8*, 2687.

(155) Wolff, S.; Wang, M.-J.; Tan, E.-H. *Rubber chemistry and technology* **1993**, *66*, 163.

(156) Rehner, J.; Kraus, G., Ed.; Interscience: New York, 1965, p 153.

(157) Hamed, G. R.; Hatfield, S. *Rubber chemistry and technology* **1989**, *62*, 143.

(158) Choi, S.-S. *Journal of Applied Polymer Science* **2004**, *93*, 1001.

(159) Fukahori, Y. *Rubber Chemistry and Technology* **2007**, *80*, 701.

(160) Leblanc, J. L. *Progress in Polymer Science* **2002**, *27*, 627.

(161) Kaufman, S.; Slichter, W. P.; Davis, D. D. *Journal of Polymer Science Part A-2: Polymer Physics* **1971**, *9*, 829.

(162) O'brien, J.; Cashell, E.; Wardell, G.; McBrierty, V. *Macromolecules* **1976**, *9*, 653.

(163) Nishi, T. *Journal of Polymer Science: Polymer Physics Edition* **1974**, *12*, 685.

(164) Fukahori, Y. *Journal of Applied Polymer Science* **2005**, *95*, 60.

(165) O'Brien, J.; Cashell, E.; Wardell, G.; McBrierty, V. *Rubber Chemistry and Technology* **1977**, *50*, 747.

(166) Serizawa, H.; Nakamura, T.; Ito, M.; Tanaka, K.; Nomura, A. *Polym. J* **1983**, *14*, 201.

(167) Kenny, J.; McBrierty, V.; Rigbi, Z.; Douglass, D. *Macromolecules* **1991**, *24*, 436.

(168) Meissner, B. *Rubber Chemistry and Technology* **1995**, *68*, 297.

(169) Medalia, A. I. *Journal of Colloid and Interface Science* **1970**, *32*, 115.

(170) Beatty, M. F. *J. Elast* **2000**, *59*, 369.

(171) Boonstra, B.; Cochrane, H.; Dannenberg, E. *Rubber Chemistry and Technology* **1975**, *48*, 558.

(172) Warrick, E.; Lauterbur, P. *Industrial & Engineering Chemistry* **1955**, *47*, 486.

(173) Clement, F.; Bokobza, L.; Monnerie, L. *Rubber chemistry and technology* **2001**, *74*, 847.

(174) Chazeau, L.; Brown, J.; Yanyo, L.; Sternstein, S. *Polymer composites* **2004**, *21*, 202.

(175) Ward, I. M.; Hadley, D. *An introduction to the mechanical properties of solid polymers*; John Wiley & Sons Ltd.; John Wiley & Sons, Inc., 1993.

(176) Roesler, J.; Harders, H.; Baeker, M. *Mechanical behaviour of engineering materials: Metals, ceramics, polymers & composites*; Springer: New York, 2007.

(177) *Polymer Handbook*; 2nd ed.; John Wiley and Sons: New York, 1975.

(178) Leger, L.; Raphael, E.; Hervet, H. *Polymers in Confined Environments* **1999**, 185.

(179) Fragiadakis, D.; Pissis, P. *Journal of Non-Crystalline Solids* **2007**, *353*, 4344.

(180) Cochrane, H.; Lin, C. *Rubber chemistry and technology* **1993**, *66*, 48.

(181) Hamed, G. R. *Rubber chemistry and technology* **2000**, *73*, 524.

(182) Camenzind, A.; Schweizer, T.; Sztucki, M.; Pratsinis, S. E. *Polymer* **2010**, *51*, 1796.

(183) Llorente, M.; Andrady, A.; Mark, J. *Journal of Polymer Science: Polymer Physics Edition* **2003**, *19*, 621.

(184) Mark, J.; Sullivan, J. *Journal of Chemical Physics* **1977**, 66.

(185) Medalia, A. *Rubber Chem. Technol* **1974**, *47*, 411.

(186) Wang, X.; Rackaitis, M. *EPL (Europhysics Letters)* **2006**, *75*, 590.

(187) Ikeda, Y.; Yasuda, Y.; Yamamoto, S.; Morita, Y. *Journal of Applied Crystallography* **2007**, *40*, 549.

(188) Beaucage, G. *Journal of Applied Crystallography* **1996**, *29*, 134.

(189) Beaucage, G.; Kammler, H.; Pratsinis, S. *Journal of applied crystallography* **2004**, *37*, 523.

(190) Ehrburger-Dolle, F.; Bley, F.; Geissler, E.; Livet, F.; Morfin, I.; Rochas, C. In *Macromolecular Symposia*; Wiley Online Library: 2003; Vol. 200, p 157.

(191) Morfin, I.; Ehrburger-Dolle, F.; Grillo, I.; Livet, F.; Bley, F. *Journal of synchrotron radiation* **2006**, *13*, 445.

(192) Patwardhan, S. V.; Taori, V. P.; Hassan, M.; Agashe, N. R.; Franklin, J. E.; Beaucage, G.; Mark, J. E.; Clarson, S. J. *European polymer journal* **2006**, *42*, 167.

(193) Schaefer, D. W.; Suryawanshi, C.; Pakdel, P.; Ilavsky, J.; Jemian, P. R. *Physica A: Statistical Mechanics and its Applications* **2002**, *314*, 686.

APPENDICES

Appendix A Figures

The Following Figures are Supplementary to Data Provided in "The Application of Time-Temperature Superposition for Carbon Black Filled Elastomers" by Prabhu, R; Ogebule, O, Klitkou, R; Medvedev, GA; Caruthers, JM

1. Payne Experiments

Payne experiment data showing G' normalized with respect to G' at the low amplitude modulus, G'(ε→0).

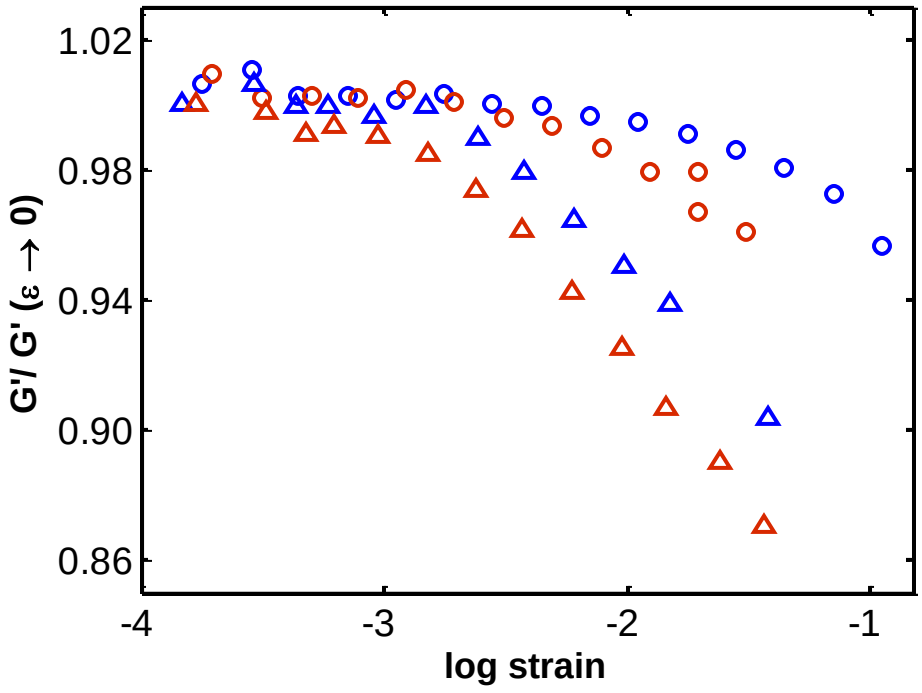

Figure A1- 1:Variation of Shear storage modulus with applied strain amplitude for 40phr N990 filled SBR+0.1phr DCP (○) and 36phr N550 filled Polybutadiene (Δ) at two temperatures each; 30°C (blue symbols) and -30°C (red symbols).

2. Isotherms from dynamic experiment

The dynamic isotherms for Tan δ, G’ and G’’ versus frequency are provided for the following materials:

2-1. 40phr N550 carbon black filled SBR cured with 0.1phr DCP

2-2. Polybutadiene

2-3. 40phr N990 carbon black filled polybutadiene

2-4. 40phr N990 carbon black filled polybutadiene

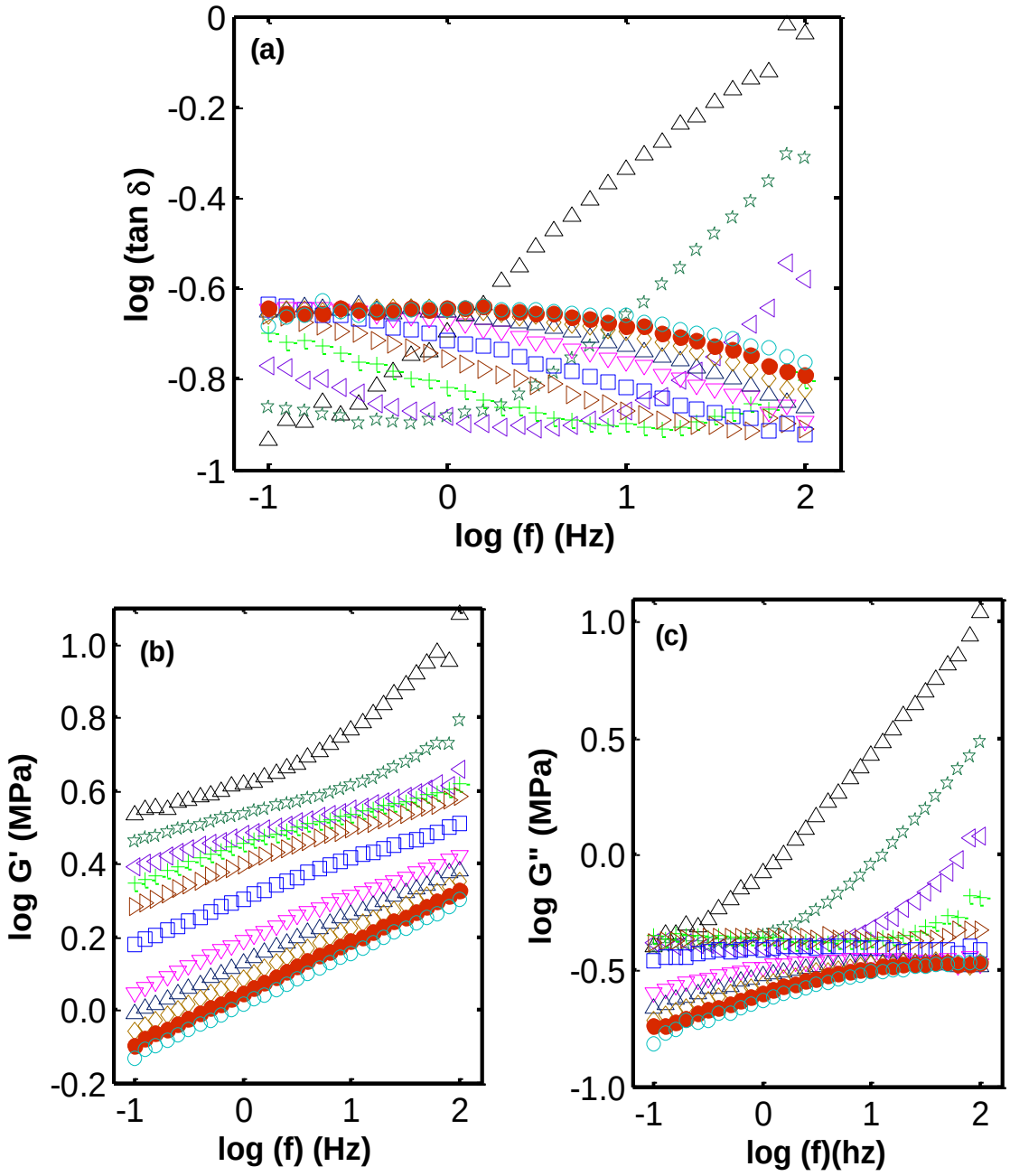

Figure A2- 1:Tanδ (a), G' (b), and G" (c) isotherms for SBR with 40 phr of N550 cured with 0.1 phr of DCP. Temperatures (in ºC) are as follows: △ -30, ☆ -20, ◁ -10, + 0, ▷ 10, □ 20, ▽30, × 40, ◇50, • 60, ○ 70.

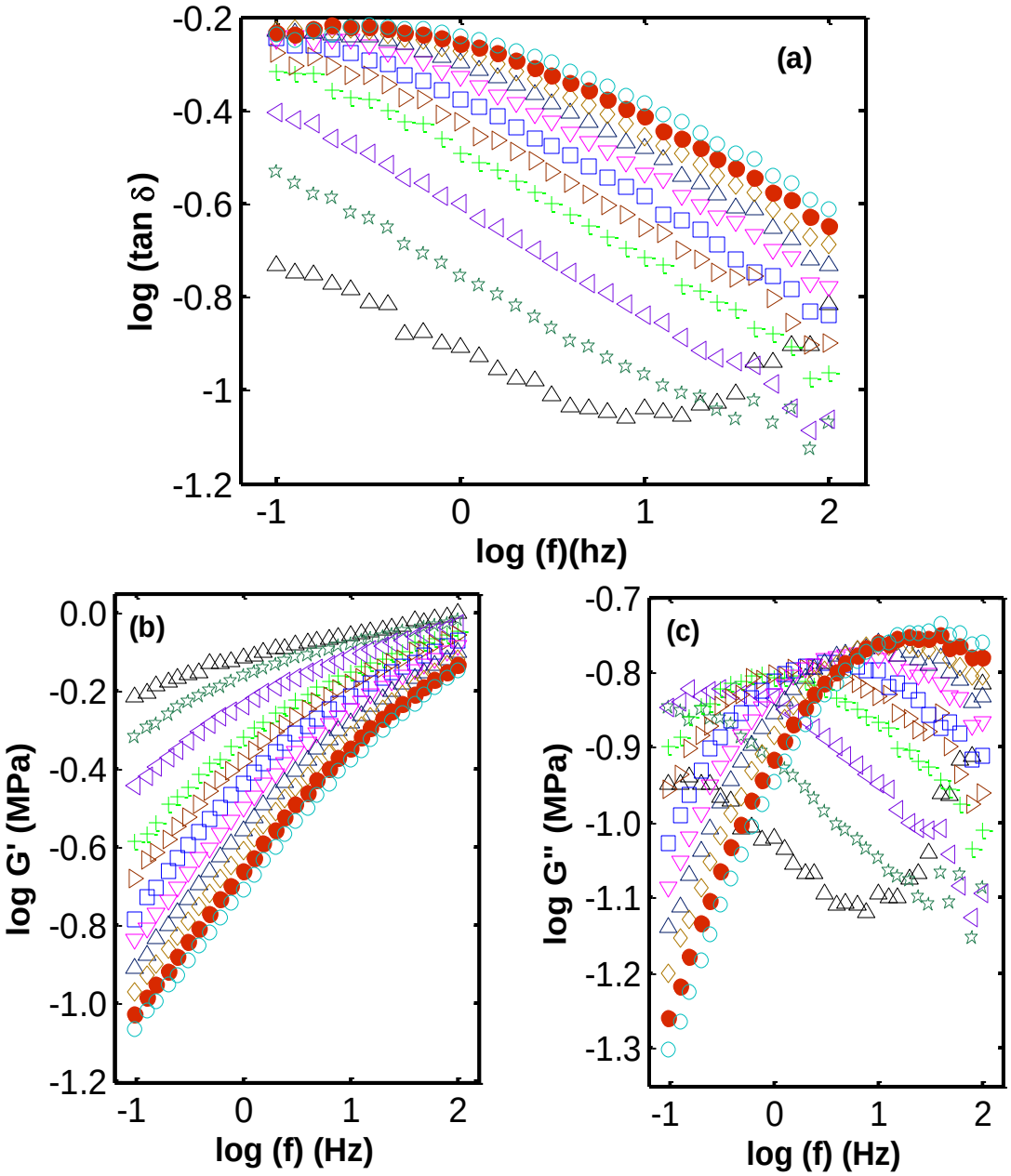

Figure A2- 2: Tanδ (a), G' (b), and G" (c) isotherms for polybutadiene. Temperatures (in ºC) are as follows: △ -30, ☆ -20, ◁ -10, + 0, ▷ 10, □ 20, ▽30, × 40, ◇50, • 60, ○ 70.

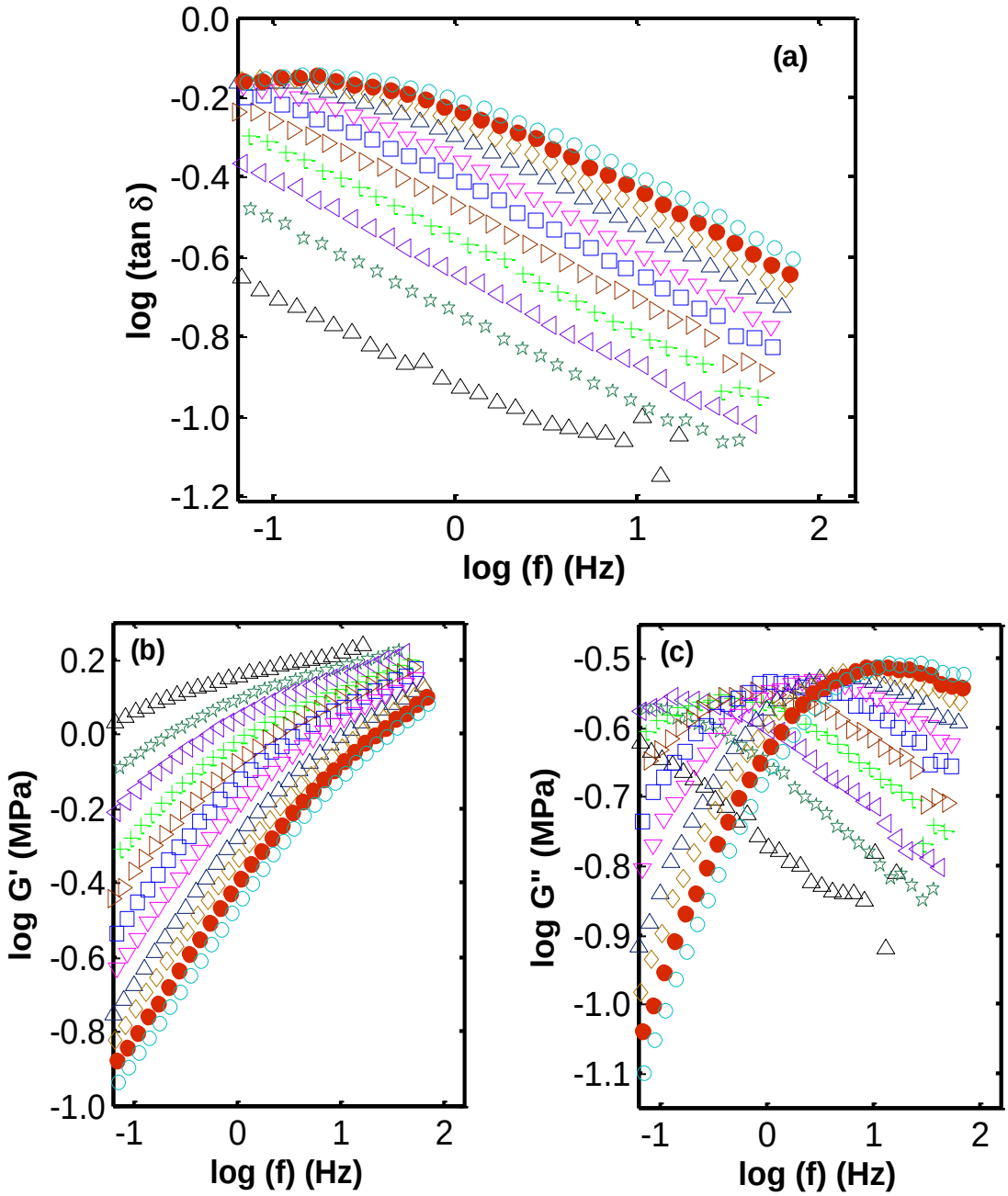

Figure A2- 3: Tanδ **(a),** G' (b), and G'' (c) isotherms for PB with 40 phr of N990. Temperatures (in ºC) are as follows: △ -30, ☆ -20, ◁ -10, + 0, ▷ 10, □ 20, ▽ 30, × 40, ◇ 50, • 60, ○ 70.

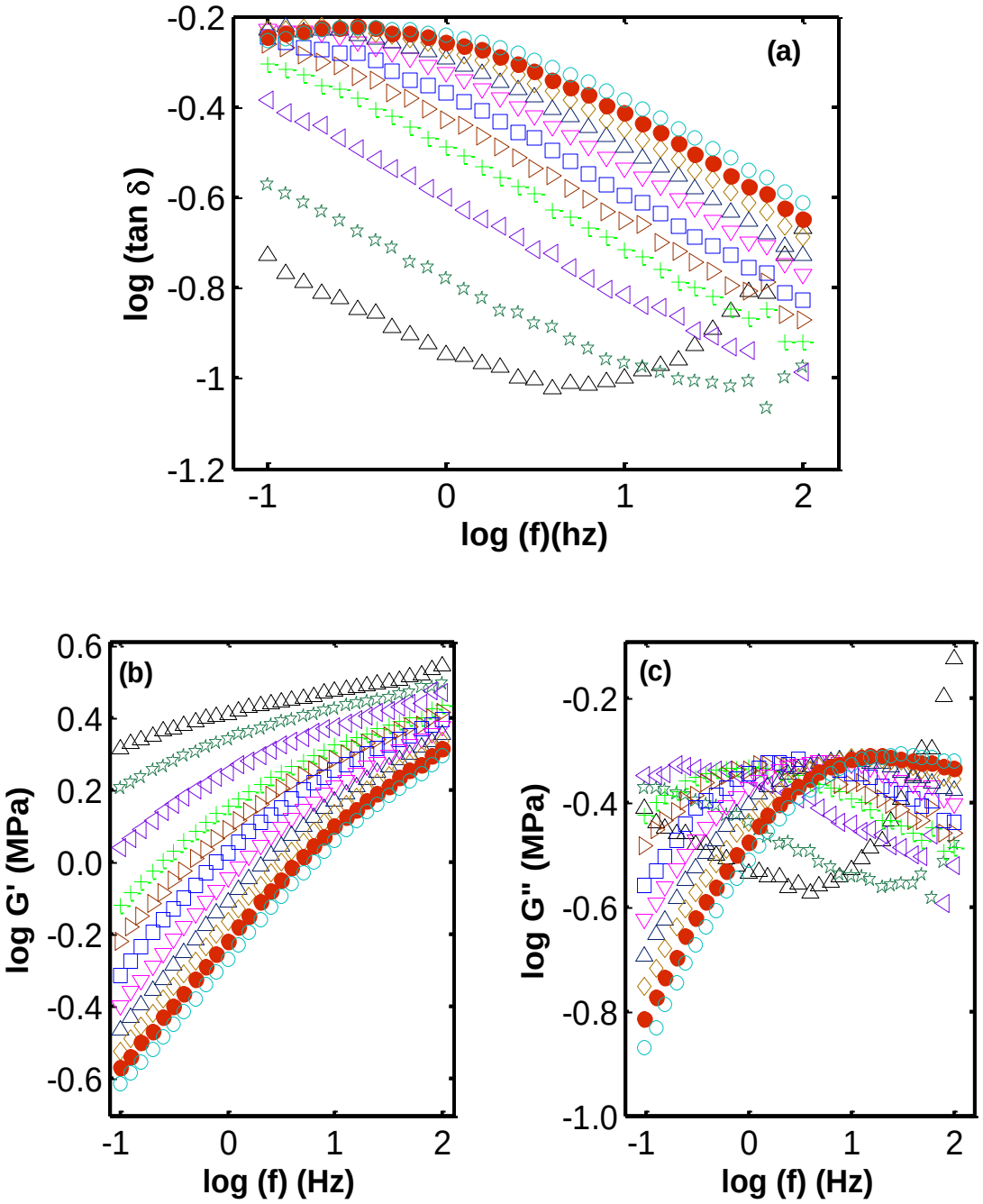

Figure A2- 4: Tanδ **(a),** G' (b), and G'' (c) isotherms for PB with 40 phr of N550. Temperatures (in ºC) are as follows: △ -30, ☆ -20, ◁ -10, + 0, ▷ 10, □ 20, ▽ 30, × 40, ◇ 50, • 60, ○ 70.

3. Isotherms from transient experiment

The isotherms from the creep experiment at several temperatures are provided below.

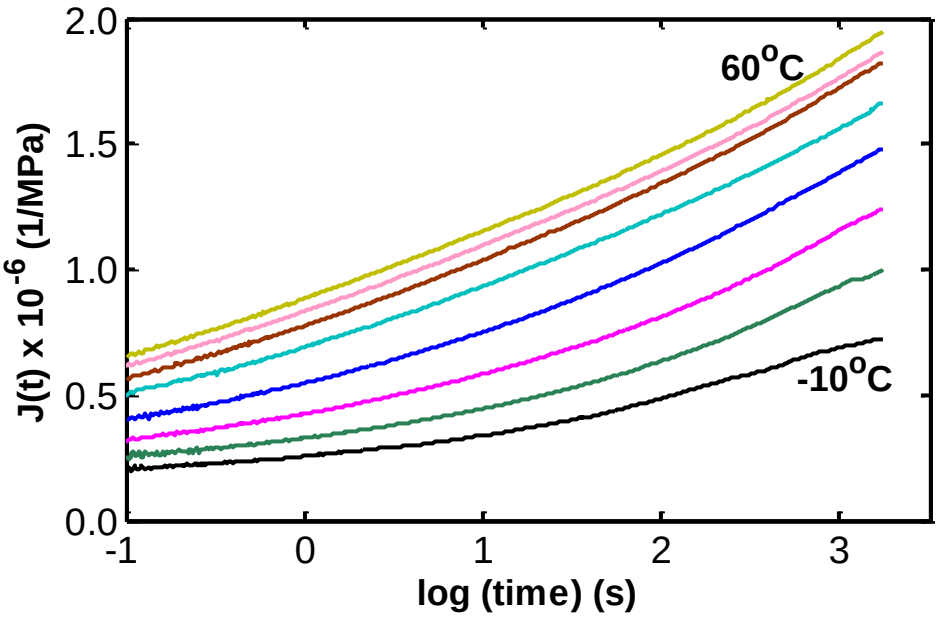

Figure A3- 1: Creep isotherms for SBR filled with 40 phr of N550 carbon black. Temperatures in 10°C increments from -10°C to 60°C.

Appendix B Figures

The Following Figures are Supplementary to Data Provided in "Critical Analysis of the Dynamic Behavior of Carbon Black Filled Elastomers: Part I. Linear viscoelastic master curves" by Ogebule, O; Medvedev, GA; Caruthers, JM.

1. Isotherms from dynamic experiment

The dynamic isotherms for Tan δ, G' and G'' versus frequency are provided for SBR cured with 0.1phr DCP containing the following carbon black composition:

3-1. 20phr N762

3-2. 10phr N762

3-3. 40phr N550

3-4. 20phr N550

3-5. 10phr N550

3-6. 40phr N990

3-7. 40phr N990

3-8. 40phr N990

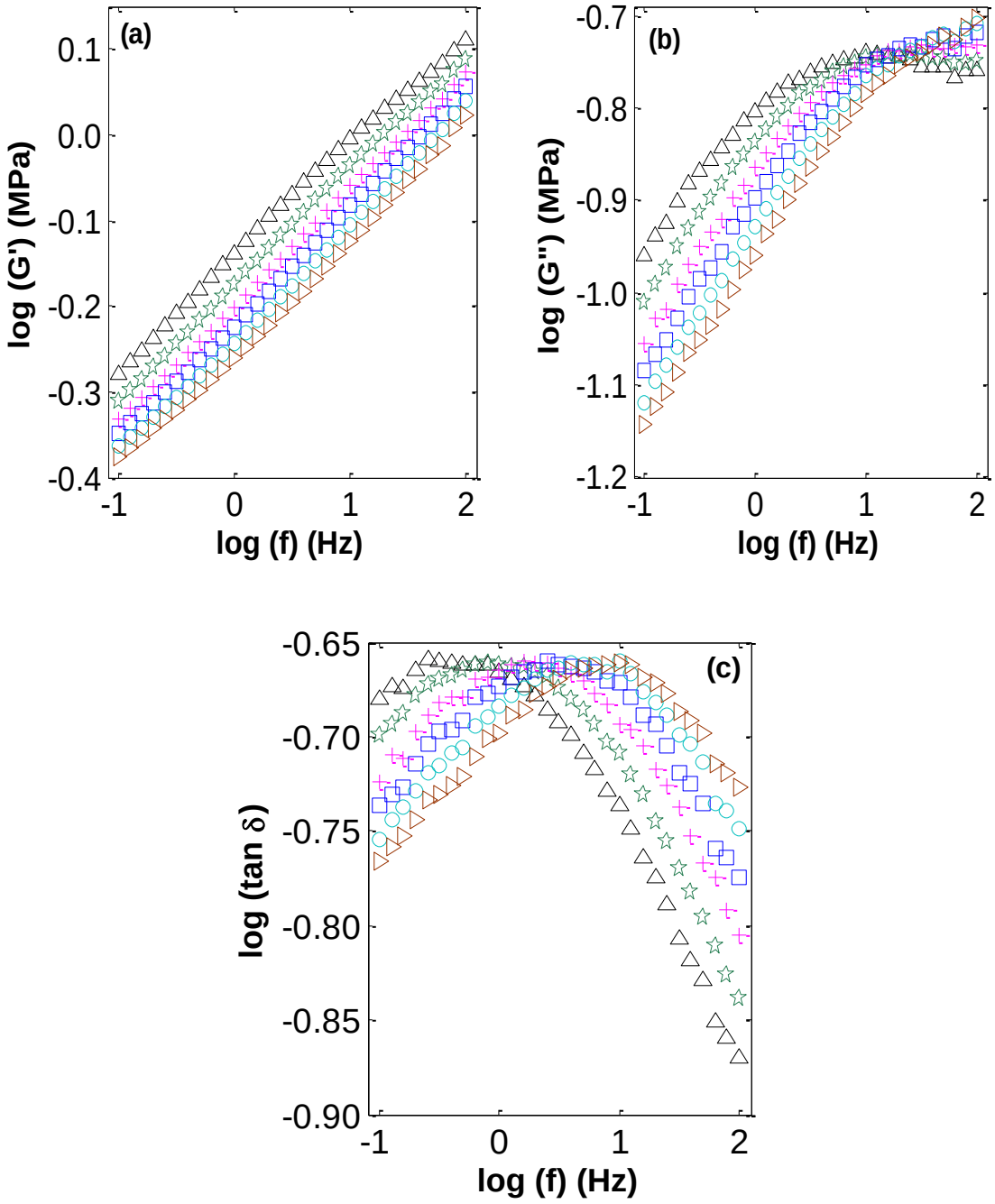

Figure B1- 1: G'(a), G'' (b), and tanδ (c) isotherms for SBR with 20 phr of N762 cured with 0.1 phr of DCP. Temperatures (in ^{o}C) are as follows: △ 30, ☆ 40, + 50, □ 60, ○ 70, ▷ 80.

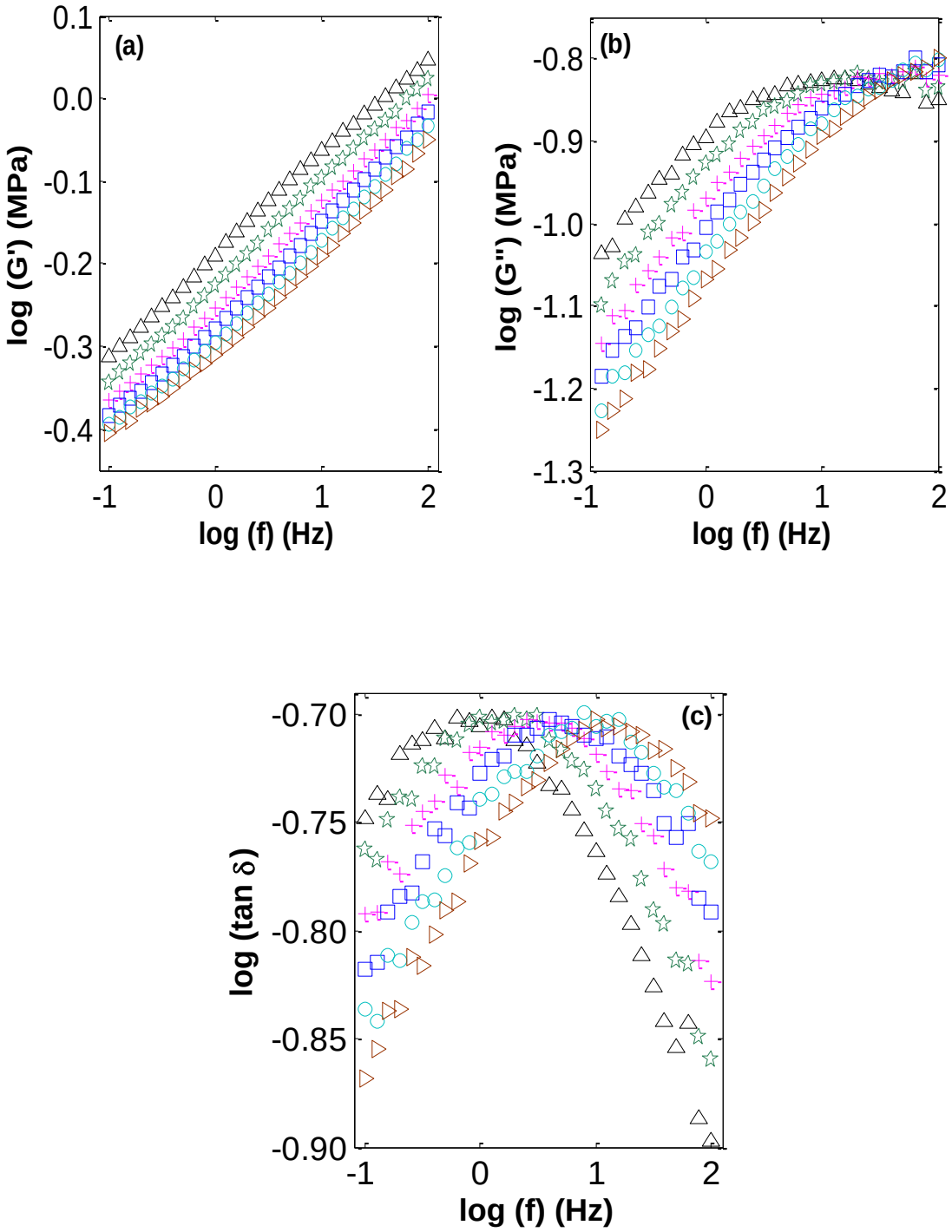

Figure B1- 2: G'(a), G'' (b), and tanδ (c) isotherms for SBR with 10 phr of N762 cured with 0.1 phr of DCP. Temperatures (in ^{o}C) are as follows: △ 30, ☆ 40, + 50, □ 60, ○ 70, ▷ 80.

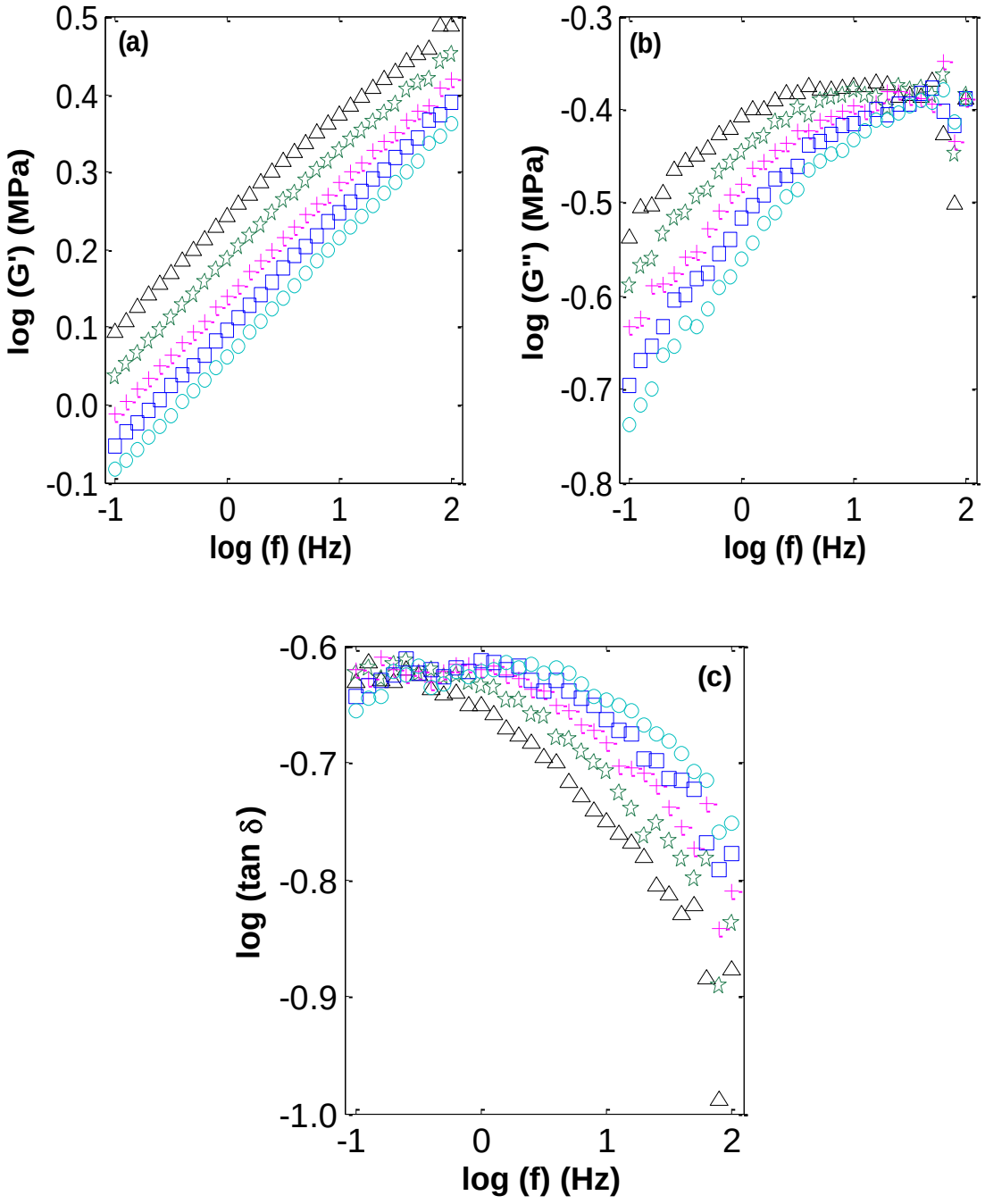

Figure B1- 3: G'(a), G'' (b), and tanδ (c) isotherms for SBR with 40 phr of N550 cured with 0.1 phr of DCP. Temperatures (in ^{o}C) are as follows: △ 30, ☆ 40, + 50, □ 60, ○ 70.

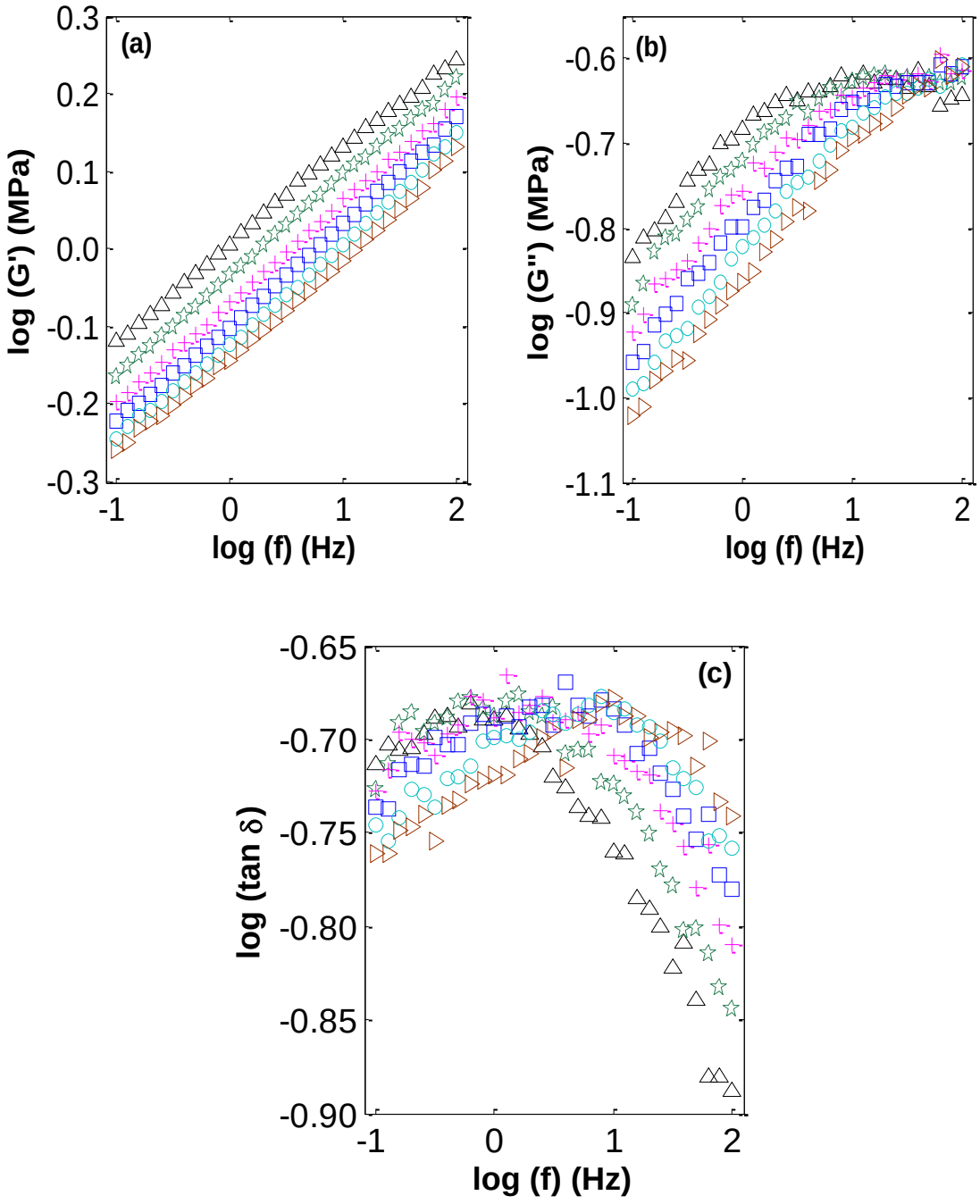

Figure B1- 4: G'(a), G'' (b), and tanδ (c) isotherms for SBR with 20 phr of N550 cured with 0.1 phr of DCP. Temperatures (in ^{o}C) are as follows: △ 30, ☆ 40, + 50, □ 60, ○ 70, ▷ 80.

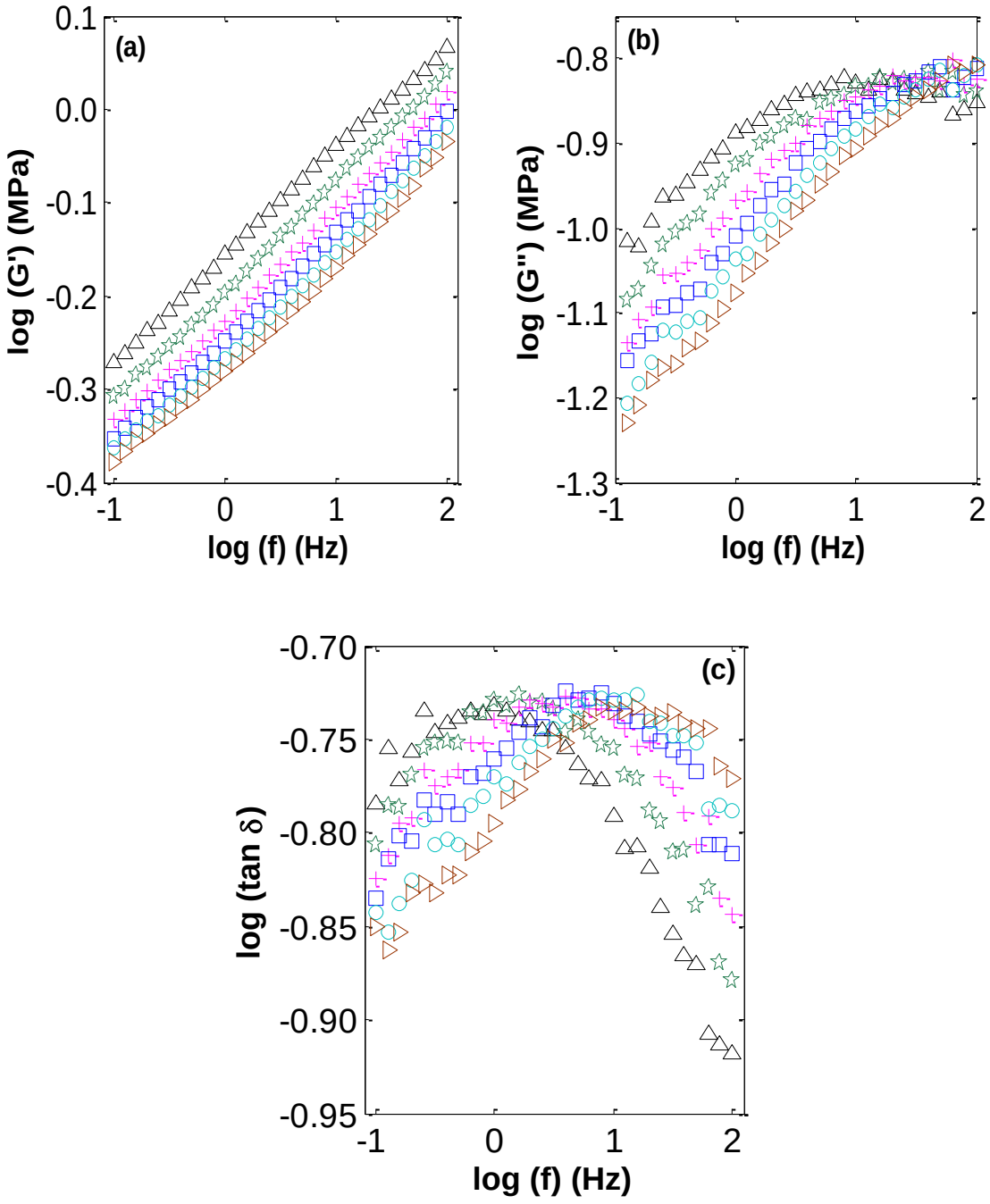

Figure B1- 5: G'(a), G'' (b), and tanδ (c) isotherms for SBR with 10 phr of N550 cured with 0.1 phr of DCP. Temperatures (in ^{o}C) are as follows: △ 30, ☆ 40, + 50, □ 60, ○ 70, ▷ 80.

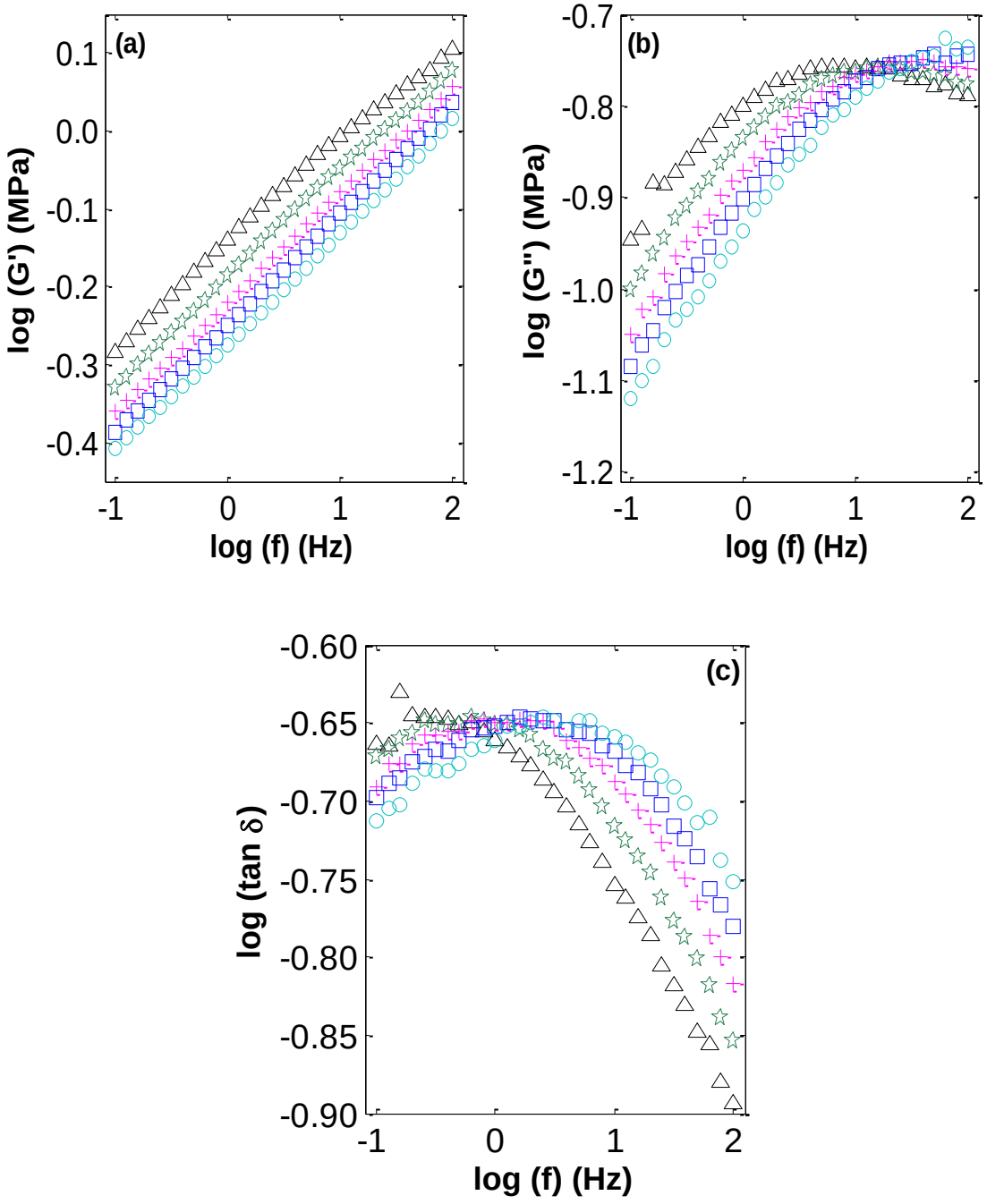

Figure B1- 6: G'(a), G'' (b), and tanδ isotherms for SBR with 40 phr of N990 cured with 0.1 phr of DCP. Temperatures (in ^{o}C) are as follows: △ 30, ☆ 40, + 50, □ 60, ○ 70.

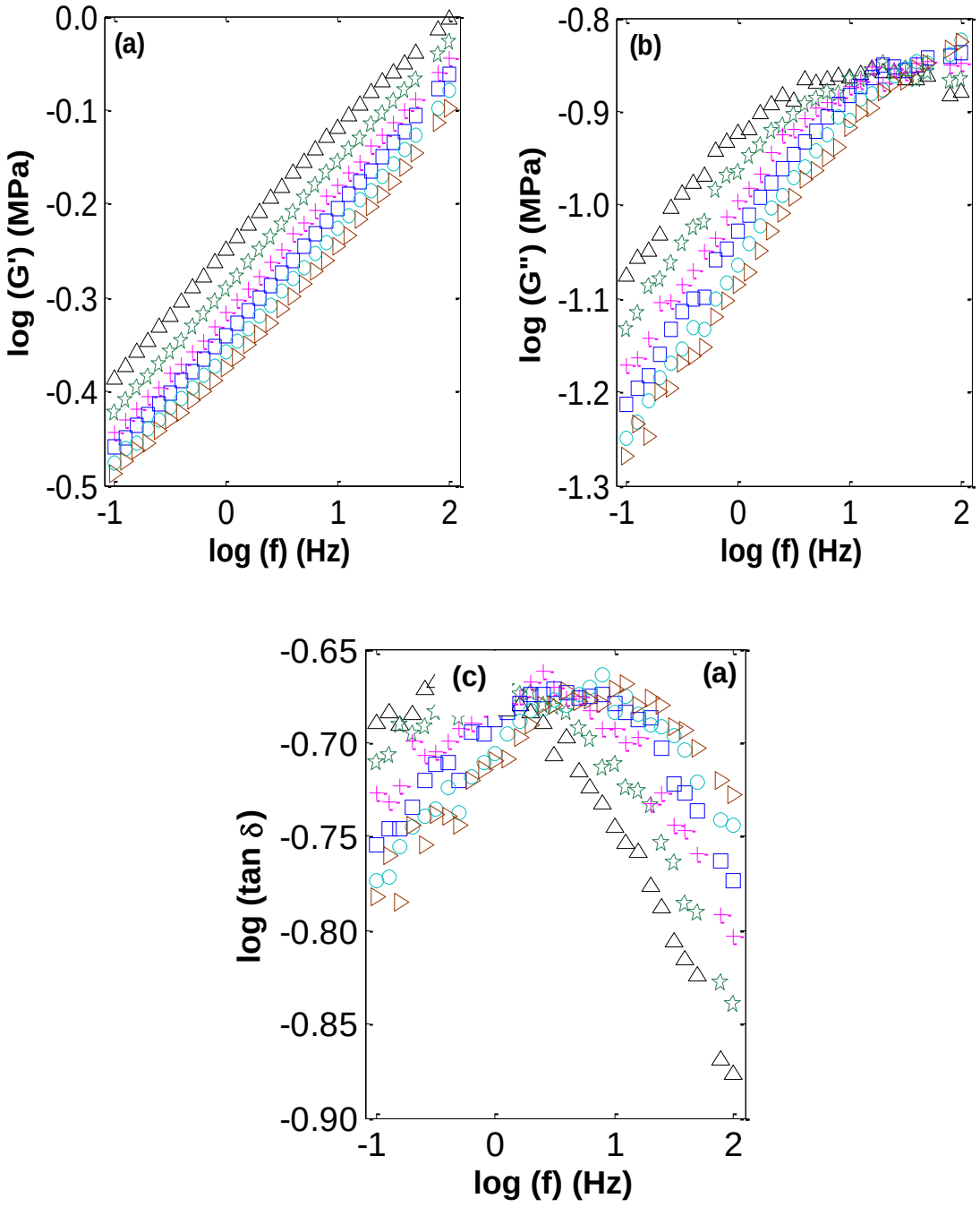

Figure B1- 7: G'(a), G'' (b), and tanδ (c) isotherms for SBR with 20 phr of N990 cured with 0.1 phr of DCP. Temperatures (in ^{o}C) are as follows: △ 30, ☆ 40, + 50, □ 60, ○ 70, ▷ 80.

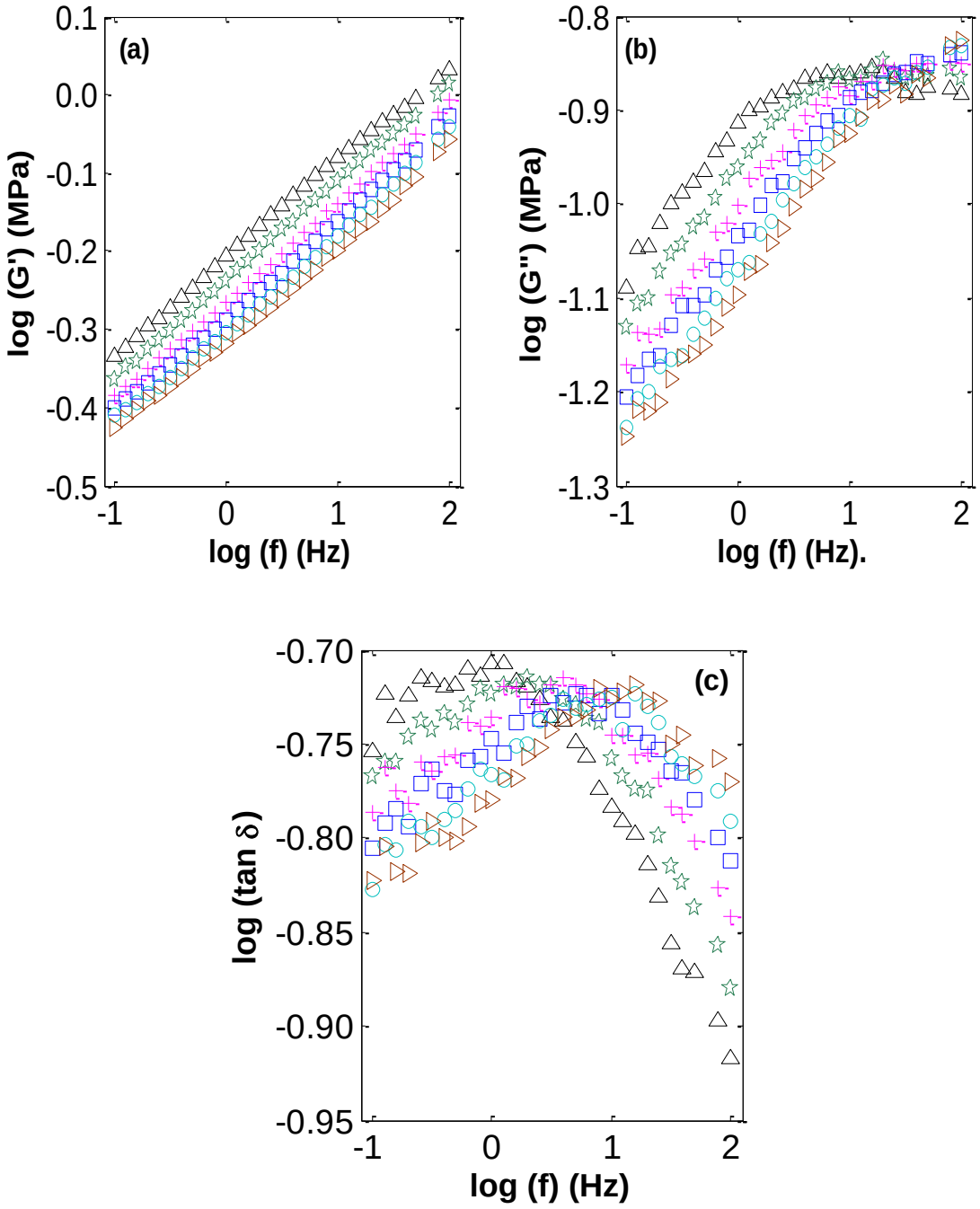

Figure B1- 8: G'(a), G'' (b), and tanδ (c) isotherms for SBR with 10 phr of N990 cured with 0.1 phr of DCP. Temperatures (in ^{o}C) are as follows: △ 30, ☆ 40, + 50, □ 60, ○ 70, ▷ 80.

Appendix C Figures

The Following Figures are Supplementary to Data Provided in "Necking in Fumed Silica Poly(Dimethylsiloxane) and the Resulting Mechanical Properties of the Necked Materials" by Ogebule, O, Medvedev, GA; Caruthers, JM. *Polymer* (2012).

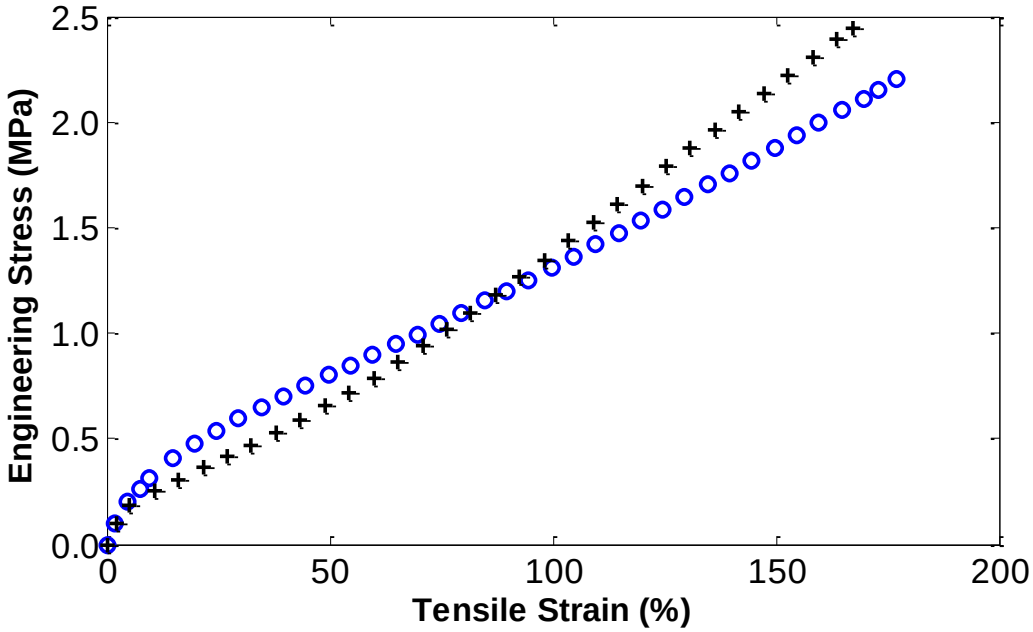

Figure C1- 1: Stress-strain behavior to failure for 60phr A150 (○) and 100phr OX50 (+).

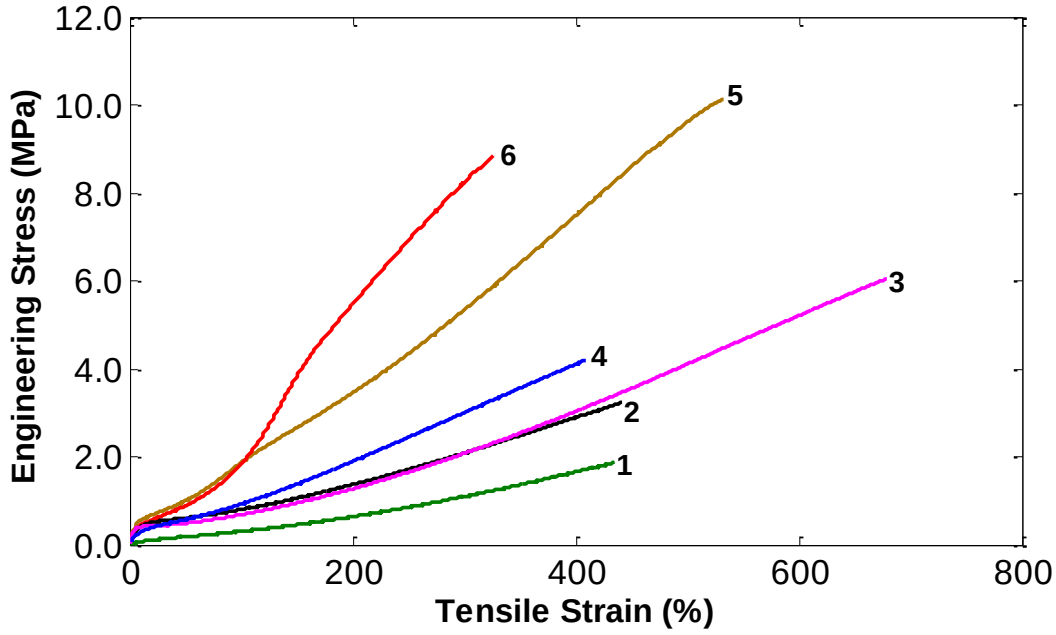

Figure C1- 2: Tensile strength of 40phr silica filled PDMS with varying surface areas; non-necking systems: 1 -50m^2/g; 2 - 150m^2/g; 3- 200m^2/g; 4- 90m^2/g; necking systems (after re-gripping of the necked portion; deformation of the virgin sample is not shown): 5 - 380m^2/ g; and 6 - 300m^2/g.

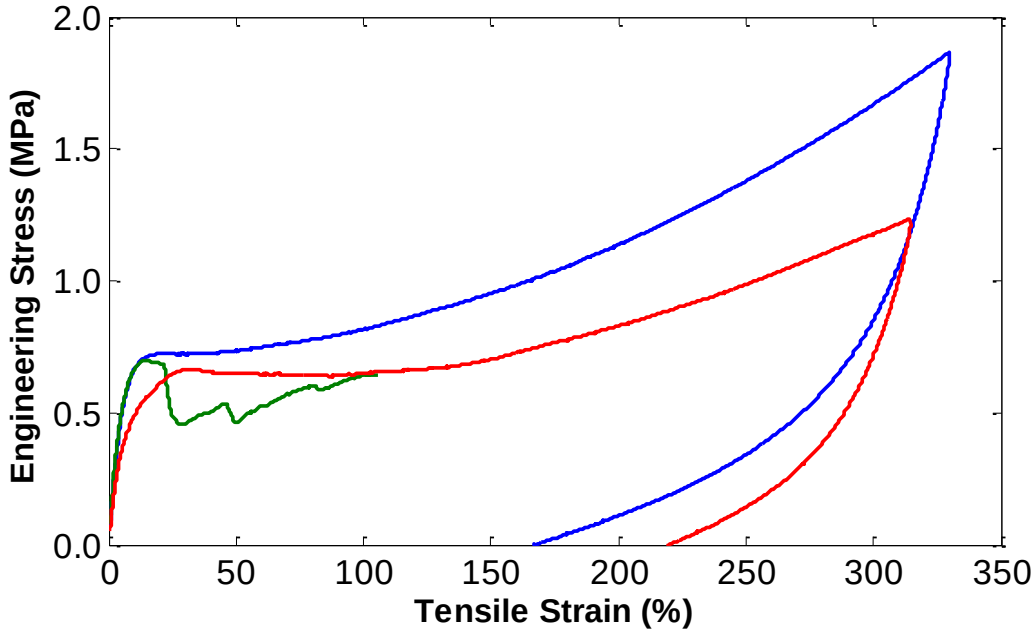

Figure C1- 3: Stress-strain behavior for 35phr A380 –PDMS with varying cross-link density; the amount of cross linking agent, DCP: 0.5 phr –green (cracks are visible on the sample during deformation), 1phr – red (necking from approximately 25% to 140% strain), 2phr – blue (necking from approximately 15% to 55% strain).

VITA

VITA

Oluwaseyi “Shay” Ogebule received her Bachelor of Chemistry degree from Alabama A&M University, Normal, Alabama in May 2007. She joined the School of Chemical Engineering at Purdue University in the Fall of 2008. Since then, she has worked with Professor James M Caruthers in the area of characterization of filled elastomers (rubbers). She is expected to receive her Ph.D. from Purdue University in October 2013 and thereafter join Intel Corporation in Rio Rancho, New Mexico